Investigation of Hydrophobic Interactions by Monte Carlo Simulation

Inaugural-Dissertation
zur Erlangung des Doktorgrades
der Mathematisch-Naturwissenschaftlichen Fakultät
der Universität zu Köln

vorgelegt von
Orkide Coskuner
aus Remscheid

Köln,

8th September 2003

Berichterstatter:	Prof. Dr. U. K. Deiters
	Priv. Doz. Dr. T. Kraska
Tag der mündlichen Prüfung	10.07.2003

For my parents and for my brother.

Zusammenfassung

In vorliegender Arbeit sind die Temperatur- und der Druckabhängigkeit hydrophober Effekte untersucht worden. Zu diesem Zweck wurden die strukturellen und thermodynamischen Eigenschaften von apolaren Molekülen und Wasser mit MC (Monte Carlo) Simulationen berechnet.

Das TIP5P Wasser Modell wurde anhand von ab initio Berechnungen optimiert. Um den hydrophoben Effekt zu untersuchen, wurde ein NPT Ensemble MC Programm in der Sprache C implementiert. Durch die Zugabe von jeweils zwei Methan-, zwei Xenon- oder zwei Ethanmolekülen zu 216 Wassermolekülen wurden hydrophoben Wechselwirkungen untersucht. Reines Wasser wurde unter den selben Bedingungen simuliert um die Veränderungen in den physikalischen Eigenschaften zu vergleichen. Zur Untersuchung der strukturellen Eigenschaften in Abhängigkeit von der Temperatur oder dem Druck, wurden die Korrelationsfunktionen und Koordinationszahlen berechnet.

Das Volumen, die innere Energie, die Enthalpie, und das chemische Potential von Wasser und von der apolaren Molekülen wurde simuliert um die Temperatur- und Druckabhaängigkeit dieser Systeme zu bestimmen. Es zeigte sich, daß der räumliche Abstand zwischen CH_4- oder C_2H_6- Molekülen mit steigender Temperatur kleiner wird. Für Xenon konnte eine derartige starke Abhängigkeit von der Temperatur nicht gezeigt werden. Im Gegensatz zu Methan und Xenon, bilden zwei Ethan Moleküle mit steigender Temperatur ein Kontanktpaar aus. Xenon Atome bzw. zwei Methanmoleküle sind auch bei hoher Temperatur durch Wasser getrennt. Ein Grund für dieses Verhalten ist die geringe Löslichkeit und die Größe der Ethanmoleküle. Die Anzahl an Wasserstoffbrücken ist am höchsten für das Wasser–Ethan System. Die O–O und H–H Korrelationsfunktionen sowie die Koordinationszahlen zeigen eine starke Temperatur Abhängigkeit für dieses System im Gegensatz zu den Wasser–Methan und Wasser–Xenon Systemen. Dieses Ergebniss ist im Einklang mit der Iceberg Theorie von Frank und Evans.

In dieser Arbeit, konnten keine starke Abhängigkeiten der Korrelationsfunktionen oder Koordinationszahlen vom Druck gezeigt werden.

Das Volumen, die innere Energie, die Enthalpie und das chemische Potential steigt mit steigender Temperatur. Es hat sich herausgestellt, daß die Veränderungen der strukturellen und thermodynamischen Eigenschaften für das Wasser–Methan System zwischen 313–318 K und für das Wasser–Ethan zwischen 303–308 K stark sind. Die Wassermoleküle zeigen eine Umordnung zwischen 308–323 K.

Zur Gewinnung einer neuen Betrachtungsweise, wurde die Auswirkung der apolaren Moleküle auf Wasser in Abhängigkeit von der Temperatur, untersucht. Hierzu wurde die Veränderung der Enthalpie und des chemische Potentials des Wassers berechnet. Die Änderungen der Enthalpie und des chemischen Potentials des Wassers sind am größten für das Wasser–Ethan System und am kleinsten für die Wasser–Xenon und Wasser–Methan Systeme. Ein Grund hierfür ist die Größe

des Ethanmoleküls.

Die Veränderung des chemischen Potentials von Wasser ist eine Kombination aus einer kleinen Abnahme der Enthalpiedifferenz sowie einer großen Abnahme der Entropiedifferenz.

Weiterhin wurden drei Methoden zur Berechnung des chemischen Potentials in Systemen von hoher Dichte untersucht: Widom insertion, Widom deletion und particle deletion scheme Methoden. Die Widom insertion Methode lieferte Ergebnisse, die am besten mit experimentellen Daten übereinstimmen.

Abstract

In this work the temperature and pressure dependence of the hydrophobic effetcs have been investigated. For this purpose, the structural and thermodynamic properties of the apolar and water molecules, with increasing temperature and pressure, have been calculated by Monte Carlo simulations.

The TIP5P model for the water dimer was optimized by ab initio calculations. To investigate the hydrophobic effects, an NPT ensemble Monte Carlo program was coded in C. The hydrophobic interactions have been studied by the addition of two methane, two xenon and two ethane molecules into 216 water molecules. To compare the change in the physical properties of water when these apolar molecules are added, pure water simulations with 216 water molecules under same conditions were performed. The correlation functions and coordination numbers of the molecules were simulated and calculated to study the structural properties with increasing temperature or increasing pressure. The volume, internal energy, enthalpy and the residual chemical potential of water and that of apolar molecules were simulated to investigate the temperature or pressure dependence of the thermodynamic properties of the systems. It is found that the methane and ethane molecules attract each other with increasing temperature and that xenon does not show strong dependence on temperature. The water–separated methane and xenon pair probability is higher, whereas the contact–pair probability is higher for the ethane molecules with increasing temperature. This must be due to the lower solubility and bigger size of ethane. The hydrogen bonds number between the water molecules is highest when two ethane molecules are added into water. This indicates, together with the oxygen–oxygen and hydrogen–hydrogen correlation functions and coordination numbers, that the water molecules reorganize and rearrange with increasing temperature when ethane molecules are added. This result is in agreement with the iceberg theory of Frank and Evans. The correlation functions and coordination numbers show no strong dependence on increasing pressure.

The volume, internal energy, enthalpy and the residual chemical potential of water and that of apolar molecules increase with increasing temperature. These properties show no clear dependence on increasing pressure. It has been found that the change in the thermodynamic and structural properties of the water–methane system is large between 313–318 K and that of the water–ethane system is remarkable between 303–308 K. The water rearrangement seems like to be stronger between 308 and 323 K.

To generate a new view of the temperature dependence of the apolar molecules effects on the water molecules, the enthalpy and residual chemical potential of water changes have been calculted when two apolar molecules are added into water. The enthalpy change is largest when two ethane molecules are added and smalles when two methane molecules are added into water. The residual

chemical potential of water shows the strongest change when ethane molecules are added, whereas this change is smallest when xenon or methane molecules are added. This must be because of the larger size of ethane. It has been found that the residual chemical potential change is a combination of a small decrease in enthalpy change. Therefore, there must be a large decrease in the entropy change.

To investigate the residual chemical potential calculation of the highly dense systems, three different methods have been studied in this work: the Widom insertion method, Widom deletion method and the particle insertion method. It has been found that the Widom insertion method yields the closest approximations to the experimental data.

Contents

Chapter 1

Introduction

Benjamin Franklin was the first who published a treatise on the immiscibility of oil in water in 1773. Lord Rayleigh repeated Franklin's experiment and made the first calculations of the size of the molecules [104]. Traube found that the amphiphilic molecules were concentrated at the air-water interface due to disaffinity between the hydrocarbon and water molecules in 1891 [105]. In 1892 Pockels developed what later became known as Langmuir trough and began with the investigation of films of oil on water.

In 1915, the word 'hydrophobic' appeared for the first time and was defined as [107]:

> "applied to a hydrosol that readily forms a precipitate and on evaporation or cooling gives rise to a solid that cannot readily be converted back into a sol."

With all these information given above, it became apparent that the disaffinity of nonpolar molecules for water drives many different types of noncovalent association in chemistry, biology and medicine.

Meyer published in 1898 the direct proportionality between oil/water partition coefficients and the anesthetic potencies of drugs [108]. McBain and Salmon discovered the reversible formation of micelles in soap solutions [109]. Gorter and Grendel investigated the lipid molecules from red blood cells and found that they could form bilayers [110]. Davson et al. published that proteins associate with the bilayer membranes through nonpolar interactions in 1935 [111]. Bull found that proteins contain a large number of nonpolar molecules and investigated their denaturation [112]. The X-ray experiments and structural studies of the localization of polar and nonpolar groups started in 1945 [113, 114].

Micelle formation was assumed to be driven by oil/oil attraction, or by charge interactions [115–117]. Hildebrand showed that the bonding between nonpolar molecules appeared due to noncovalent interactions [118].

The term 'hydrophobic' has become a common usage with the information mentioned above:

- The affinities are defined by free energies and not by enthalpies.
- 'bond' term refers to certain types of noncovalent interactions.
- the term 'hydrophobic' should be used for interactions between water and at least two apolar molecules and should be distinguished from 'hydration' that means interactions of one apolar molecule with water.

Hydrophobic interaction plays an important role in many processes like binding, development and structure of membranes and micelles, clathrate and hydrate formation, ligand–protein and protein–protein interactions, nucleic acid interactions, partitioning of drugs, toxins and metabolites in the environment and body, protein folding, oil and water immiscibility etc.

The terms, "hydrophobic interaction", "hydration" and "hydrophobic effect" describe the observation that apolar molecules tend to oppose their interaction with water molecules with characteristic thermodynamic properties that vary with the temperature."Hydrophobic hydration" as mentioned above refers to the structural and energetic response of water near to a hydrophobic solute [1–4, 34]."Hydrophobic interaction" describes the interaction of nonpolar molecules with water, each other and the interaction between water molecules in the presence of two or more hydrophobic solutes [5, 6, 73].

The low solubility of apolar molecules makes the experimental studies of pairwise interactions to investigate hydrophobic interactions extremely difficult. The analysis of hydrocarbon hydration thermodynamics of Ben-Naim and Yacobi provides qualitative support for the traditional view of hydrophobic hydration [125]. A few experimental studies measured the deviation of nonpolar solubility from Henry's law of limiting behaviour [126,127]. For example, it is found that isolated benzene molecules in water tend to aggregate and that this tendency increases with temperature [126,128]. In general, data for other nonpolar solutes are consistent with the benzene results, but are subject to large uncertainty [127, 129, 130]. In solutions where solubilities are appreciable, due to inclusion of hydrophilic groups in otherwise nonpolar solutes theoretical evaluation of experimental information is complicated by the existence of competing effects.

The experimental solvation process of a molecule is defined as the process of transferring the molecule from a fixed position in an ideal gas phase into a fixed position in the liquid phase. The solvation process is carried out experimentally at constant temperature, pressure and composition [9].

Broadbent and Neilson performed neutron scattering experiments to investigate the hydration structure of argon in water at elevated pressure and found a pronounced first hydration shell with weak long range correlations [26].

The low solubility of apolar molecules in water results from the fact that the transfer of apolar molecules from the gas phase into infinitely diluted aqueous solution involves an increase in the Gibbs energy. This Gibbs energy change is a combination of a small decrease in enthalpy and a large decrease in entropy

near to room temperature, as observed by Butler, along with a negative volume of solution and an increase in the heat capacity of the solution [10–12]. These thermodynamic observations are surprising in view of the large heat of vaporization and also the surface tension of water, which seem to indicate that water has rather a strong cohesive energy, so that the creation of a cavity to accomodate a solute molecule would require an input of enthalpy. Of course, some of the enthalpy should be recovered when the solute is placed in the cavity. It could then be argued that the whole process involves replacing the strong water–water attractive forces by the weaker water–apolar molecule ones. This could lead to a net positive enthalpy change that could explain the observed positive free energy change.

Most of the structural theories proposed to account for the thermodynamic observations mentioned above [13] rely on the idea that the apolar molecule increases the degree of hydrogen bonding of water molecules in the solvation shell. This leads to an increase in water–water attraction which is characterized by a negative contribution to the enthalpy and the entropy increases. The negative entropy change can be viewed as a result of some ordering or rearranging of water molecules in the hydration shell. It is believed to cause the decrease in the solubility of apolar molecules in water [219].

The inert gases form crystalline clathrate hydrates at high pressure and temperatures in which each inert gas molecule is surrounded by a polyhedral cage in the lattice of host water molecules [15]. It has been claimed that the hydration shell of apolar solutes in water should resemble these cages, since there would be a tendency for the hydrogen-bonding groups of the water molecules to avoid being direct toward the solute molecules. Such an orientation allows the number of water-water hydrogen bonds in the hydration shell to be close to that in bulk water [13].

A different picture of hydrophobic hydration comes from the hydrogen bonding properties of water molecules [16]. As the hydration shell adjusts to accomodate the apolar molecule, water molecules start to reorganize and rearrange around the apolar molecule in order to maintain the highest number of hydrogen bonds. The orientational freedom is restricted because of the inability of the nonpolar molecule to participate in hydrogen bonding with water molecules, so that some orientations of the water molecules become energetically unfavorable.

Hydrophobic interaction can also be regarded as resulting from a thermodynamic force in water that drives hydrocarbon molecules towards each other in contrast to the situation in a nonpolar solvent; because the surface area the apolar molecules would present to water as a cluster is less than that if they are separate. The entropy change should be positive, bringing two apolar molecules together, and should lower the free energy. The association of apolar molecules in water can be regarded as partial reversal of the thermodynamically unfavorable process of solution [13].

Traditional descriptions of the stability of biologically important structures

relied on the concept of a hydrophobic interaction that represents some sort of effective attraction between nonpolar molecules of these structures [13, 14]. This effective attraction has been thought to be because of the peculiar structure of water. Therefore, much effort has been invested in the studies of nonpolar molecules in water [27, 32, 34]. One specific aspect of this broad area of research is being referred to as the hydrophobic bond, or hydrophobic interaction problem [60, 124, 153, 215, 219, 220].

There are several phenomena that are referred by the term hydrophobic interaction. It is possible to distinguish between two extreme cases; all others can be regarded as intermediary. The first case involves the folding of a polymer in a way that side-chain nonpolar groups are removed from water and transferred into the interior of the protein. The second case involves the dimerization of two dissolved nonpolar particles in water. The actual process of polymer folding that was pointed out by Scheraga [219] involves side-chain nonpolar groups that are partially surrounded by water molecules, attracting each other so that part of the water molecules in between are being squeezed out, with thus the formed dimer still being surrounded by water molecules. In a review Kauzmann [215] made the comparison between the process transfer of a nonpolar molecule from water to benzene or CCl_4, and the process of transferring of the side-chain nonpolar group into the interior of a protein. However, the actual cases are likely to belong to the intermediary class as Scheraga et al. [219] have argued: Even when the hydrophobic region is formed in the interior of the protein, it will still retain some water molecules.

In the second case, one investigates the dimerization process, the thermodynamic properties of which may indicate to what extent two nonpolar molecules have the tendency to adhere to each other. This approach encounters some theoretical and experimental difficulties. If one investigates dimerization, the proper definition of a dimer has to be given. The easiest way to define a dimer could be according to the relative distances of the two nonpolar molecules. However, if the two nonpolar molecules are simple enough, there is no available method to see the formed dimers and to distinguish them from the separate monomers.

When one investigates dimerization of somewhat more complex molecules, like alanine, where an operational definition, in terms of a suitable measuring technique, can be given to the alanine dimer, the shortcomings of this approach are evident. The driving forces that bring the two nonpolar molecules closer to each other originate from both the hydrophobic interaction and hydrophobic bond formed between the two nonpolar molecules. It is difficult to differentiate between the various contributions. The geometry of the formed dimer may be such that the two nonpolar molecules will not be at a typical distance that is essential for hydrophobic interaction.

Theoretical and computer simulation works have provided valuable insight into the nature of hydrophobic interactions. It has been claimed that a solvent–separated apolar pair may be more important than a contact apolar pair in de-

termining the hydrophobic effects [61, 62]. In addition, it has been claimed that two simple nonpolar solutes in water are not strongly attracted as it is assumed traditionally [67–69, 131].

The approximate integral equation theory of Pratt and Chandler was the first one that demonstrated the existence and importance of solvent-separated pairs [61]. Using experimentally determined water correlation functions, the van der Waals diameter of water, and a hard sphere solute solvent potential energy, they calculated the potential mean force for hard spheres in water, and for comparison in a hard sphere solvent. The potential of mean force in the two solvents differed primarily in the solvent-separated region, where the aqueous potential of mean force was more stable. Thus, the nature of pairwise interactions was observed to depend on the solvent-separated region. Upon increasing the temperature, the stability of the solvent-separated pair decreases. The net attraction between the solute particles, measured by osmotic second virial coeffient, was found to decrease as the temperature was increased. This is in conflict with the traditional theory. Finally, when attractive interactions are included in Pratt and Chandler calculation, two additional effects are noted [62]; the enthalpy of association is closer to the traditional view and the contact–pair is destabilized. For the specific case of methane considered, including the attractive interaction causes the solvent separated free energy to be lower than the contact free energy. This observation can be interpreted as being consistent with the structure of clathrate and hydrates, in which nonpolar molecules are never observed in contact [132]. Nevertheless the observation is in conflict with the traditional ideas of nonpolar aggregation. Pettitt, Rossky and Karplus et al. also calculated the free energy, entropy, enthalpy, and internal energy of association by using the integral equation theory [63–65]. The internal energy was found to stabilize the contact pair. Their simulation results were in conflict with the usual prediction of positive enthalpy of association.

Berne and co-workers calculated the potential of mean force of Lennard-Jones solutes in ST2 water and obtained agreement with the Pratt and Chandler theory. Other simulations of free energy of association of nonpolar solutes predicted stable solvent separated configurations [67, 70, 71, 133]. The same observation was made by Wallqvist and Berne for a nonpolar solute near a paraffin wall in water [72].

However, Smith and Haymet calculated the potential of mean force of methane molecules in water and concluded that the contact pair is more stable than the water separated pair [73]. Mancera reported, based on molecular dynamics an increased tendency for methane particles to form contact pair with increasing temperature [74].

Dang, however, attributed the temperature effects reported by Mancera to a density effect, his own simulations showed no temperature effect [75]. Steinhauser et al. investigated the temperature dependence of free energy especially between 300 and 350 K. By using the parameters of Pratt and Chandler and the Lorentz–Berthelot mixing rules, they found out that a global minimum at contact distance

exists for methine like molecules [76].

Mackie pointed out that the early simulations seemed to support the theory of water structure enhancement and that it would not be the case according to their radial distribution function investigations of water–methane system, where the interactions would lead to a negative free energy. Thus, the negative free energy of solvation would be determined by water–methane interactions and not by positive reorganization of the water molecules, according to Mackie [77]. Chan et al. investigated the temperature dependence of hydrophobicity by using the Pratt and Chandler theory and TIP4P as water model. They showed that the heat capacity of the desolvation is large and positive, and that the entropy increases when methane molecules form a contact pair. But at the same time there would be a drastic heat capacity change in the system [78].

The temperature dependence of hydrophobic effects was also investigated by Skipper, who simulated four methane molecules in 256 water molecules, at a fixed density and concluded that the tendency of methane molecules to aggregate increases with increasing temperature from 275 to 317 K [79, 134]. This was followed by many more extensive studies using similar systems of semiconcentrated methane solutions. However, some scientists pointed out that the results of Skipper contain some ambiguity because of methane–methane interaction [78]. Furthermore, Dang reported a very small temperature dependence of aggregation and suggested that the discrepancy might be caused by Skippers use of a temperature–independent water density [75].

Guillot and Guissani investigated the temperature dependence of hydration of noble gases and methane in simple point charge water by performing molecular dynamics simulations [25]. They argued that the bigger the apolar molecule, the more negative the value of the water–apolar molecule interaction that leads to an increase in the solubility of the apolar molecule. On the other hand, the bigger the apolar molecule, the more negative the entropy of cavity formation that leads to a decrease in the solubility of the apolar molecule.

The rather low solubility of inert gases in water attracted interest for a long time, and much effort has been invested in experimental studies [39–42]. The behaviour of xenon is here of special interest: A large number of proteins are well known to fix small ligands, like organic solvent molecules. The inert gas chosen to simulate was xenon due to the attractive properties not only in the physical chemistry but also in biology, medicine etc. Xenon is able to bind to discrete sites in hydrophobic cavities, pores of channel like structures and also to the substrate and ligand binding pockets [?, 45–48]. Dichloromethane and Cyclopropane can also bind to the proteins, but because of their greater size some distortions and rearrangements in the protein structure and amino acid chains are noticed. Xenon complexes can also be used as highly isomorphous heavy-atom derivatives [51–54].

The rotational degrees of freedom of water show a decrease upon xenon binding. Local rearrangements and displacement of water molecules may occur upon inert gas binding, as was evident by the analysis of krypton binding to elas-

tase [46, 47, 55, 56, 58, 59].

Because of the lack of experimental work about hydrophobic interactions and to compare the simulation results with the available experimental data, the hydration process of xenon at different temperatures and pressures had to be simulated and compared with the experimental results.

The literature contains many discussions of hydrate and clathrate behavior. Hence, it was also necessary to investigate inert gases in water and compare the structural, thermodynamic properties and their temperature and pressure dependence with the alkanes; methane and ethane molecules. In this work Monte Carlo simulations were performed to investigate the methane, ethane and xenon molecules in water to predict the structural and thermodynamic properties and also the temperature and pressure dependence of these properties. Another idea was to simulate also pure liquid water and compare the structural and thermodynamic results of pure water when two methane or two ethane molecules are added into the system under same conditions. The temperature and pressure dependence of the water-xenon system was important to understand especially the effect of xenon to water molecules rearrangement that was pointed out by Tilton et al. [47] which is explained above.

The simulation of the chemical potential of highly dense systems is still a problem in the statistical mechanics, and one can find several methods for it. In this work, the residual chemical potential was investigated by using different methods.

Chapter 2

Theoretical Background

2.1 Theory of the hydrophobic effect

In general the hydrophobic interaction is expressed in terms of differences in Gibbs energy. The nonpolar pairs are characterized mainly by their interaction, or by their binding energy, with the rest of the system [9]. A system containing N_A molecules of species A and N_B molecules of species B, at a given temperature and pressure is considered. The Gibbs energy change for bringing A and B molecules from fixed positions to some close distance R, where R is of the order of magnitude of the average molecular diameters of A and B, $R \approx (\sigma_A + \sigma_B)/2$, is defined [9]. A and B molecules are assumed as spherical molecules for simplicity, so that the Gibbs energy of the process is a function of R only and not a function of the orientation of the two molecules.
The Gibbs energy change is defined as [227].

$$\Delta G_{AB}(r) = U_{AB}(R) + \delta G_{AB}(R) \tag{2.1}$$

where $U_{AB}(R)$ is the direct pair potential at distance R and $\delta G_{AB}(R)$ is the indirect part of the Gibbs energy change. The pair potential $U_{AB}(R)$ depends on the properties of the pair of molecules A and B and is irrelevant for studying the solvent properties. The value $\delta G_{AB}(R)$ is referred to as the hydrophobic interaction thermodynamic property between the molecules A and B [228].
$\delta G_{AB}(R)$ is defined as:

$$\delta G_{AB}(R) = \Delta G^*_{AB}(R) + \Delta G^*_{AB}(\infty) \tag{2.2}$$

where $\Delta G^*_{AB}(R)$ and $\Delta G^*_{AB}(\infty)$ are the hydration Gibbs energies for the pair at a distance R and ∞, respectively.
The equation above was simplified further by noting that the binding energy of A and B molecules, at infinite separation may be viewed as the sum of the binding energies of A and B separately.

$$\begin{aligned} \delta G_{AB}(R) &= -kT \ln \langle \exp\left[-\beta B_{AB}(\infty)\right] \rangle_* \\ &= -kT \ln \langle \exp(-\beta B_A) \rangle_* - kT \ln \langle \exp(-\beta B_B) \rangle_* \\ &= \Delta G_A^* + \Delta G_B^* \end{aligned} \tag{2.3}$$

Therefore

$$\delta G_{AB}(R) = \Delta G_{AB}^*(R) - \Delta G_{AB}^*(R) - \Delta G_A^* - \Delta G_B^* \tag{2.4}$$

The quantity $\delta G_{AB}(R)$ is also related to the apolar–apolar molecule distance distribution. According to Ben-Naim [228], the pair correlation function $g_{AB}(R)$ is related to the Gibbs energy change $\delta G_{AB}(R)$.

$$\begin{aligned} g_{AB}(R) &= \exp\left[-\beta \Delta G_{AB}(R)\right] \\ &= \exp\left[-\beta U_{AB}(R)\right] \exp\left[-\beta \delta G_{AB}(R)\right] \end{aligned} \tag{2.5}$$

One can find many quasichemical theories about the hydrophobic effect in the literature [224]. However, the quasichemical theories break down for real systems, because these theories treat hard core solutes.
As pointed out in Section 1, the first widely accepted explanation for the thermodynamic properties of aqueous solutions of apolar molecules was the "iceberg" hypothesis of Frank and Evans [217], which states that the structure of water around apolar molecules is more ordered than the bulk water. This accounts for both the negative entropy change (increased ordering) and the negative enthalpy change (increase in degree of hydrogen bonding). The correlation functions and coordination numbers, explained in following sections when one adds different pairs of apolar molecules, and the dependence on temperature and pressure of these structural quantities can give information about the structural changes of water as well as apolar molecules.
In this work the internal energy was calculated under the assumption of pairwise interactions, namely Lennard-Jones and Coulombic interactions between the molecules present in the system under investigation. The simulation of the internal energy for different systems provided the investigation of the interactions of different systems with increasing temperature and increasing pressure. The enthalpy was calculated according to:

$$H = E + PV \tag{2.6}$$

where P is the pressure and V is the volume.
The heat capacity, a thermodynamic property that indicates the amount of broken hydrogen bonds and rearrangement of molecules with increasing temperature and increasing pressure, is given by:

$$C_p = \left(\frac{\partial H}{\partial T}\right)_P \tag{2.7}$$

The residual chemical potential of water and apolar molecules as well as its temperature and pressure dependences, which include energetic and entropic contributions and are characteristic properties for defining hydrophobic effects, is calculated according to the Widom method which is explained in detail in following sections. The theoretical aim of this work is to simulate and calculate the structural and thermodynamic properties by using as few approximations of statistical mechanics as possible in the simulations.
When the hydrophobic bonds are formed, water–apolar molecules interactions decrease in extent and this decrease should be accompanied by an energy loss according to Scheraga et al. [219, 221–223]. The enthalpy difference with increasing temperature is calculated according to:

$$\Delta H_{\text{hydro}} = H_{\text{w,a}} - H_{\text{w}} \tag{2.8}$$

ΔH_{hydro} is the difference in enthalpy, $H_{\text{w,a}}$ is the enthalpy of water/apolar system, and H_{w} is the pure water enthalpy under same conditions. The residual chemical potential difference of water with increasing temperature is calculated according to the following formula:

$$\Delta\mu_{\text{hydro}} = \mu_{\text{w,e}} - \mu_{\text{w}} \tag{2.9}$$

where $\Delta\mu_{\text{hydro}}$ is the difference in residual chemical potential, $\mu_{\text{w,e}}$ is the residual chemical potential of water in water/apolar system and μ_{w} belongs to pure liquid water chemical potential under same conditions.

2.2 Statistical thermodynamics

Statistical mechanics provides the connection between the microscopic states of a molecular system and its macroscopic properties. Statistical mechanics is based on the principle that thermodynamic properties are averages of microscopic properties, and it sets up a scheme for calculating these thermodynamic averages [92].

The techniques of statistical mechanics have been used in a wide variety of physical investigations. Statistical mechanics has been applied to gases, liquids, solutions, polymers, metals, spectroscopy, transport theory, the helix–coil transition of DNA, cell mebranes etc.

Thermodynamics provides connections between many properties, like mathematical relations between the experimental property of an macroscopic system in equilibrium, but does not supply information concerning the magnitude of any property. Thermodynamics does not need to recognize or rely upon the existence of atoms or molecules. Thermodynamics provides general relations without

the need of ever considering the ultimate constitution of matter, while statistical mechanics, on the other hand, assumes the existence of atoms and molecules to calculate and investigate thermodynamic properties from a molecular point of view.

Statistical mechanics deals with ensembles of members. An ensemble of members is defined to be a number of independent members in contact with the environment under some conditions [92]:

- The environment should be so large that the intensive properties are not affected by the interactions of the members.
- Every ensemble member presents a model of the system under consideration, and all members should be identical.
- The ensemble and environment should be isolated from the rest of the universe.
- The interactions which are possible between a member and the environment should be same for all members.

Within the statistical mechanics, several paths lead to the same procedure for calculating or simulating the thermodynamic properties. The two fundamental postulates for the paths of various lengths are:

- Postulate 1: The mechanical-thermodynamical value of a property in a system in equilibrium is given by the value belonging to the most probable distribution of ensemble members.
- Postulate 2: The most probable distribution of ensemble members among the possible states is the distribution for which the number of possible states of the ensemble and enviroment is a maximum.

A mechanical-thermodynamic property is a macroscopic quantity which has a defined value like pressure, volume, energy etc.

2.2.1 Ensembles

By Monte Carlo or Molecular Dynamics simulations one is able to generate information at the microscopic level and to convert microscopic information into macroscopic properties [91–94].

The microscopic mechanical state of the N particle system is defined by positions and momenta. This means that these positions and momenta can be regarded as coordinates in a phase space. Hence, a microscopic state is a point $\mathbf{\Gamma}$ in the phase space. On the other hand, a macroscopic state is defined through

macroscopic properties like pressure P, number of particles N and temperature T.

Systems treated by statistical mechanics can be classified according to the natures of the surfaces bounding the systems and the general displacement rules. The following systems have been studied widely:

- Systems surrounded by surfaces that do not permit energy or mass passage: microcanonical ensemble.
- Systems surrounded by surfaces that permit energy passage but not mass passage: canonical ensemble.
- Systems surrounded by surfaces that permit passage of energy and of mass: grandcanonical ensemble.

The isobaric-isothermal ensemble (N, P and T are constant) and the Gibbs ensemble are those ensembles which are used besides the classical ensembles in computer simulations [93, 94].

2.2.2 Ensemble averages

The methods of statistical mechanics have to include a procedure, for predicting, from the results of statistics, values of macroscopic mechanical quantities. This requirement is met by the following procedure [92]:

An ensemble is a collection of points in phase space. The probabilities of the microscopic states of a canonical ensemble with N particles are not all equal. The probability p_s of a microscopic state with the energy E_s is proportional to the Boltzmann factor:

$$p_\mathrm{s} \propto \exp\left(-\frac{E_\mathrm{s}}{k_\mathrm{B}T}\right) \tag{2.10}$$

k_B : Boltzmann constant

The points in phase space are distributed according to a probability density

$$\rho(\mathbf{\Gamma}) = \frac{1}{N}\exp\left(-\frac{E_\mathrm{pot}(\mathbf{\Gamma}) + E_\mathrm{kin}(\mathbf{\Gamma})}{k_\mathrm{B}T}\right) \tag{2.11}$$

The probability function is essentially in a non-normalized form and the partition function Q is acting as the normalizing factor to calculate the probability density $u(\mathbf{\Gamma})$.

$$u(\mathbf{\Gamma}) = \frac{\rho(\mathbf{\Gamma})}{Q} \text{ with } Q = \int \rho(\mathbf{\Gamma})\,\mathrm{d}\mathbf{\Gamma} \tag{2.12}$$

The ensemble average of a property a is calculated from this probability distribution in the following way:

$$\langle a \rangle_{\text{ens}} = \int a(\mathbf{\Gamma}) u(\mathbf{\Gamma}) \, \mathrm{d}\mathbf{\Gamma} \tag{2.13}$$

Because the energy is a sum of potential and kinetic energy, the phase space- and probability densities can be subdivided into two terms. The residual thermodynamic properties can be calculated by using the configurational term.

2.2.3 Ergodicity

The fundamental problem of classical statistical mechanics is known as the ergodic problem. The system, no matter how it is prepared, relaxes on a reasonable time scale towards a statistical equilibrium. The definition of equilibrium is that all macroscopic variables are constant in time.

Consider a random process described by a function $x(t)$. If one repeats the process for N times, one obtains the function $x(t, \alpha), \alpha = 1, ..., N$. The mathematical abstraction of this is to consider a family of functions $x(t, \alpha), \alpha$ may be discrete as well as continuous. If α is taken to be a random variable with a probability density $\rho(\alpha) d\alpha$, then $x(t, \alpha)$ is a stochastic process. Then, a stochastic process is a function of two variables t and α, where t is time and α is a random variable. More precisely, the random process $X(t)$ is described by a set of probability distributions. At any time, one can find the fraction of the total number of functions which have a value between x and $x + \mathrm{d}x$. This fraction, $w_1(x, t)\mathrm{d}x$ is called the first probability distribution.
$w_2(x_1, t_1; x_2, t_2)\mathrm{d}x_1\mathrm{d}x_2$ is the joint probability of finding X between x_1 and $x_1 + \mathrm{d}x_1$ at time t_1 and between x_2 and $x_2 + \mathrm{d}x_2$ at time t_2. This process can be continued for the 3th, 4th etc. probability distribution. If one knows the functions w_j for all j, knows all that can be known about the random process. The function w_j has to satisfy the following conditions:

- $w_n \geq 0$
- $w_n(x_1, t_1; x_2, t_2; \cdots; x_n, t_n)$ is a symmetric function in the set of (x_j, t_j).
- $w_k(x_1, t_1; \cdots; x_k, t_k) = \int \cdots \int w_n(x_1, t_1; \cdots; x_n, t_n)\mathrm{d}x_{k+1} \cdots \mathrm{d}x_n$.

The complete determination of the set of probability distributions given above is not feasible. Thus the time evolution of a large number of similarly prepared system has to be observed. Fortunately, there are several assumptions that can be made that greatly simplify matters. It has to be assumed that the random process is stationary in time. Thus the form of the probability distribution functions does not depend on the shift of the origin of the time. More precisely, the random process is stationary when the probability distributions of $|x(t, \alpha)|$ and $|x(t+\tau, \alpha)|$ are the same for any time period, τ.

For a stationary random process, the various probability distributions from the experimental observation of $x(t)$ for one system over a long period of time should be determined. This long-time record can be divided into pieces of length T, where T is much longer than the time periods occurring in the process, and these pieces may be treated as observations of different systems in an ensemble of similarly prepared systems. The underlying assumption here is called the the ergodic hypothesis. It states that for a stationary random process, a large number of observations made on a single system at N arbitrary instants of time have the same statistical properties as observing N arbitrarily chosen systems at the same time from an ensemble of similar systems.
When one deals with general random processes, there are two types of mean values. One is obtained by observations made on any systems at some fixed time t, ($\langle x \rangle$) and the other is the time average made on the system as a function of time, ($\hat{x}$). For a stationary random process, the averages yield the same result.

$$\hat{x} = \lim_{T \to \infty} \frac{1}{2T} \int_{-T}^{T} x(t) \mathrm{d}t \tag{2.14}$$

and

$$\langle x \rangle = \int_{-\infty}^{\infty} x w_1(x) \mathrm{d}x \tag{2.15}$$

and for a stationary random process:

$$\hat{x} = \langle x \rangle \tag{2.16}$$

according to the ergodic hypothesis.
For a large number of physical processes, it is assumed that the process is a Markov process. The time axis is divided into small intervals, δ. and t is defined as $t_j = j\delta$. When one introduces the conditional probability $\rho_n(x_n, t_n \mid x_{n-1}, t_{n-1})$, $t_0 < t_1 < \cdots < t_n$, that X lie in $(x_n, x_n + \mathrm{d}x_n)$ at time t_n given that $X(t_0) = x_0$, $X(t_1) = x_1$, etc. The Markov process can be defined as:

$$\rho_n(x_n, t_n \mid x_0, t_0; \cdots; x_{n-1}, t_{n-1}) = \rho(x_n, t_n \mid x_{n-1}, t_{n-1}) \tag{2.17}$$

The probability that the system is in the state n at time t_n depends upon its state directly preceding t_n and not upon the previous history of the process.

2.2.4 The Monte Carlo method

At the end of the Second World War, von Neumann, Ulam and Metropolis developed the Monte Carlo method to investigate the diffusion of neutrons in fissionable materials. Because of the use of random numbers in the calculation, the name Monte Carlo was chosen for this method.

The expression 'Monte Carlo method' is actually very general. Monte Carlo (MC) methods are stochastic techniques, meaning they are based on the use of random numbers and probability statistics to investigate problems. One can find Monte Carlo methods used in everything from economics to nuclear physics to regulating the flow of traffic.

Monte Carlo or molecular dynamics simulations involve the numerical determinations of the statistical thermodynamics and related structural, energetics and dynamic properties of atomic or molecular assemblies on a high speed digital computer. Applications to molecular systems range from the study of the motions of atoms or groups of atoms of a molecule or macromolecule under the influence of intramolecular energy functions to the exploration of structure and energetics of fluid phases such as liquid water based on intermolecular potential functions. The quantities determined in a typical Monte Carlo or Molecular Dynamics simulations include the average or mean configuration energy, various spatial distribution functions for equilibrium systems and time correlation functions for dynamical systems, along with detailed structural and energetic analyses.

The use of Monte Carlo methods to model physical problems allows us to examine more complex systems than we otherwise can. Solving equations which describe the interactions between two atoms is fairly simple; solving the same equations for thousands of atoms is impossible. With Monte Carlo methods, a large system can be sampled in a number of random configurations, and that data can be used to describe the system as a whole.

2.2.5 The Metropolis method

The so-called Metropolis Method was introduced by Metropolis in 1953 [95]. The configurations $\mathbf{\Gamma}_k$ are generated with the probability $\exp(E(\mathbf{\Gamma}_k)/(k_\mathrm{B}T))$. The mean value is calculated according to:

$$\langle a \rangle_\mathrm{MC} = \frac{1}{M} \sum_{k=1}^{M} a(\mathbf{\Gamma}_k) \tag{2.18}$$

whereby M is the number of Monte Carlo steps.

The average number of accepted trial moves that results in leaving a state has to be equal to the number of accepted trial moves from other states to this state. In equilibrium, the average number of accepted moves from a state to any other state is equally canceled by the number of reverse moves. The Markov chain process is used in this method [96]. The advantage of this theory is that the algorithm to generate the configurations permits also the reverse moves.

$$
\begin{aligned}
u_i p_{ij} &= u_j p_{ji} \qquad (2.19)\\
& u_i : \text{ configurational probability } i\\
& p_{ij} : \text{ transition probability from state } \quad i \quad \text{to state } \quad j
\end{aligned}
$$

If $B(i)$ is the number of states:

$$
p_{ij} = \begin{cases} 0 & \text{for } \mathbf{\Gamma}_j \notin B(i) \\ \frac{1}{Z} & \text{for } \mathbf{\Gamma}_j \in B(i) \text{ and } \rho(\mathbf{\Gamma}_j) \geq \rho(\mathbf{\Gamma}_i) \\ \frac{1}{Z}\frac{\rho(\mathbf{\Gamma}_j)}{\rho(\mathbf{\Gamma}_i)} & \text{for } \mathbf{\Gamma}_j \in B(i) \text{ and } \rho(\mathbf{\Gamma}_j) < \rho(\mathbf{\Gamma}_i) \end{cases} \qquad (2.20)
$$

The reversibility can be demonstrated as follows:

- When $\mathbf{\Gamma}_j \notin B(i)$ is, then $\mathbf{\Gamma}_i \notin B(j)$ and $p_{ij} = 0 = p_{ji}$.
- When $\rho(\mathbf{\Gamma}_j) \geq \rho(\mathbf{\Gamma}_i)$ then

$$
\begin{aligned}
p_{ij} &= \frac{1}{Z} \text{ and } p_{ji} = \frac{1}{Z}\frac{\rho(\mathbf{\Gamma}_i)}{\rho(\mathbf{\Gamma}_j)} = \frac{1}{Z}\frac{u_i}{u_j}\\
&\Rightarrow \quad u_j p_{ji} = u_i p_{ij}
\end{aligned}
$$

  and vice versa.

To accept a move with the probability $p = \frac{\rho(\mathbf{\Gamma}_j)}{\rho(\mathbf{\Gamma}_i)}$, one calculates p and compares this value with a random number $\xi \in [0, 1]$. If $p > \xi$, the move is accepted and otherwise rejected.

2.2.6 The isothermal–isobaric ensemble

The isobaric-isothermal ensemble is generally used in this work because most of the available experimental data have been measured under controlled temperature and controlled pressure.

The NPT ensemble Monte Carlo simulations were first described by Wood [97] in the context of a simulation work of two dimensional hard disks. However, the method used by Wood is not readily applicable to arbitrary continuous potential systems. McDonald applied NPT Monte Carlo simulations to a Lennard-Jones mixture with continuous intermolecular potential [82]. This method is now being used in simulations.

In the NPT ensemble Monte Carlo method, the volume is treated as an additional coordinate. The trial moves of volume consist of an attempted change of the volume from V to $V' = V + \Delta V$ where ΔV is randomly chosen and distributed uniformly over an interval $[-\Delta V_{\max}, +\Delta V_{\max}]$. According to the

Metropolis scheme, the volume move will be accepted or rejected with a probability that is explained in coming sections. Instead of random changes in volume, one can also attempt to use trial moves in the box length. Such trial moves are allowed as long as the symmetry of the underlying Markov chain is maintained.

The probability density for the isothermal-isobaric ensemble is proportional to $\exp(-(E+PV)/(k_{\mathrm{B}}T))$.

The summation over all possible volumes can be written as an integral [97]. For an atomic system:

$$Q_{\mathrm{NPT}} = \frac{1}{N!}\frac{1}{h^{3\mathrm{N}}}\frac{1}{V_o}\int\int \exp(-(E+PV)/k_{\mathrm{B}}T)\mathrm{d}\vec{r}^{N}\mathrm{d}\vec{p}^{N}\mathrm{d}V \tag{2.21}$$

2.2.7 Periodic boundary conditions and minimum image convention

By implementing the periodic boundary conditions, the problem of surface effects can be overcome [98]. An infinite lattice is formed by replicating the cubic box throughout the space. When one particle moves in the original box, its periodic image moves exactly in the same way and direction in each neighbouring box. Hence, when one molecule leaves the box, one of its images will enter through the opposite site.

The properties of a small, periodic system and the macroscopic system are same for a fluid of Lennard-Jones atoms. This feature depends on the range of the chosen intermolecular function and the phenomenon under investigation. When the chosen potential is long ranged, the particle and its image will interact substantially; this problem will be discussed below. Pratt et al. developed some theoretical methods to investigate the effects of periodic boundary conditions on equilibrium properties [99].

The common experience that can be found in the literature is that periodic boundary conditions have negligibly small effects on the thermodynamic properties and structural quantities of fluids.

The important part of Monte Carlo and molecular dynamics simulations is the calculation of the potential energy of a configuration. Hence we have to include all the interactions between a particle and every other particle in the box. But we have to include also the interactions between the particle and all its images placed in neighbouring boxes. We may restrict this summation of interactions by making an approximation that is called 'Minimum Image Convention' for a short-range potential energy function. Minimum Image Convention means that one constructs a box of the same size as the simulation box around a selected particle, and then considers only the interaction between this particle and the other particles in this box. The chosen particle interacts with all other particles whose centers are in this region i.e. with the closest images of other $N-1$ particles. This technique was first used by Metropolis et al. in 1953 [95].

2.2.8 The Ewald sum method

The Ewald sum method was developed by Ewald and Madelung between 1918 and 1921 for ionic crystal systems [100, 101]. The mathematical details of this method can be found in the literature [102, 103]. Its purpose is the computation of long-range contributions to the potential energy in a system which includes the periodic boundary conditions. When one investigates a system with charged particles assumed to be located in a cube with diameter L, and the periodic boundary conditions are included, the Ewald sum method is a method to calculate the long-range interactions. The Coulombic interactions energy formula will not be enough to calculate the long-range interactions, because it contains a poorly converging sum. This can be improved by the expression for charge density. The contribution to the electrostatic potential due to the point charges would decay as $1/r$, where r is the distance. It would not be a problem, if every particle i with charge q_i was surrounded by a diffuse charge distribution of the opposite sign, the total charge of the surrounding cloud would cancel the charge q_i. The Gaussian distribution for the screening charge is usually assumed.

For the Ewald sum method, it is assumed that each point charge is surrounded by two diffuse charge clouds of opposite sign. There are three contributions to the electrostatic potential; the one due to the point charge q_i, the second one due to (Gaussian) screening charge cloud with opposite charge, and the last one due to the compensating charge cloud with the point charge. In order to exclude coulombic self interactions, only the contribution due to compensating charge distribution should be included. Because the compensating charge distribution is not only a smoothy varying function, but is also periodic, this function can be presented by a Fourier series. In the end of the calculation, a correction for the inclusion of a spurious self interaction between the point charge and the compensating charge cloud is necessary.

The compensating charge distribution surrounding an ion i is a Gaussian, where $\sqrt{2/\alpha}$ is the width and α parameter characterizes the shape of the Gaussian charge distributions.

$$\rho_{\text{Gauss}}(r) = -q_i(\alpha/\pi)^{3/2}\exp(-\alpha r^2) \tag{2.22}$$

The charge density $\rho_1(r)$ at location r due to the presence of the Gaussian charge cloud is:

$$\rho_1(r) = \sum_{j=N}^{N}\sum_{n} q_j(\alpha/\pi)^{3/2}\exp\left[-\alpha|\mathbf{r}-(\mathbf{r}_j+\mathbf{n}L)|^2\right] \tag{2.23}$$

Fourier transforming the charge density ρ_1 yields:

$$\begin{aligned}
\rho_1(\mathbf{k}) &= \int_V \exp(-i\mathbf{k}\cdot\mathbf{r})\rho_1(\mathbf{r})\mathrm{dr} \qquad (2.24)\\
&= \int_V \exp(-i\mathbf{k}\cdot\mathbf{r}) \sum_{j=1}^{N}\sum_{n} q_j(\alpha/\pi)^{3/2}\exp\left[-\alpha|\mathbf{r}-(\mathbf{r}_j+\mathbf{n}L)|^2\right]\mathrm{dr}\\
&= \int_{\text{all space}} \exp(-i\mathbf{k}\cdot\mathbf{r}) \sum_{j=1}^{N} q_j(\alpha/\pi)^{3/2}\exp\left[-\alpha|\mathbf{r}-\mathbf{r}_j|^2\right]\mathrm{dr}\\
&= \int_{j=1}^{N} q_j \exp(-i\mathbf{k}\cdot\mathbf{r}_j)\exp(-k^2/4\alpha)
\end{aligned}$$

where $\mathbf{k} = (2\pi/L)\mathbf{l}$ with $\mathbf{l} = (l_x, l_y, l_z)$ are the lattice vectors in the Fourier space and r_i and r_j present the positions of particle i and j. If the above expression is inserted into the Poisson equation, $-\nabla^2\Phi_1(r) = 4\pi\rho_1(r)$, it yields:

$$\Phi_1(k) = \frac{4\pi}{k^2}\sum_{j=1}^{N}\exp(-i\mathbf{k}\mathbf{r}_j)(-\mathrm{k}^2/4\alpha) \qquad (2.25)$$

The above equation is for $\mathbf{k} \neq 0$, where $\Phi(r_i)$ is the electrostatic potential at the position of ion i. For the contribution of Φ_1 to the potential energy, one should first compute:

$$\begin{aligned}
\Phi_1(r) &= \frac{1}{V}\sum_{\mathbf{k}\neq 0}\Phi_1(\mathbf{k})\exp(\mathrm{i}\mathbf{k}\mathrm{r}) \qquad (2.26)\\
&= \sum_{\mathbf{k}\neq 0}\sum_{j=1}^{N}\frac{4\pi q_j}{k^2}\exp(i\mathbf{k}(\mathbf{r}-\mathbf{r_j}))\exp(-k^2/4\alpha)
\end{aligned}$$

The electrostatic potential term is:

$$\begin{aligned}
U &= \frac{1}{2}\sum_i q_i\Phi_1(r_i) \qquad (2.27)\\
&= \frac{1}{2}\sum_{k\neq 0}\sum_{j=1}^{N}\frac{4\pi q_i q_j}{Vk^2}\exp\left[i\mathbf{k}(\mathbf{r_i}-\mathbf{r_j})\right]\exp(-k^2/4\alpha)\\
&= \frac{1}{2V}\sum_{k\neq 0}\frac{4\pi}{\mathbf{k}^2\epsilon_0}|\rho(k)|^2\exp(ikr_i)
\end{aligned}$$

where $\rho(\mathbf{k}) \equiv \sum_{i=1}^{N} q_i\exp(i\mathbf{k}\mathbf{r_i})$. The contribution to the potential energy given above includes the term $(1/2)Q_i\Phi_{\text{self}}(r_i)$ because of the interaction between a

continuous Gaussian charge cloud and a point charge q_i located at the center of the Gaussian. This term should be corrected. By using the Poisson equation to compute the electrostatic potential due to the charge distribution, including the spherical symmetry of the Gaussian charge cloud and integrating, the following spurious contribution to the potential energy can be achieved:

$$\begin{aligned} U_{\text{self}} &= \frac{1}{2}\sum_{i=1}^{N} q_i \Phi_{\text{self}}(r_i) \\ &= (\alpha/\pi)^{1/2} \sum_{i=1}^{N} q_i^2 \end{aligned} \tag{2.28}$$

The spurious self interaction term has to be substracted from the sum of the real space and Fourier contributions to the Coulomb energy.

The electrostatic energy yielded by the point charges screened by the oppositely charged Gaussian has to be computed. By applying the error function to the Poisson equation used to compute the electrostatic potential and the spherical symmetry of the Gaussian charge cloud, the total contribution of the screened Coulomb interactions to the potential energy is given as [93]:

$$U_{\text{short-range}} = \frac{1}{2}\sum_{i\neq j}^{N} q_i q_j \text{erfc}(\sqrt{\alpha} r_{ij})/r_{ij} \tag{2.29}$$

the error function is defined as; $\text{erfc}(x) \equiv 1 - \text{erf}(x)$. The total electrostatic contribution to the potential energy becomes [93]:

$$\begin{aligned} U_{\text{Coulomb}} = \frac{1}{2V}\sum_{k\neq 0} \frac{4\pi}{k^2} |\rho(k)|^2 \exp(-k^2/4\alpha) \\ - (\alpha/\pi)^{1/2} \sum_{i=1}^{N} q_i^2 + \frac{1}{2}\sum_{i\neq j}^{N} \frac{q_i q_j \text{erfc}(\sqrt{\alpha} r_{ij})}{r_{ij}} \end{aligned} \tag{2.30}$$

The Ewald sum method can be used also for dipolar particle systems, to simulate the dielectric constant of a polar fluid etc.

So far, the calculation of the energy is performed in two parts in the Ewald summation method: the real space part and the Fourier space part.

For the energy, the real space cutoff error of the total energy deviation expression is:

$$\delta E_{\text{R}} = Q \left(\frac{r_{\text{c}}}{2L^3}\right)^{1/2} \frac{1}{(\alpha r_{\text{c}})}^{2} \exp\left(-\alpha^2 r_{\text{c}}^2\right) \tag{2.31}$$

and for the Fourier part, it looks like:

$$\delta E_{\mathrm{F}} = Q\frac{n_{\mathrm{c}}^{1/2}}{\alpha L^2}\frac{1}{\left(\pi n_{\mathrm{c}}/\alpha L\right)^2}\exp\left[-\left(\pi n_{\mathrm{c}}/\alpha L\right)^2\right] \tag{2.32}$$

where $Q = \sum_i q_i^2$

2.2.9 Correlation functions

The atom–atom pair correlation functions, $g(r)$, represent the number of atoms whose distance from a given atom in the fluid lies in the $(r, r+\delta r)$ interval. The correlation function is [94]:

$$\rho g(r) = \lim_{\delta r \to 0} \frac{\langle N_0(r, r+\delta r)\rangle_N}{4\pi r^2 \delta r} \tag{2.33}$$

where $\langle N_0(r, r+\delta r)\rangle$ is the ensemble average of the number of atoms in the spherical shell, δr is the thickness of the given shell and ρ is the density. The location of the first minimum of correlation functions defines the first hydration shell. The coordination number of atoms can be calculated by the following expression:

$$N_{\mathrm{c}} = 4\pi\rho \int_0^{r_{\min}} r^2 g(r)\mathrm{d}r \tag{2.34}$$

where N_{c} is the coordination number, and ρ is the density.

2.3 The free energy problem

Free energies are difficult to calculate, because they are related directly to the partition function, Q_{NPT}, which is a complete sum over states. The principal difficulty in the Monte Carlo simulations of free energy is the absence of a corresponding microscopic analogue, i.e., a function of configuration space variables to be averaged to obtain the required result. Nonetheless, knowledge of free energy is a key quantity for understanding molecular phenomena, such as hydration, solvation, hydrophobic interactions, conformational transitions in proteins and other macromolecules, phase transitions etc.

Formally, we may write expressions allowing us to calculate the free energy, but these typically involve averages of properties where the most significant contributions come from phase space regions where the sampling is poorest.

Diverse problems in structural and reaction chemistry of molecules in solution, such as solvation potentials, solvent effects on stability, the effect of solvent on chemical kinetics and mechanism via activated complex theory etc. also require a particular knowledge of the configurational free energy, which in principle directly follows from the statistical thermodynamic partition function for the system.

The configurational free energy is:

$$A = -k_{\mathrm{B}}T \ln\left(\frac{Z_{\mathrm{N}}}{V^{\mathrm{N}}}\right) \tag{2.35}$$

The determination of mean energy via simulation involves essentially calculating the area under the curve $E_{\mathrm{N}}P(E_{\mathrm{N}})$ or $E_{\mathrm{N}}\exp(-E_{\mathrm{N}}/k_{\mathrm{B}}T)$ by generating various configurations of the system and calculating their respective energies and probabilities. Only a narrow range of E_N values contributes significantly to the integrand, since the region in which E_{N} or $\exp(-E_{\mathrm{N}}/k_{\mathrm{B}}T)$ are simultaneously large is limited. A random selection of configurations in a simulation is thus an inefficient approach to the numerical determination of mean energy, since an extraordinary amount of time would be spent sampling configurations which make relatively insignificant contributions to the mean energy integrand. This problem in Monte Carlo theory was taken up by Metropolis et al. [152] who devised an importance sampling scheme which is now followed in essentially all Monte Carlo studies of fluids. The Metropolis method is a Markov walk through configuration space, sampling states of the system with a frequency proportional to the Boltzmann factor. The evaluation of mean energy reduces to the summation:

$$\sum_{j=1}^{n} E_{\mathrm{N}}(R_j)/nR_j \in M \tag{2.36}$$

where the n configurations R_j are chosen by the Metropolis method (M). Convergence studies indicate that the Metropolis method makes mean energy determinations feasible at presently accessible sampling rates. Other properties of the system computed in parallel with mean energy each found to have their own profile of convergence, and in general structural properties and simple average quantities such as mean energy converge more rapidly than the fluctuation properties like the heat capacity [153–155].

An analogous consideration can be made for the free energy. The ensemble average expression for the excess free energy yields,

$$A = k_{\mathrm{B}}T \ln \langle \exp[E_N/k_{\mathrm{B}}T] \rangle \tag{2.37}$$

expanding the exponential in powers of E_N and rearranging terms, it can be shown that,

$$A = k_{\mathrm{B}}T \ln \frac{[1 + \frac{U}{k_{\mathrm{B}}T} + (\frac{U}{2k_{\mathrm{B}}T})^2 + \frac{C_v'}{2k_{\mathrm{B}}} + \frac{<E_N^3>}{(k_{\mathrm{B}}T^3)} + ...]}{V^N} \tag{2.38}$$

Thus the convergence problem in free energy is equivalent to the problem of determining ensemble averages of the mean energy (first moment) and higher moments of energy distribution. This indicates that a significant increase in

sampling would be required to achieve convergence in free energy relative to mean energy in a simulation.

A broader range of sampling could be accomplished by a Monte Carlo approach, but in practice the configuration space of molecules is so immense that convergence for the partition functions integral cannot reasonably be expected. Metropolis sampling, concentrated in regions where $E_N \exp(-E_N/k_\mathrm{B}T)$ is large, is optimal for internal energy, but would not sample broadly enough to provide accurate estimates of the partition function and the free energy. Thus we are left with no viable means of the calculation of free energy by the numerical methods for molecular systems of interest and with the indication that an extent of sampling significantly beyond that suitable for mean energy determinations must be part of the free energy simulations.

The chemical potential is an important property for the study of hydrophobic interactions. There exist several techniques for measuring the chemical potential in a single Monte Carlo simulation. On closer inspection, what we measure is not the chemical potential itself but the residual chemical potential, the difference between the chemical potential and that of an ideal gas under same conditions. To simulate dense liquids and calculate their chemical potential, much effort has gone into the chemical potential method development and a number of methods have been proposed. Examples of these are: thermodynamic integration [136–139], particle insertion [135,140], perturbation methods [137,141–143], multistage sampling [144], umbrella sampling [145–147], acceptance ratio method [148,149], expanded ensemble method [150], etc.

No single method for free energy simulations can be considered as clearly superior to others and the choice depends on the system under consideration. One limitation of the umbrella sampling is that the more the sampling is to be extended, the larger will be the range of the modification of the energy, making the calculation of $\langle \exp(E_\mathrm{w}/k_\mathrm{B}T) \rangle_\mathrm{w}$ (where E_w is the modification of the energy that serves to extend the sampling), prine to roundoff errors [160]. The more complex the parameters chosen in the umbrella sampling simulation, the more difficult is the determination of an efficient modification of the energy.

2.3.1 Widom method

A general method for calculating the chemical potential μ of a species in a fluid or in a mixture is the so called Widom method [135]. The definition of the chemical potential μ_a of a species a is:

$$\begin{aligned} \mu_{\mathrm{a}} &= \left(\frac{\partial G}{\partial N_{\mathrm{a}}}\right)_{\mathrm{NPT}} \\ &= \left(\frac{\partial F}{\partial N_{\mathrm{a}}}\right)_{\mathrm{NVT}} \\ &= -T\left(\frac{\partial S}{\partial N_{\mathrm{a}}}\right)_{\mathrm{NVE}} \end{aligned} \tag{2.39}$$

where G, F, and S are the Gibbs free energy, Helmholtz free energy and the entropy, respectively. When we assume that we deal with a system of N particles in a cubic volume with diameter L and volume $V = L^3$ at constant temperature and pressure, the Gibbs free energy is given by:

$$G = -k_{\mathrm{B}}T \ln\left(\int \frac{V^N \exp\left(-\beta PV\right)}{\Lambda^{dN} N!}\mathrm{d}V \int \exp\left(-\beta U\left(s^N; V\right)\right)\mathrm{d}s^N\right) \tag{2.40}$$

in which the scaled coordinates $s = r/L$ are introduced. $U(s^N; L)$ indicates that U depends on the real rather than scaled distances between particles.

To evaluate $\mu = (\partial G/\partial N)_{\mathrm{P}T}$, the expression $\mu = G(N+1, P, T) - G(N, P, T)$ is evaluated

$$\mu = -k_{\mathrm{B}}T \ln\left\langle \frac{V}{\Lambda^d (N+1)} \int \exp\left(-\beta \triangle U\right)\mathrm{d}s_{N+1}\right\rangle \tag{2.41}$$

$$\begin{aligned} &= -k_{\mathrm{B}}T \ln\left(k_{\mathrm{B}}T/P\Lambda^d\right) - k_{\mathrm{B}}T \ln\left\langle \frac{PV}{(N+1)k_{\mathrm{B}}T} \int \exp\left(-\beta \triangle U\right)\mathrm{d}s_{N+1}\right\rangle \\ &= \mu_{\mathrm{ideal}} + \mu_{\mathrm{excess}}(P) \end{aligned} \tag{2.42}$$

The Widom method requires the addition of a particle to the system. However, in dense systems it can be applied only to small molecules.

2.3.2 Particle deletion scheme

The inverse Widom method is based on the comparison between the free energies of a system with N particles and that with $N-1$ particles [28, 29]. Theodorou et al. presented the calculation of the chemical potential by using the particle deletion scheme in 1999 [161]. They presented a new formulation of the chemical potential based on the removal of a test particle (inverse Widom) scheme. The particle deletion scheme method introduces an intermediate stage in the calculation of chemical potential where the removed test particle is replaced by a hard sphere. Because the $N-1$ molecules in the system can never occupy the remaining hole, this produces a bias to the simulation. To remove this bias, Theodorou

et al. measured the difference between a N- and $N-1$- particle system by calculating the accessible volume for inserting a hard sphere into the system. The Gibbs free energy is defined as:

$$G(N,P,T) = -\frac{1}{\beta}\ln\left(Q(N,P,T)\right) \tag{2.43}$$

The chemical potential of the system can be calculated according:

$$\begin{aligned}\beta\mu &= \beta\left(\frac{\partial G}{\partial N}\right)_{P,T} \\ &= \beta\mu^{\mathrm{ig}} - \ln\left(\left\langle\frac{1}{V}\right\rangle\frac{Z(N,P,T)}{Z(N-1,P,T)}\right)\end{aligned} \tag{2.44}$$

where $\beta\mu^{\mathrm{ig}}$ represents the chemical potential of an ideal gas under the same conditions. The ratio of the configurational integrals can be transformed according to:

$$\begin{aligned}\frac{Z(N,P,T)}{Z(N-1,P,T)} &= \frac{\int\exp\left(-\beta PV\right)V^N\mathrm{d}V\int\exp\left(-\beta U_N\left(s_1\ldots s_N\right)\right)\mathrm{d}^3s_1\ldots s_N}{\int\exp\left(-\beta PV\right)V^N\mathrm{d}V\int\prod_{i=1}^{N-1}\bar{H}_{\left(s_{i,N}\right)}\frac{\exp\left(-\beta U_{N-1}\left(s_1\ldots s_{N-1}\right)\right)}{V}\mathrm{d}^3s_1\ldots\mathrm{d}^3s_N} \\ &\times\frac{\int\exp\left(-\beta PV\right)V^N\mathrm{d}V\int\prod_{i=1}^{N-1}\bar{H}\left(s_{i,N}\right)\frac{\exp\left(-\beta U_{N-1}\left(s_1\ldots s_N\right)\right)}{V}\mathrm{d}^3s_1\ldots\mathrm{d}^3s_N}{\int\exp\left(-\beta PV\right)V^N\mathrm{d}V\int\frac{\exp\left(-\beta U_{N-1}\left(s_1\ldots s_{N-1}\right)\right)}{V}\mathrm{d}^3s_1\ldots\mathrm{d}^3s_N} \\ &= \frac{1}{\frac{\int\exp(-\beta PV)V^N\mathrm{d}V\int\prod_{i=1}^{N-1}\bar{H}\left(s_{i,N}\right)\frac{\exp\left(-\beta U_{N-1}\left(s_1\ldots s_{N-1}\right)\right)}{V}\mathrm{d}^3s_1\ldots\mathrm{d}^3s_N}{\int\exp(-\beta PV)V^N\mathrm{d}V\int\exp(-\beta U_N(s_1\ldots s_N))\mathrm{d}^3s_1\ldots\mathrm{d}^3s_N}} \\ &\times\frac{\int\exp\left(-\beta PV\right)V^{N-1}\mathrm{d}V}{\int\exp\left(-\beta PV\right)V^{N-1}\mathrm{d}V} \\ &\times\frac{\int\prod_{i=1}N-1\bar{H}\left(s_{i,N}\right)\exp\left(-\beta U_{N-1}\left(s_1\ldots s_{N-1}\right)\right)\mathrm{d}^3s_1\ldots\mathrm{d}^3s_N}{\int\exp\left(-\beta U_{N-1}\left(s_1\ldots s_{N-1}\right)\right)\mathrm{d}^3s_1\ldots\mathrm{d}^3s_N} \\ &= \frac{\left\langle\prod_{i=1}^{N-1}H\left(r_{i,N}\right)\right\rangle_{N-1,P,T}}{\left\langle\prod_{i=1}^{N-1}H\left(r_{i,N}\right)\frac{\exp(\beta U_N(r_1\ldots r_N))}{V}\right\rangle_{\mathrm{N,P,T}}}\end{aligned} \tag{2.45}$$

Here $\bar{H}\left(s_{i,N}\right)$ denotes the Heaviside step function,

$$\bar{H}\left(s_{i,N}\right) = \begin{cases} 0 & \text{for } \mid s_i - s_N \mid < s_{\mathrm{core}}(\beta,P) \\ 1 & \text{for } \mid s_i - s_N \mid \geq s_{\mathrm{core}}(\beta,P)\end{cases} \quad \text{for } i = 1,\ldots,N-1 \tag{2.46}$$

The hard core diameter (s_{core}) that is in reduced units is chosen arbitrarily.

The excess chemical potential μ^{ex} can be formulated as:

$$\begin{aligned} \beta\mu^{\text{ex}} &= \beta\mu - \beta\mu^{\text{ig}} \\ &= -\ln\left[\left\langle\frac{1}{V}\right\rangle_{\text{N},P,T}\frac{\left\langle\prod_{i=1}^{N-1}H\left(r_{i;N}\right)\right\rangle_{\text{N}-1,P,T}}{\left\langle\frac{\prod_{i=1}^{N-1}H\left(r_{i,N}\right)\exp(\beta U^{N}(r_1\ldots r_N))}{V}\right\rangle_{\text{N},P,T}}\right] \end{aligned} \tag{2.47}$$

The term $\left\langle\prod_{i=1}^{N-1}H\left(r_{i,N}\right)\right\rangle$ presents the accessible volume fraction for a molecule with a diameter of s_{core} that is interacting through the repulsive potential of a hard sphere.

Chapter 3

Molecular Models

3.1 TIP5P water model

The structure of water has been discussed in the literature ever since scientists were concerned with the peculiar properties of water and aqueous solutions. Much effort has gone into the development of intermolecular potential functions for the water dimer. Some of them are; SPC [176], SPC/E [174], ST2 [170], SCF [169], CI [166], BF [171], PM [164] and TIPS [163, 165]. Each potential function has its advantages and disadvantages. The TIP3P and TIP4P models [172,173] for water dimer were presented in 1983. The SPC, SPC/E, TIP3P and TIP4P models have been the most widely used models for the water dimer for a long time.

One of the best known experimental properties of liquid water is the density as a function of temperature and pressure. Liquid water exhibits density of maximum at about 4 °C [177–179]. None of the water models written above can reproduce the density behavior in the temperature range of interest [184,186–188]. The density behaviour with increasing pressure of the earlier calculations was also questionable [187–189, 191, 192].

The ST2 model yields a density maximum at about 27 and 40 °C and SPC/E gives a maximum density at about -38 °C. TIP4P yields a maximum density near -13 °C. Although the phenomenon of a maximum density exists for some water models, the lack of the quantitative agreement is evident, and the shape of the density function with increasing temperature could not be well reproduced.

Some attempts have been made to improve the potential function for the water dimer by addition of bond flexibility [196–198], variable electronic degrees of freedom [192,197], etc. However, the most complex models do not describe the dependence of the dipole moment change on water structure [199, 200].

Jorgensen et al. presented the TIP5P model of water in the beginning of 2000 [162]. The average error in the density between -37.5 °C and 62.5 °C at 1 bar pressure is only 0.006 g/cm^3. These authors optimized the parameters and also the negative charge positions along the lone-pair directions by Monte Carlo

calculations. They did also foundthat the TIP5P model represents the density maximum near 4 °C at 1 bar pressure [162]. The TIP5P model represents the pressure dependence of the thermodynamic properties well. The density of water at 25 °C was reproduced with an average error of about 2% between 1 and 10^4 bar. The expected shift of the temperature of maximum density to lower values with increasing pressure could be also obtained by using TIP5P model of water dimer.
The TIP5P model for water has four tetrahedrally arranged coulombic interaction sites, two of them belonging to hydrogens and the other two belonging to the lone electron pairs.
The parameters of TIP5P are presented in Table 3.1:

Table 3.1: Parameters for TIP5P water model

q_{H} (e)	σ_{o} ()	ε_{o} (kJ/mol)	r_{OH} ()	θ_{HOH} (∘)	r_{OL} ()	θ_{LOL} (∘)
0.241	3.21	0.6694	0.9572	104.52	0.70	109.47

3.2 Optimized TIP5P water model

The electronic wave function of a diatomic molecule is a function of the internuclear distance. In contrast to this, the electronic wave function of a polyatomic molecule depends on several parameters—the bond distances, bond angles, and dihedral angles of rotation about single bonds that define the molecular conformation. A theoretical treatment of a polyatomic molecule involves calculation of the electronic wave function for a range of each of these diameters; the equilibrium bond distances and angles are then found as those values that minimize the electronic energy [**?**].

To optimize the TIP5P model of water that is mentioned above, the calculation began with the choice of a basis set.

For diatomic molecules, the basis functions are generally taken as atomic orbitals. Each atomic orbital can be represented as a linear combination of one or more Slater-type orbitals. An Slater-type orbital (STO) centered an atom a has the form $Nr_a^{n-1}e^{-\zeta r_a}Y_l^m(\theta_a, \Phi_a)$. For nonlinear molecules the Slater-type orbital form with Y_l^m (spherical harmonic) is replaced by $(Y_l^{m*} \pm Y_l^m)/2^{1/2}$. Each molecular orbital is expressed as $\Phi_i = \sum_r c_{ri}\chi_r$ where χ_r is the Slater-type orbital basis function [?].

For polyatomic molecules, in this case water, the LC-STO method uses STOs centered on each of the atoms. The one-center expansion (OCE) method takes each molecular orbital (MO) as a linear combination of STOs, all of which are centered at the same point in the space. The OCE method is especially applicable to alkanes, because most of the electron propbability density is located near to

the carbon atoms and the hydrogen atoms introduce only small cusps into the wave function.

In 1950 Boys proposed the use of Gaussian-type functions (GTF) to simplify the molecular integral evaluation. A Cartesian Gaussian centered on an atom a is defined as:

$$g_{ijk} = N x_a^i y_a^i z_a^k e^{-\alpha r_a^2} \tag{3.1}$$

N is the normalization constant, i, j and k are positive integers and α is a positive orbital exponent. In general, linear combinations of Cartesian Gaussians can be formed:

$$N r_a^l e^{-\alpha r_a^2} (Y_l^{m*} \pm Y_l^m)/2^{1/2} \tag{3.2}$$

To obtain an accurate representation of an atomic orbital, a linear combination of several Gaussians must be used. The LC-GTF SCF MO calculation involves the evaluation of more integrals than the LC-STO SCF MO calculation due to the number of two-electron integrals is proportional to the fourth power of the number of basis functions. However, Gaussian integral evaluation takes much less CPU time than Slater integral evaluation, since the product of two Gaussian functions, centered at two different points is equal to a single Gaussian centered at a third point.

A minimal basis set consists of one STO for each inner-shell and valence-shell atomic orbital (AO) of each atom. A double-zeta (DZ) basis set is obtained by replacing each STO of a minimal basis set by two STOs which differ in their orbital exponents ζ. A split-valence (SV) basis set uses two STOs for each valence AO but only one STO for each inner-shell AO [?].
Instead of using the Gaussian functions as basis functions, each basis function can be taken as a linear combination of a small number of Gaussians, according to:

$$\chi_r = \sum_a d_{ur} g_u \tag{3.3}$$

g_u's are Cartesian Gaussians centered on the same atom and having the same i, j ank k values as one another, but different α's, d_{ur} are constants that are held fixed during the calculation. χ_r is called a constracted Gaussian-type function (CGTF) and the g_u is called primitive Gaussian.

The 3-21G and 4-31G basis sets are the commonly used split-valence sets of CGTFs. In the 3-21G basis set, each inner-shell AO is presented by a single CGTF which is a linear combination of primitive Gaussians. There are two basis functions, one of which is a CGTF that is a linear combination of two Gaussian primitives and one that is a single diffuse Gaussian. The 4-31G set uses four primitives in each inner-shell CGTF and represents each valence-shell AO by one CGTF with three primitives and one Gaussian with one primitive.

The 6-31G* basis set is a split-valence set with some polarization functions added. It uses a linear combination of six primitives in each inner-shell AO and adds a single set of six d-type Cartesian Gaussian polarization functions for each nonhydrogen atom [?].

The 6-31G* basis set was developed by Pople et al. and is available in the widely used ab-initio program Gaussian [8].

The 6-31G* basis set and MP2 (Moller–Plesset) method [?] have been used to optimize the TIP5P model of water. The calculated total electronic energy of the optimized TIP5P model of water was about -76.4 E_{h} (Hartree energy unit) whereas the experimental value is -76.48 E_{h} [7]. The calculated θ_{HOH} is 104.5° agrees with the experimental one; that of Jorgensen et al. is 104.52°. Also the thermodynamic properties simulated with the optimized TIP5P model are practically identical with the experimental for liquid water that are presented in the following sections.

3.3 Apolar molecule models

In this work, OPLS models (optimized intermolecular potential functions) [183] have been chosen for methane and ethane. To develop the OPLS models that yield accurate structural and thermodynamic properties, Jorgensen et al. [183] carried out Monte Carlo simulations for 15 hydrocarbon liquids; methane, ethane, propane, n-butane, isobutane, n-pentane, neopentane, cyclopentane, n-hexane, 1-butene etc.

The parameters were obtained by fitting to the gas phase dimer data and tested in Monte Carlo simulations [204, 210]. For these functions, molecules are presented by interaction sites located on their nuclei. Hydrogens on carbon atoms are implicit while those on heteroatoms are retained [211]. The use of implicit hydrogens is computationally cheaper. The hydrocarbons are all considered neutral. This was also supported by ab initio calculations on alkanes [205] and also by the lack of dipole moment for gauche n-butane [206]. The methane parameters were adapted from the work of Verlet and Weis [207] and these parameters were optimized again by Jorgensen et al. by Monte Carlo simulations.

Four different methyl group parameters were defined depending on the branching. For nonbranched molecules, the methyl parameters were optimized separately in Monte Carlo simulations of ethane.

The thermodynamic results with these models are in very good agreement with the experimental data and revealed also the trends for isomeric series [183]. The radial distribution functions were obtained by X-ray diffraction for methane, ethane and neopentane [208, 209]. For methane, the experimentally determined locations and heights of the first two peaks are; 4.1 , 2.7 and 7.6 , 1.3, while the simulation results were 4.1 , 2.9 and 7.8 , 1.3.

The parameters for methane, ethane and the Lennard-Jones parameters for

xenon are presented at Table 3.2

Table 3.2: OPLS parameters.

	σ ()	ε (kJ/mol)
Methane	3.730	1.2301
Ethane	3.775	0.8661
Xenon	4.1	1.7992

3.4 Lorentz–Berthelot mixing rules

For the interactions between unlike atoms A and B in different molecules the Lorentz–Berthelot mixing rules were used in this work. The σ and ε cross values are given by [94]

$$\sigma_{AB} = \frac{1}{2}\left[\sigma_{AA} + \sigma_{BB}\right] \tag{3.4}$$

and

$$\varepsilon_{AB} = \left[\varepsilon_{AA}\varepsilon_{BB}\right]^{1/2} \tag{3.5}$$

Chapter 4

Simulation Details

All 216 water molecule and apolar molecule coordinates were generated with the program STARTCONFIG. This program subsequently places 8^3 molecules on a face centered cubic lattice. The molecules are rotated, and by increasing the pressure the desired density is reached.

In this work, 3 programs (HYDRO, EXPERT and THEO) were coded in C to investigate the hydrophobic interactions of 2 methane, 2 ethane or 2 xenon in 216 water molecules, as well as the hydration of a single xenon atom in 216 water molecules.

Because the chemical potential is an important quantity for characterizing hydrophobic interactions, 3 different methods for its calculation were coded and the obtained results were compared.

4.1 HYDRO and EXPERT

HYDRO is an NPT ensemble Monte Carlo program. All the thermodynamic and structural values are initialized during the program run. The program uses periodic boundary conditions and the minimum image convention. Metropolis acceptance criteria are used to accept and reject the generated configurations. The particle energy, including Lennard-Jones and Coulombic interactions are calculated. The long range interactions are treated by using the Ewald sum method. The random number generator ran2.c is used, which was coded by M. Hloucha [122].

The translation steps for each Cartesian coordinate are calculated according to $(2\xi - 1)\Delta X_{\max}$, where ξ is a random number in the range $[0; 1]$ and $\Delta X_{\max}$ is the maximum displacement. The rotational steps are calculated according to $(2\xi - 1)\Delta r_{\max}$ where $\Delta r_{\max}$ is the maximum rotational angle. The volume change steps are calculated according to $(2\xi - 1)\Delta V$, where the ΔV value was chosen before the simulation.

By using HYDRO the correlation functions, potential energy, enthalpy, resid-

ual chemical potential of water and residual chemical potential of apolar molecules according to the Widom insertion method are calculated [135].

Simulation runs for the study of hydrophobic effects were made with 216 water molecules and 2 apolar molecules consisting of 2.000.000 equilibration moves followed by up to 7 million production moves. The statistical uncertainty was calculated by using block average analysis, where each run was subdivided into 100 blocks.

The EXPERT program is a NVT ensemble Monte Carlo program. All the structural and thermodynamic properties except the residual chemical potential are simulated as by HYDRO. The residual chemical potential is calculated by the Widom deletion method [28], where a particle is removed from the system and the difference in potential energy is calculated.

Because the remaining hole generates a bias in sampling, the equilibration time for this program was longer, and it took usually 3.5 million equilibration moves followed by 8 million production moves for pure liquid water to generate the desired thermodynamic data.

4.2 The program THEO

The program THEO (named according to Theodorou) is an NPT ensemble Monte Carlo program. All the structural and thermodynamic properties except the residual chemical potential are simulated as by HYDRO and EXPERT.

The particle deletion scheme method [161] was coded to simulate the chemical potential. As explained before, a rigorous application of the Widom deletion scheme requires two separate runs, one with $N-1$ molecules, where the accessible volume for the hard sphere particle is calculated (the accessible volume part of the chemical potential), and one with N molecules, where the energy part of the chemical potential is calculated.

The size of the hard core, which is utilized in an intermediate step of the method, is very important for the CPU time as well as the accuracy of the results. The rule presented by Theodorou et al [161] is that the hard core diameter should not be smaller than the minimum distance between two molecules interacting in the system. The clear optimum value for the hard core diameter is 0.9 . Similar calculations were performed by Theodorou et al. [161] and they obtained 0.95 for the hard core diameter. The equilibration period took 2 million moves followed by 7 million production moves for all pure liquid water simulations at different temperatures. Statistical uncertainty is calculated by block average analysis, where each run is subdivided into 100 blocks, so that the variance is calculated from the expression:

$$\delta\mu^{\mathrm{ex}} = \left[\left(\delta\mu^{ex}_{\mathrm{energy}}\right)^2 + \left(\delta\mu^{ex}_{\mathrm{volume}}\right)^2\right]^{1/2} \tag{4.1}$$

By using THEO one is able to simulate the correlation functions, potential energy, enthalpy, and the residual chemical potential according to particle deletion scheme method.

4.3 Cutoff values

The cutoff values used to simulate all four systems by using HYDRO, EXPERT or THEO are presented in Table 4.1.

Table 4.1: Cutoff radius

System	Cutoff Radius ()
pure water	4.5
water-methane	5.0
water-ethane	6.0
water-xenon	6.5

4.4 Required CPU time

The CPU time required by each of the three methods for estimating (Widom insertion method, Widom deletion method and particle deletion scheme) the chemical potential of 216 water molecules at different temperatures are presented in Table 4.2

T (K)	HYDRO	THEO	EXPERT
298	1	0.83	0.67
303	1	0.85	0.66
308	1	0.85	0.70
313	1	0.91	0.75
318	1	0.89	0.77

Table 4.2: Comparison of CPU times of the MC simulation programs.

The CPU times for EXPERT and THEO are given as fractions of the CPU time required by HYDRO under same conditions. The CPU time of EXPERT, where the Widom deletion method is, is less than the CPU time required by the program THEO (particle deletion scheme).

The results for the residual chemical potential for TIP5P water are presented in the following sections.

Chapter 5

Results

The structural and thermodynamic properties with increasing temperature or increasing pressure of the systems presented in Table 5.1 have been studied to investigate hydrophobic interactions.

Table 5.1: Systems investigated in this work.

system	number of water molecules	number of apolar molecules
water–methane	216	2
water–ethane	216	2
water–xenon	216	2

The notion "iceberg" formation [217] around apolar molecules in water, introduced by Frank and Evans, has become a central feature of descriptions of hydrophobic interactions. According to the "iceberg" formation, water molecules in the first layer around apolar molecules are more ordered and participate more in hydrogen bonding than bulk water as explained before. This may explain the dissolution of rare gases and hydrocarbons in water [89]. One can find in the literature several works about the proportionality of the number of water molecules in the surface layer to the free energy, enthalpy and entropy of the solution [89,219]. Roughly linear correlations have been reported for these quantities [180, 182] by using the solute cavity surface area calculations, solute volume, number of carbon atoms, or number of hydrogen atoms in the solute. The number of water molecules in the first hydration shell is also a key parameter in theoretical treatments of aqueous solutions including the significant structure theory of Eyring and co–workers [181] and Nemethy–Scheraga [219] model that is explained in detail in following sections. However, the methods for estimating the number of water molecules in the first layer [219] or cavity surface areas [180] are crude and ambiguous, while the correlations with number of hydrogens [185] have been criticized for having a limited theoretical basis [226]. In the literature one can find also several discussions about the temperature dependence of the structural properties. In this work, both the temperature and pressure dependence of the

structural and thermodynamic properties of the systems have been investigated and a novel approach for hydrophobic effects is presented.

5.1 Structural properties

5.2 Temperature dependence of the structural properties

The temperature dependence of the correlation functions and coordination numbers of the pure water, water–methane, water–ethane and water–xenon systems has been investigated at a pressure of 1 bar.

The structure of water was experimentally investigated by Soper and Phillips [193] by neutron scattering experiments at 298 K. The simulated correlation functions in this work are in good agreement with these data.

Figures 5.1– 5.3 show the oxygen–oxygen, oxygen–hydrogen and hydrogen–hydrogen pair correlation functions of pure liquid water with increasing temperature between 298 and 318 K. At 298 K the computed first peak in g_{OO} of pure liquid water is located at about 2.85 Å and has a height of 3.0, while the experimental values are 2.875 Å and 3.092 [193]. The second maximum in g_{OO} of pure liquid water is located at about 4.5 Å according to optimized TIP5P and has a height of almost 1.25, whereas the experimental values are 4.525 Å and 1.136 [193].

The g_{OH} and g_{HH} also reveal decreasing structure with increasing temperature, though the effect is less pronounced than for g_{OO}. At 298 K the computed first peak in g_{OH} of pure liquid water is located at about 1.9 Å and has a height of 1.3, whereas the experimental values are 1.85 Å and 1.385 [193]. The second peak in g_{OH} is located at about 3.15 Å and has a height of 1.85, and the experimental values are 3.35 Å and 1.6. The first peak in g_{HH} at 298 K of pure liquid water is located at 2.45 Å and has a height of 1.8, whereas the experimental values are 2.45 and 1.26. The second maximum in g_{HH} is located at 3.9 Å and has a height of 1.4, the experimental values are 3.85 and 1.2 [193].

In order to detect possible structural stabilization due to the introduction of two nonpolar molecules, the temperature dependence of the water–methane, water–ethane and water–xenon system correlation functions was investigated between 298 and 333 K for water–methane and water–ethane, and between 298 and 338 K for the water–xenon system at a pressure of 1 bar.

The oxygen–oxygen, oxygen–hydrogen and hydrogen–hydrogen correlation functions of these three systems with increasing temperature can be found in Appendix A. They show almost the same structural change with increasing temperature as those of pure liquid water.

The height of the first maximum of g_{OH} at 298 K, which can be regarded as a measure of the degree of hydrogen bonding, is as follows.

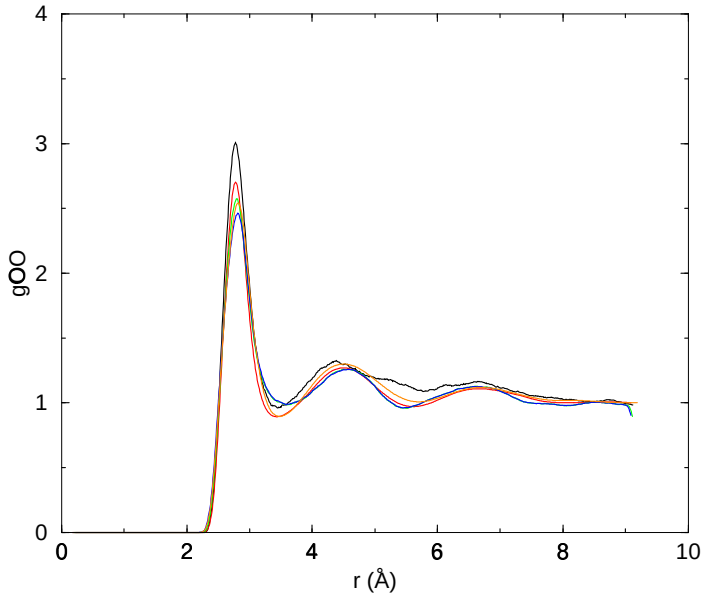

Figure 5.1: Temperature dependence of g_{OO} of pure water. 298 K black, 303 K red, 308 K green, 313 K blue, 318 K magenta

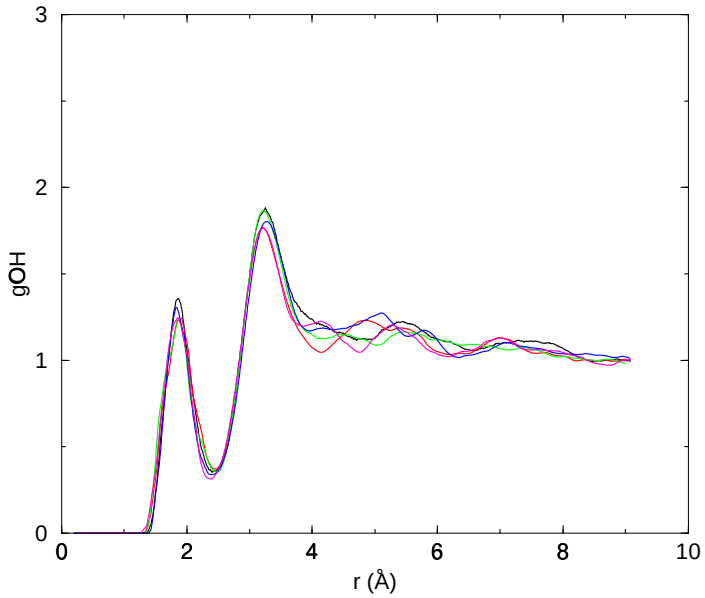

Figure 5.2: Temperature dependence of g_{OH} of pure water. 298 K black, 303 K red, 308 K green, 313 K blue, 318 K magenta

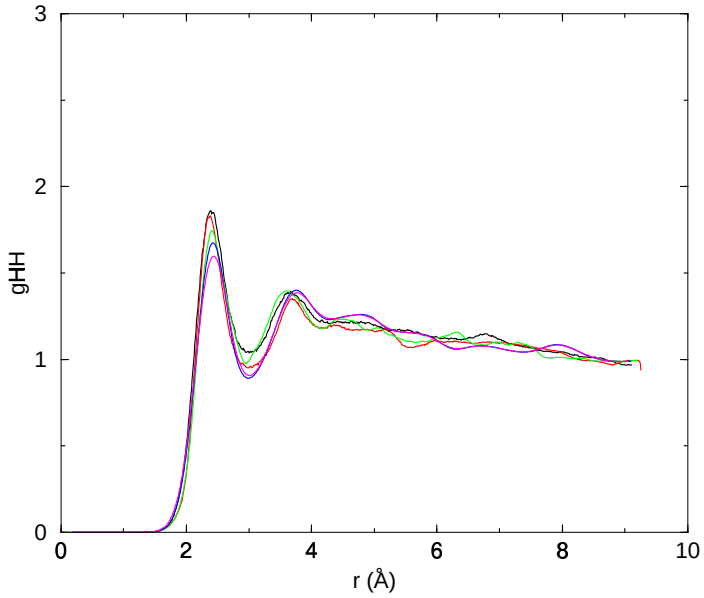

Figure 5.3: Temperature dependence of g_{HH} of pure water. 298 K black, 303 K red, 308 K green, 313 K blue, 318 K magenta

Table 5.2: Height of g_{OH} at 298 K

pure water	water–methane	water–ethane	water–xenon
1.4	1.42	1.7	1.4

Higher correlation of g_{OH} indicates a more pronounced hydrogen bonding structure of water. Ethane is the biggest apolar molecule, and the first peak of g_{OH} of all four systems is the highest for the water–ethane system. The highest correlation of g_{OO} was found for the water-xenon system, this can be because xenon represents a behaviour like clathrate hydrates, which means the nonpolar molecules do not attract each other and water molecules are placed between the nonpolar molecules.

The methane–methane correlation functions, which are presented in Figure 5.15, show that the first peak, which represents the contact pair at about 4 increases. The second peak, which represents the water–separated methane pair at about 6.7 , decreases and vanishes into the first peak with increasing temperature at 1 bar pressure.

The ethane–ethane correlation functions with increasing temperature between 298 and 333 K are presented in Figure 5.5. The second peak, which represents water–separated ethane molecules at about 7.4 , decreases and vanishes into the

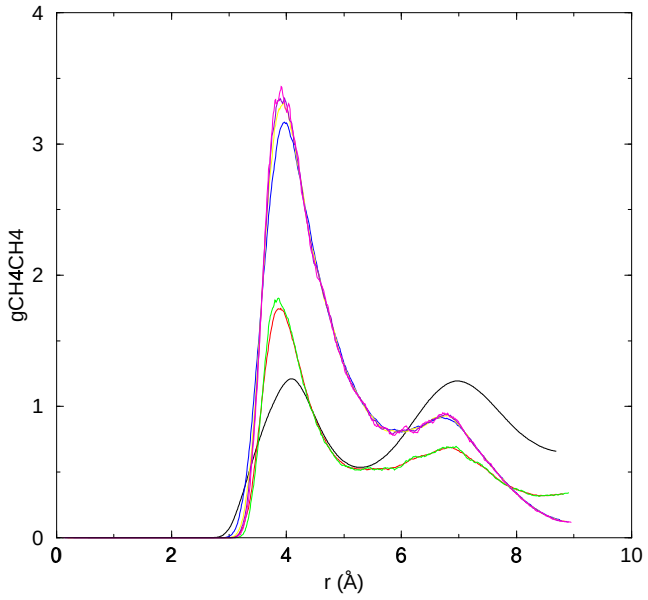

Figure 5.4: Temperature dependence of $g_{\mathrm{CH_4CH_4}}$ of the water–methane system, 298 K black, 303 K red, 308 K green, 313 K blue, 318 K yellow, 323 K violet, 333 K magenta.

first peak, which represents the contact pair; the first peak increases after 308 K at 1 bar pressure.

The temperature dependence of the xenon–xenon correlation function between 298 and 338 K is presented in Figure 5.6. The first peak at 5.3 and the second peak at 7.5 decrease slightly with increasing temperature, but water separated pairs seem to be stable at higher temperatures.

Temperature dependence of the coordination number

Although overall structural information can be obtained from the correlation functions, a more detailed analysis can be done with coordination number calculation.

The oxygen–oxygen, oxygen–hydrogen, hydrogen–hydrogen as well as the methane–methane, ethane–ethane and xenon–xenon coordination numbers at different temperatures and pressures were calculated according to the following formula which is explained in Section 2.2.9 in detail:

$$N_{\mathrm{c}} = 4\pi\rho \int_0^{r_{\mathrm{min}}} r^2 g(r) \mathrm{d}(r) \tag{5.1}$$

where ρ is the density of the system and $g(r)$ denotes the radial distribution function and r the distance.

The location of the first minimum of the correlation functions defines the first hydration shell and the second minimum defines the second hydration shell.

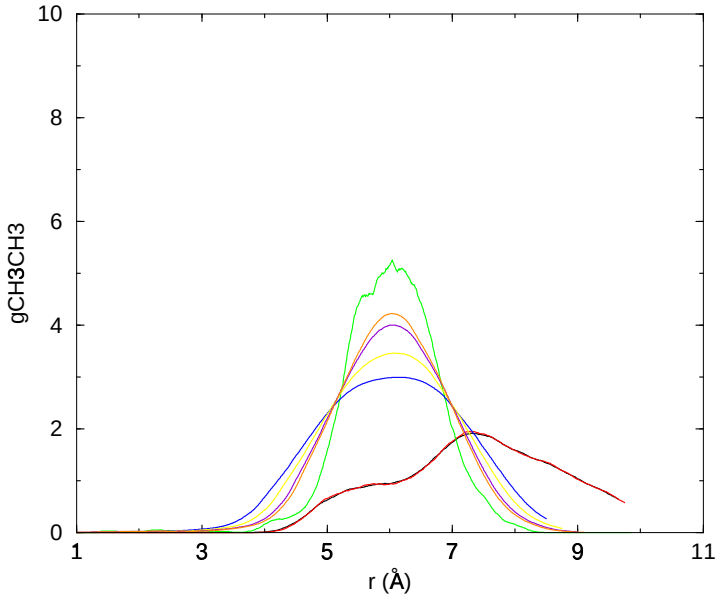

Figure 5.5: Temperature dependence of the $g_{CH_3CH_3}$ of the water–ethane system at 1 bar pressure, 298 K black, 303 K red, 308 K green, 313 K blue, 318 K yellow, 323 K violet, 328 K orange, 333 K magenta.

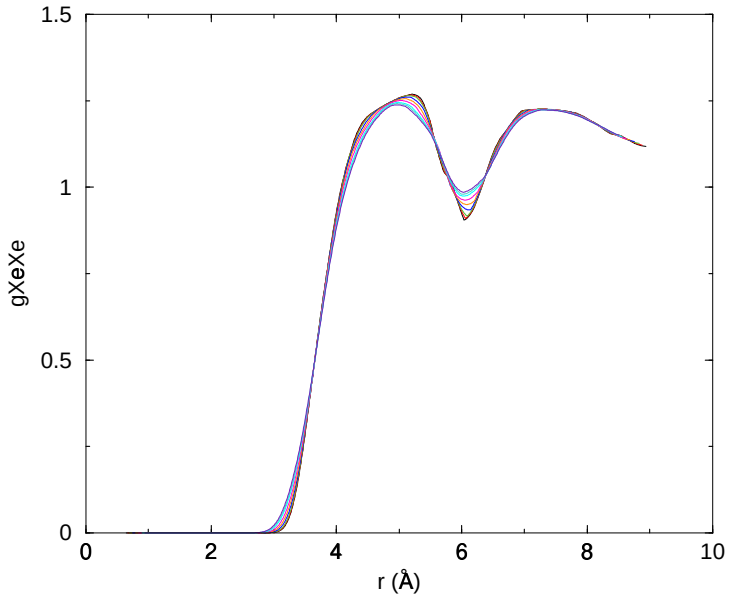

Figure 5.6: Temperature dependence of g_{XeXe} of the water–xenon system at 1 bar pressure, 298 K black, 303 K red, 308 K green, 313 K blue, 318 K orange, 323 K yellow, 328 K cyan, 333 K turqis, 338 K indigo.

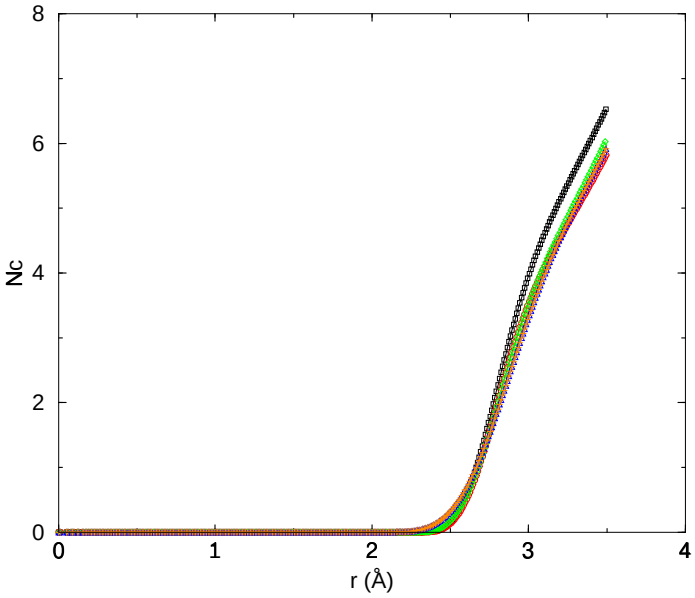

Figure 5.7: Temperature dependence of the oxygen–oxygen coordination number of water in the first hydration shell. 298 K black, 303 K red, 308 K green, 313 K blue, 318 K orange, 323 K brown, 328 K cyan, 333 K indigo.

Figures 5.7– 5.10 show the oxygen–oxygen coordination number of pure water, water–methane, water–ethane and water–xenon systems. Integration of the first peak in g_{OO} to 3.5 yielded a similar value to the experimental data (5.0). The oxygen–oxygen coordination number of pure water and the water–xenon system at different temperatures is larger than that of the water–methane and water–ethane systems. The change in coordination number of water–ethane system is sharp with increasing temperature.

The temperature dependence of the oxygen–hydrogen coordination number of pure water, water–methane, water–ethane and water–xenon systems in the first hydration shell, is shown in Table 5.3. The change of the oxygen–hydrogen coordination number with increasing temperature is remarkably sharp for the water–ethane system.

Figures 5.11– 5.14 show the hydrogen–hydrogen coordination number in the first hydration shell of pure water, water–methane, water–ethane and water–xenon with increasing temperature. The hydrogen–hydrogen coordination number of the water–ethane and the water–methane systems is less than that of the water–xenon system and pure water under same conditions. The change in hydrogen–hydrogen coordination number with increasing temperature is sharp for the water–ethane system.

The oxygen–oxygen, oxygen–hydrogen and hydrogen–hydrogen coordination number in the second hydration shell of all four systems were calculated with increasing temperature and the results can be found Appendix A. The coordi-

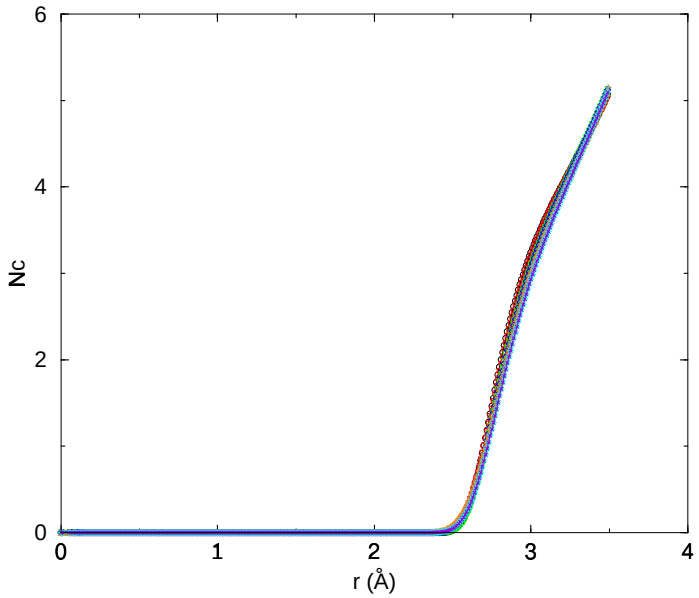

Figure 5.8: Temperature dependence of the oxygen–oxygen coordination number of the water–methane system in the first hydration shell. 298 K black, 303 K red, 308 K green, 313 K blue, 318 K orange, 323 K brown, 328 K cyan, 333 K indigo.

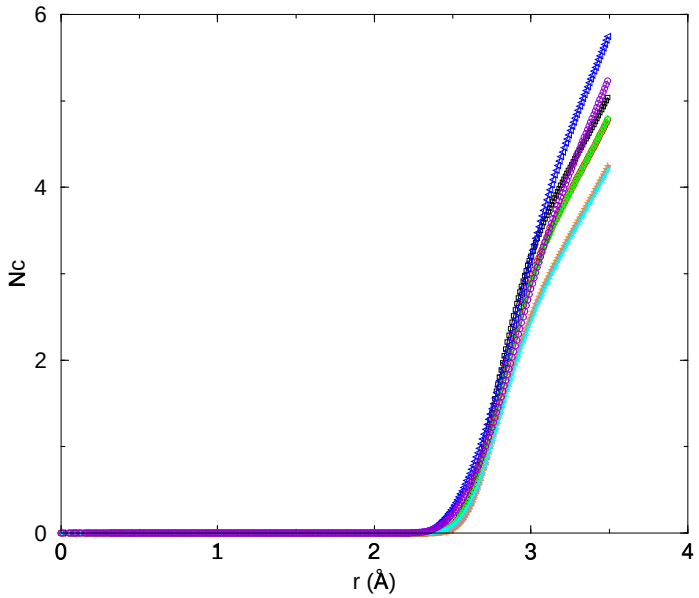

Figure 5.9: Temperature dependence of the oxygen–oxygen coordination number of the water–ethane system in the first hydration shell. 298 K black, 303 K red, 308 K green, 313 K blue, 318 K orange, 323 K brown, 328 K cyan, 333 K indigo, 338 K magenta.

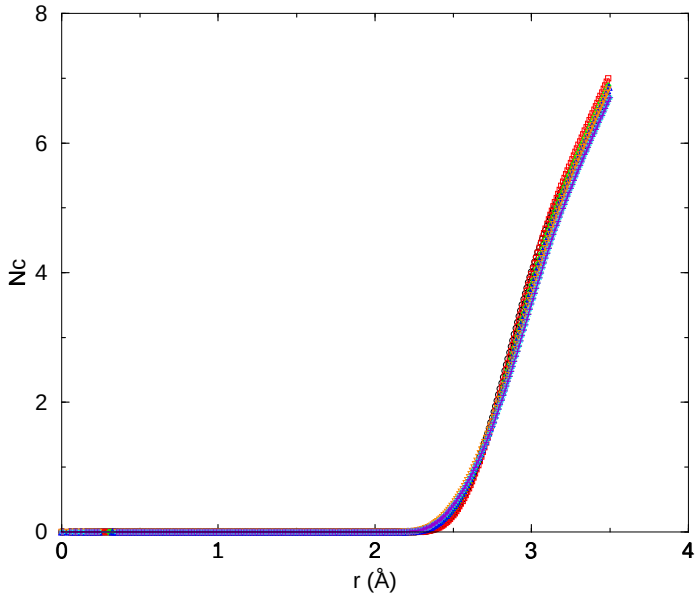

Figure 5.10: Temperature dependence of the oxygen–oxygen coordination number of the water–xenon system in the first hydration shell. 298 K black, 303 K red, 308 K green, 313 K blue, 318 K orange, 323 K brown, 328 K cyan, 333 K indigo, 338 K magenta.

Table 5.3: Hydrogen Bonding in the First Hydration Shell

T (K)	bulk water	water–methane	water–ethane	water–xenon
298	3.27	3.00	3.03	3.49
303	3.28	2.99	2.98	3.48
308	3.22	2.92	2.96	3.48
313	3.19	2.89	2.92	3.47
318	3.16	2.87	2.89	3.46
323	-	2.84	2.85	3.46
328	-	2.80	2.78	3.44
333	-	2.73	2.75	3.42

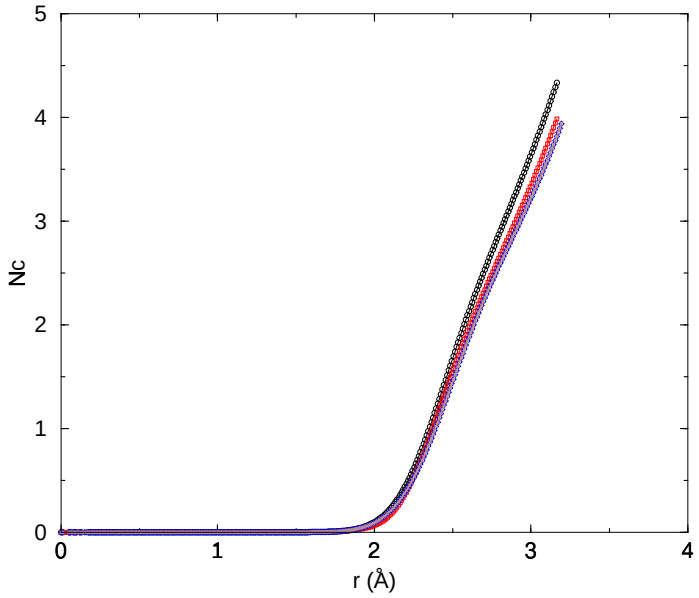

Figure 5.11: Temperature dependence of the hydrogen–hydrogen coordination number of water in the first hydration shell. 298 K black, 303 K red, 308 K green, 313 K blue, 318 K orange, 323 K brown, 328 K cyan, 333 K indigo.

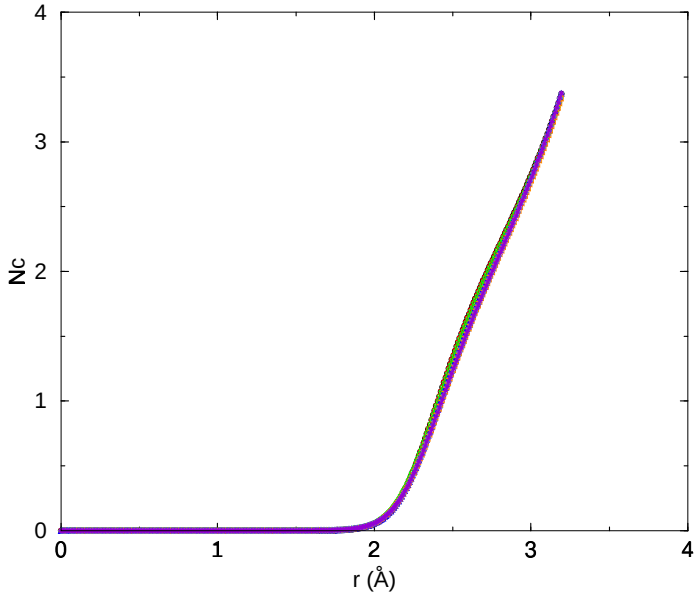

Figure 5.12: Temperature dependence of the hydrogen–hydrogen coordination number of the water–methane system in the first hydration shell. 298 K black, 303 K red, 308 K green, 313 K blue, 318 K orange, 323 K brown, 328 K cyan, 333 K indigo.

nation number of pure water and water–xenon systems are higher than those of water–methane and water–ethane systems. However, the change in coordination

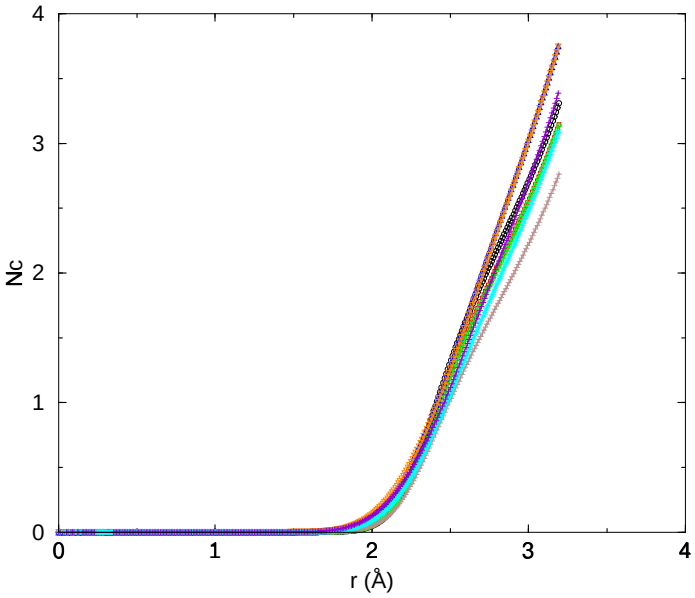

Figure 5.13: Temperature dependence of the hydrogen–hydrogen coordination number of the water–ethane system in the first hydration shell. 298 K black, 303 K red, 308 K green, 313 K blue, 318 K orange, 323 K brown, 328 K cyan, 333 K indigo, 338 K magenta.

number with increasing temperature at constant 1 bar pressure is more noticeable for the water–methane and water–ethane systems than for pure water and the water–xenon system.

Figure 5.15 shows the methane–methane coordination number of the first hydration shell with increasing temperature. The coordination number of methane stays almost constant between 323 and 333 K. The methane molecules attract each other with increasing temperature especially between 308 and 313 K according to the correlation functions and calculated coordination numbers.

The temperature dependence of the second hydration shell coordination number of methane around methane in water is presented in Figure 5.16. The coordination number of methane in the second hydration shell decreases with increasing temperature and stays almost constant after 318 K, this indicates that the water–separated methane pair probability is higher at lower temperatures.

The ethane–ethane coordination number in the first hydration shell with increasing temperature is presented in Figure 5.17. The ethane molecules attract each other with increasing temperature according to the correlation functions and coordination numbers.

Figure 5.18 shows the ethane–ethane coordination number in the second hydration shell with increasing temperature at a pressure of 1 bar. The ethane–ethane coordination number decreases with increasing temperature.

Figure 5.19 displays the coordination number of xenon–xenon in the first

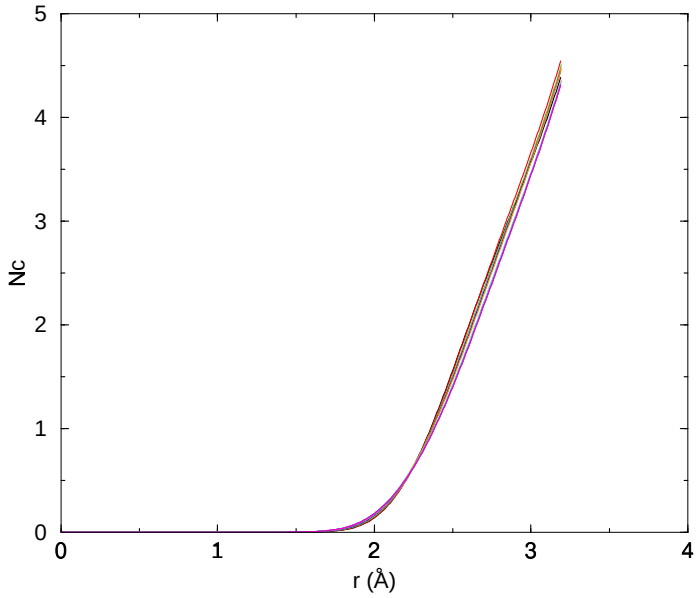

Figure 5.14: Temperature dependence of the hydrogen–hydrogen coordination number of the water–xenon system in the first hydration shell. 298 K black, 303 K red, 308 K green, 313 K blue, 318 K orange, 323 K brown, 328 K cyan, 333 K indigo, 338 K magenta.

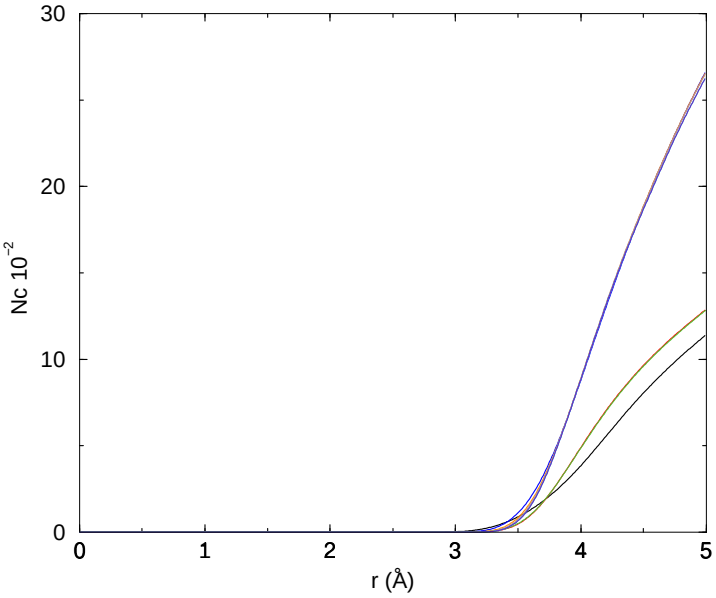

Figure 5.15: Temperature dependence of the methane–methane coordination number of the water–methane system in the first hydration shell, 298 K black, 303 K red, 308 K green, 313 K blue, 318 K orange, 323 K brown, 328 K cyan, 333 K indigo.

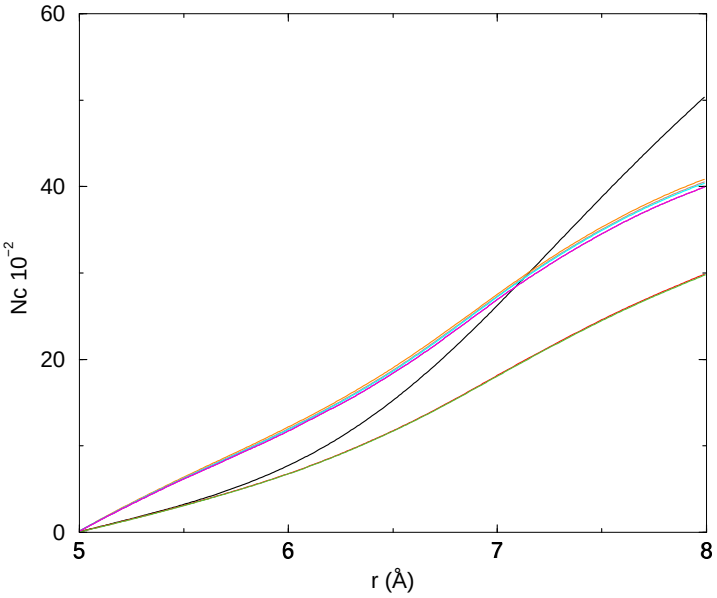

Figure 5.16: Temperature dependence of the methane–methane coordination number of the water–methane system in the second hydration shell, 298 K black, 303 K red, 308 K green, 313 K blue, 318 K orange, 323 K brown, 328 K cyan, 333 K indigo.

hydration shell with increasing temperature. The coordination number of xenon around xenon does not show any strong dependence on temperature.

The xenon–xenon coordination number in the second hydration shell with increasing temperature at a pressure of 1 bar is presented in Figure 5.20 . The coordination number of xenon stays almost constant with increasing temperature.

5.2.1 Pressure dependence of the structural properties

The pressure dependence of the correlation function and coordination number of pure water, water–methane, water–ethane and water–xenon system has been investigated at 298 K temperature.

Figures 5.21– 5.23 present the pressure dependence of the oxygen–oxygen, oxygen–hydrogen, hydrogen–hydrogen correlation functions of pure liquid water with increasing pressure between 1 and 25 bar. The first peak at about 2.85 of the oxygen–oxygen correlation function decreases and the second peak at 4.4 of the oxygen–oxygen correlation function decreases between 15 and 25 bar with increasing pressure.

The oxygen–hydrogen correlation function shows that the first peak at about 1.9 and the second peak at 3.3 decrease with increasing pressure between 1 and 25 bar at 298 K temperature.

The pressure dependence of the simulated correlation function of the water–methane, water–ethane and water–xenon systems is presented in Appendix B.

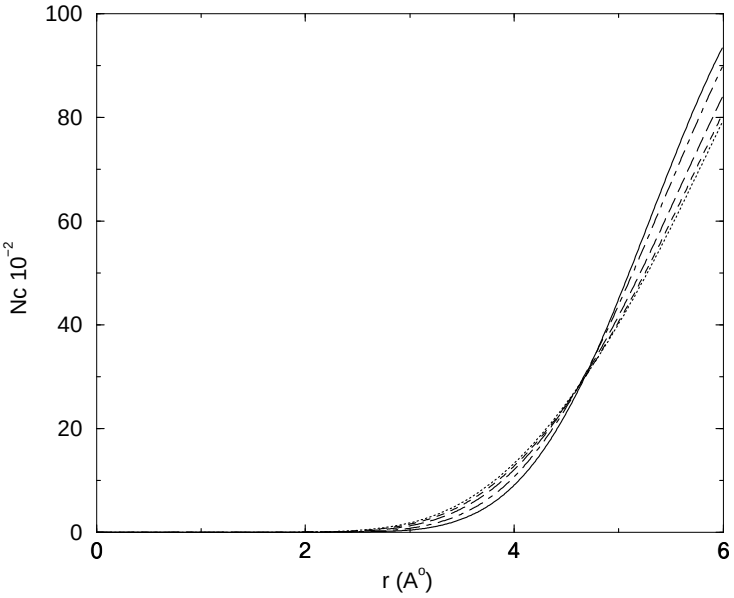

Figure 5.17: Temperature dependence of the ethane–ethane coordination number of the water–ethane system in the first hydration shell, 298 K dotted line, 308 K dot dashed line, 318 K dashed line, 323 K long dashed line, 333 K solid line.

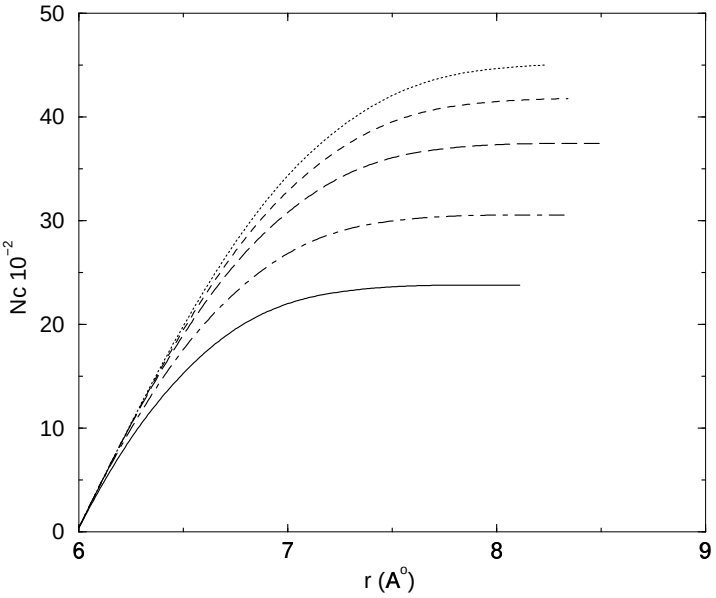

Figure 5.18: Temperature dependence of the ethane–ethane coordination number of the water–ethane system in the second hydration shell. 298 K dotted line, 308 K dot dashed line, 318 K dashed line, 323 K long dashed line, 333 K solid line.

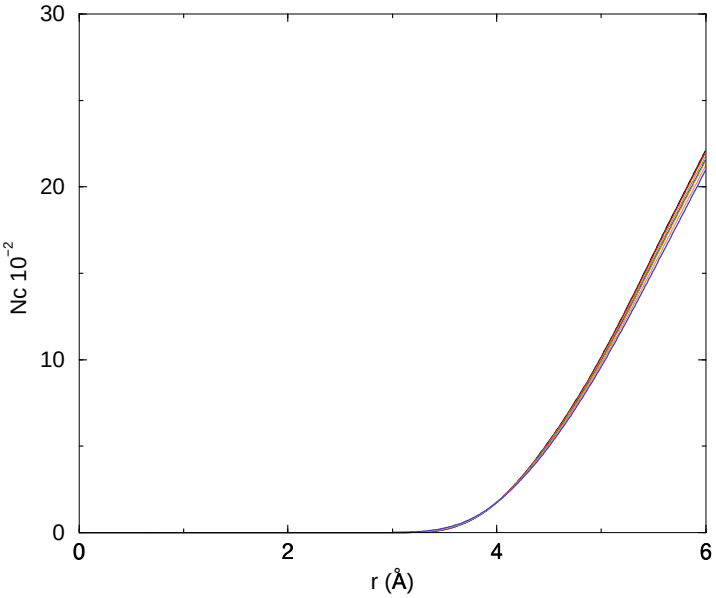

Figure 5.19: Temperature dependence of the xenon–xenon coordination number of the water–xenon system in the first hydration shell, 298 K black, 303 K red, 308 K green, 313 K blue, 318 K orange, 323 K brown, 328 K cyan, 333 K indigo, 338 K magenta.

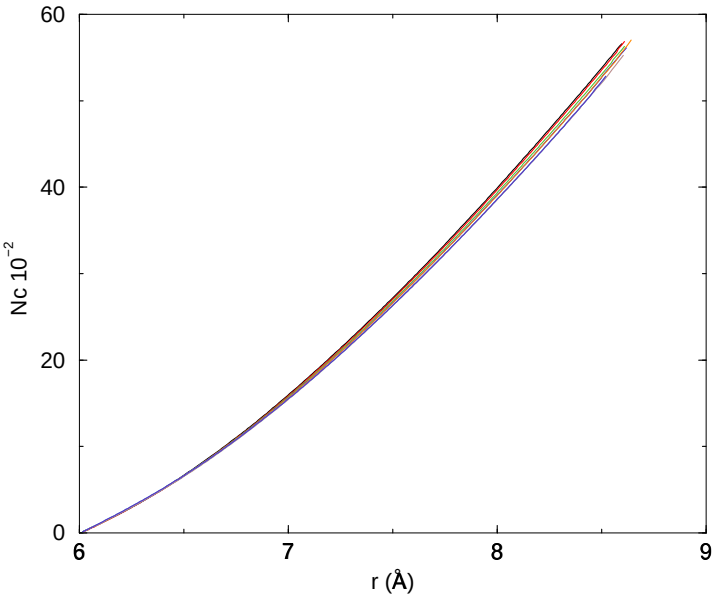

Figure 5.20: Temperature dependence of the xenon–xenon coordination number of the water–xenon system in the second hydration shell, 298 K black, 303 K red, 308 K green, 313 K blue, 318 K orange, 323 K brown, 328 K cyan, 333 K indigo, 338 K magenta.

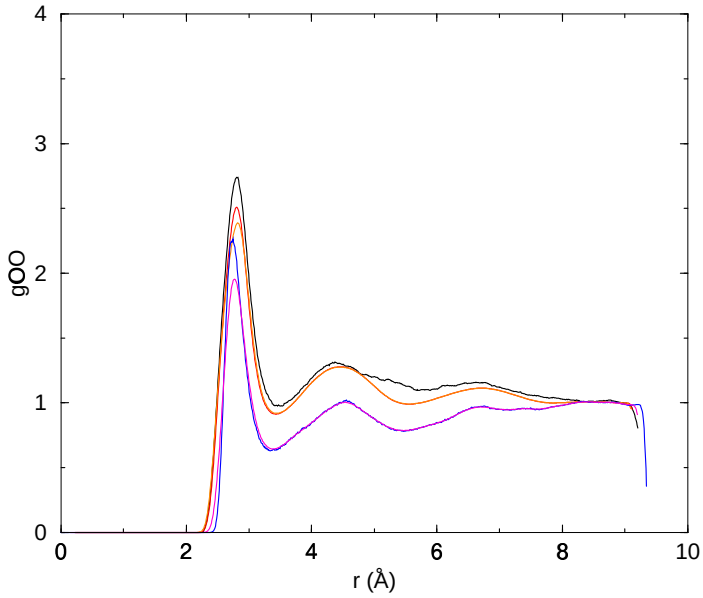

Figure 5.21: Pressure dependence of the g_{OO} of pure water between 1–25 bar, at 298 K temperature: 1 bar black, 5 bar red, 10 bar orange, 15 bar blue, 25 bar magenta.

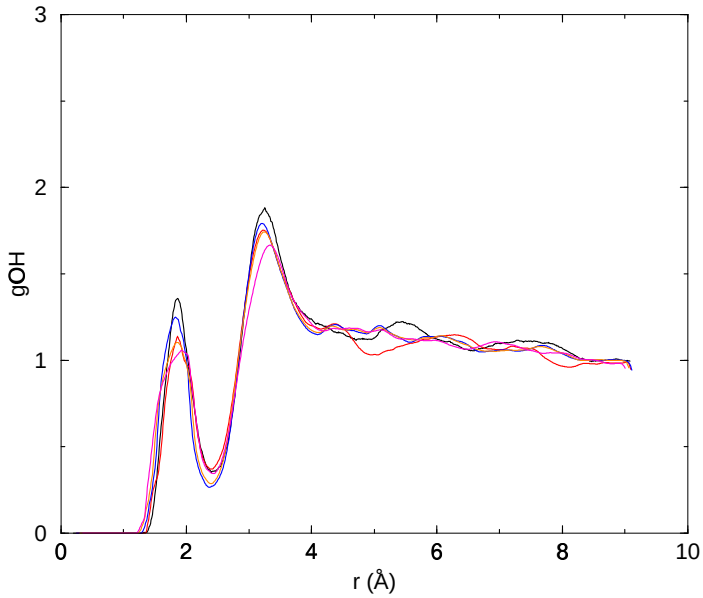

Figure 5.22: Pressure dependence of the g_{OH} of pure water between 1–25 bar, at 298 K temperature: 1 bar black, 5 bar red, 10 bar orange, 15 bar blue, 25 bar magenta.

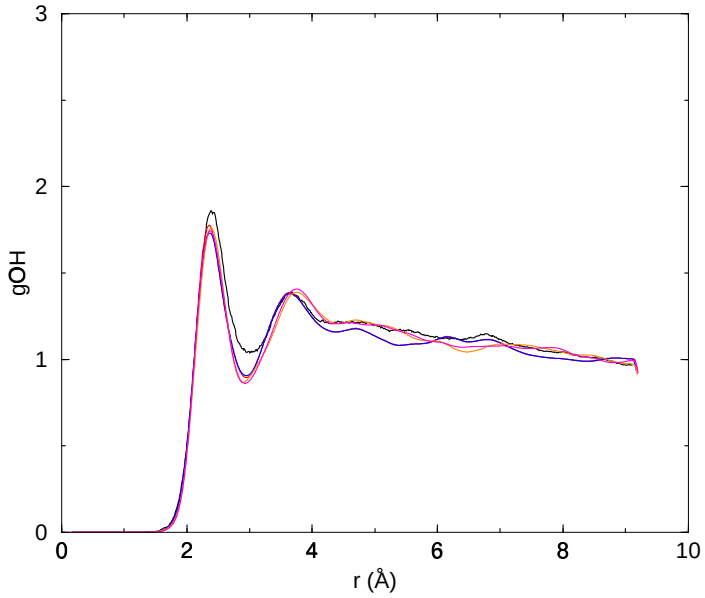

Figure 5.23: Pressure dependence of the g_{HH} of pure water between 1 and 25 bar at 298 K temperature: 1 bar black, 5 bar red, 10 bar orange, 15 bar blue, 25 bar magenta.

The g_{OO}, g_{OH} and g_{HH} of these three systems show almost the same structural change with increasing pressure as those of pure liquid water, which is presented above.

The methane–methane correlation function with increasing pressure between 1 and 35 bar at 298 K temperature is displayed in Figure 5.24. The first peak at about 4 decreases slightly between 1 and 35 bar and the second peak at 5 decreases between 25 and 35 bar. The methane–methane coordination number shows no strong dependence on pressure.

Figure 5.25 presents the ethane–ethane coordination number in the first hydration shell with increasing pressure at 298 K temperature.

The coordination number of oxygen–oxygen of pure liquid water decreases slightly with increasing pressure. The oxygen–oxygen coordination number of the water–methane system stays almost constant with increasing pressure at 298 K temperature. The oxygen–oxygen coordination number of the water–ethane system increases slightly with increasing pressure, whereas that of the water–xenon system decreases slightly as that for pure water. The overall oxygen–oxygen coordination number of the water–methane and water–ethane systems is less than that of pure liquid water and that of the water–xenon system under same conditions. The coordination number of oxygen–hydrogen of pure water and of the water-ethane system decreases with increasing pressure. The oxygen–hydrogen coordination number of the water–methane and the water–xenon systems stays almost constant with increasing pressure at constant 298 K temperature. The oxygen–hydrogen coordination number of the water–methane and the

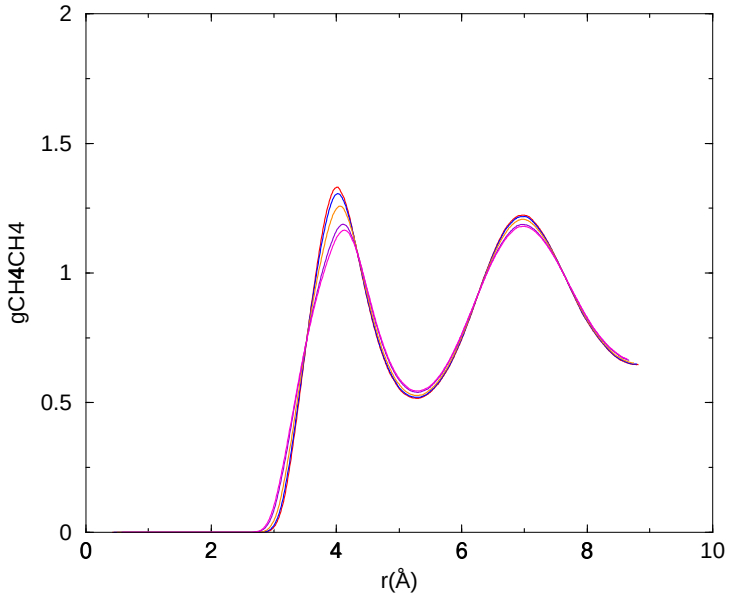

Figure 5.24: Pressure dependence of the methane-methane correlation functions between 1 and 35 bar at 298 K temperature. 1 bar black, 5 bar red, 10 bar blue, 16 bar indigo, 25 bar orange, 35 bar magenta.

water–ethane systems are almost the same and less than that of the water–xenon system and pure liquid water under same conditions. The hydrogen–hydrogen coordination number of the water–ethane system is less than that of the water–methane system. The water–methane system hydrogen–hydrogen coordination number is less than that of pure liquid water and that of the water–xenon system under same conditions.

5.2.2 The effect of apolar molecule number

The effect of the number of apolar molecule on the correlation functions and coordination numbers has been investigated by adding 6 methane molecules to 216 water molecules at 298 K and 1 bar pressure. The correlation functions were compared with those of the water–methane system under same conditions.

Figures 5.27– 5.28 show the comparison of the oxygen–oxygen, oxygen–hydrogen and hydrogen–hydrogen correlation functions of 6 methane molecules in 216 water molecules. The changes in first and second peaks of oxygen–oxygen, oxygen–hydrogen and hydrogen–hydrogen correlation functions are stronger for 2 methane + 216 water molecules system than for the 6 methane + 216 water molecules system with increasing temperature.

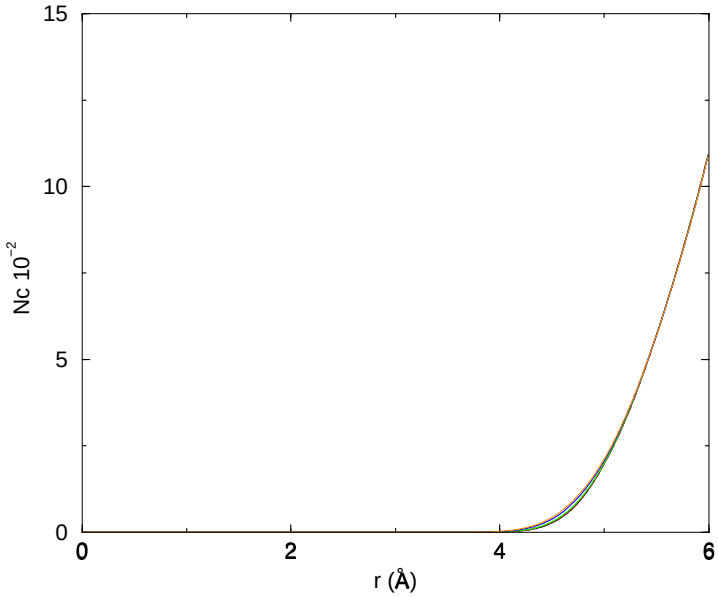

Figure 5.25: Pressure dependence of ethane–ethane coordination number in the 1^{st} hydration shell of water–ethane system. 1 bar black, 5 bar red, 10 bar green, 15 bar blue, 25 bar orange, 30 bar brown.

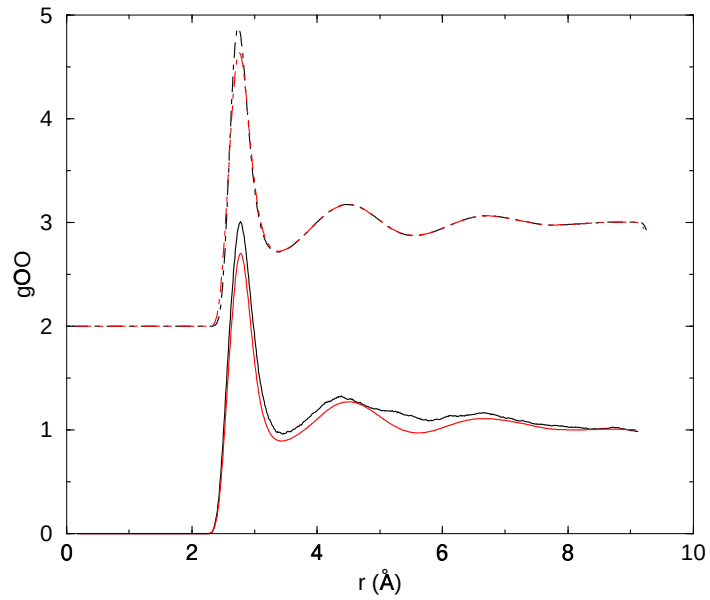

Figure 5.26: Comparison of the oxygen–oxygen correlation functions for 6 methane + 216 water molecules (dot dashed line) and the water–methane (solid line) system at 298 K (black) and 303 K (red).

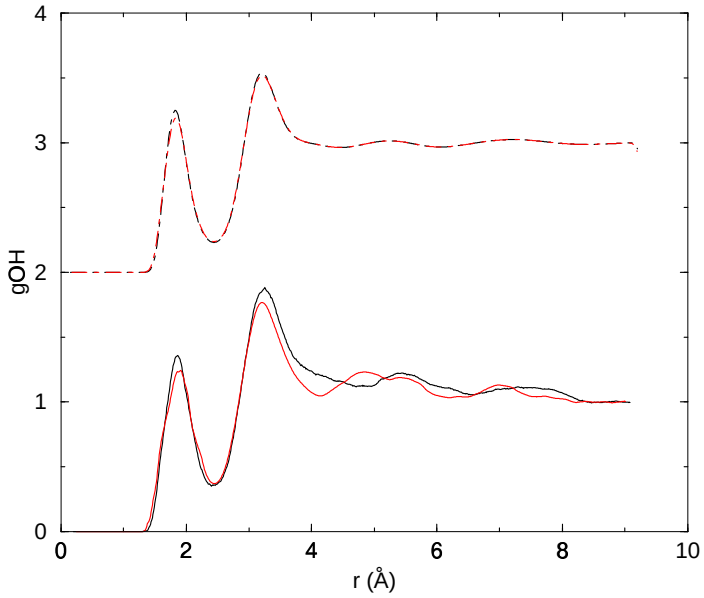

Figure 5.27: Comparison of the oxygen–hydrogen correlation functions for 6 methane + 216 water molecules (dot dashed line) and the water–methane (solid line) system at 298 K (black) and 303 K (red).

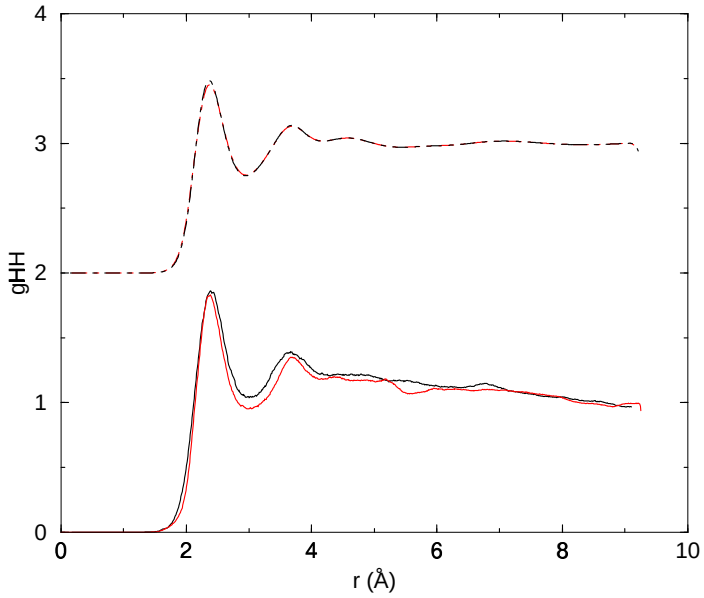

Figure 5.28: Comparison of the hydrogen–hydrogen correlation functions for 6 methane + 216 water molecules (dot dashed line) and water–methane (solid line) system at 298 K (black) and 303 K (red).

5.3 Thermodynamic properties

5.3.1 Temperature dependence of the thermodynamic properties

The thermodynamic properties like volume, potential energy, enthalpy, heat of vaporization, heat capacity, residual chemical potential have been simulated and calculated for pure liquid water, water–methane, water–ethane and water–xenon system to investigate hydrophobic interactions. Furthermore, the temperature dependence of 1 xenon in 216 water molecules has been studied to investigate the hydration process.

The residual chemical potential values presented in this section were obtained with the Widom insertion method [135]. The results of chemical potential methods are presented in the following sections.

The simulated and calculated thermodynamic properties of TIP5P pure liquid water with increasing temperature, between 298 and 318 K and at 1 bar constant pressure, are presented in Table 9.1 in Appendix C. The calculated density of 216 water molecules at 298 K and 1 bar pressure is 1.8051 10^{-5} m^3/mol, which corresponds to 0.997 g/cm^3. The experimental density is also 0.997 g/cm^3 [187].

The heat of vaporization of pure liquid water can be obtained from the simulated potential energy with a reasonably good accuracy by

$$\Delta H_{\mathrm{vap}} \approx \frac{-E_{\mathrm{liq}}}{N} + \mathrm{RT} \tag{5.2}$$

The simulated potential energy at 298 K and 1 bar pressure is -41.74 kJ/mol, the experimental potential energy at 298 K and 1 bar is -41.506 kJ/mol [187].

The experimental ΔH_{vap} at 298 K and 1 bar is 43.97 kJ/mol [187], whereas the simulated ΔH_{vap} value obtained with HYDRO is 44.18 kJ/mol.

The simulated enthalpy and the residual chemical potential of water are presented in Table 5.4 with the experimental data [120, 194].

The temperature dependence of the enthalpy of pure water is shown in Figure 5.29.

The residual chemical potential of water, which is presented in Figure 5.30 increases with increasing temperature between 298 and 318 K at a pressure of 1 bar.

Ji, Cagin and Pettitt also simulated the residual chemical potential of water at 298 K by molecular dynamics simulations, and they obtained almost -23 kJ/mol for 216 water molecules [213]. Herman and co-workers used the thermodynamic integration method and obtained a residual chemical potential of -23.43 kJ/mol for 80 SPC water molecules with a density of 0.995 g/cm^3 at 300 K.

The thermodynamic properties of the water–methane system with increasing temperature between 298 and 333 K and at a pressure of 1 bar have been inves-

	H (kJ/mol)		μ_{res} (kJ/mol)	
T (K)	simulated	experimental	simulated	experimental
298	-41.71±0.04	-41.73[a]	-23.06±0.02	-26.47[b]
303	-41.12±0.04	-41.57[b]	-22.67±0.02	-26.22[b]
308	-40.96±0.05	-41.38[b]	-22.04±0.02	-25.97[b]
313	-40.87±0.06	-41.19[b]	-21.60±0.02	-25.72[b]
318	-40.79±0.06	-40.86[a]	-21.14±0.02	-25.48[b]

Table 5.4: Temperature dependence of the optimized TIP5P water enthalpy and residual chemical potential, a represents Ref. [120] and b represents Ref. [194].

tigated. The simulated and calculated thermodynamic properties are presented in Table 9.2 in Appendix C.

The simulated enthalpy of the water–methane system with increasing temperature between 298 and 333 K is presented in Figure 5.31. The enthalpy increases almost linearly with increasing temperature.

Figure 5.32 shows the simulated residual chemical potential of water and the residual chemical potential of methane of water–methane system with increasing temperature between 298 and 333 K temperature. The residual chemical potential of water and the residual chemical potential of methane increase almost linearly with increasing temperature.

The simulated and calculated thermodynamic properties of the water–ethane system are presented in Table 9.3 in Appendix C.

The enthalpy, the residual chemical potential of water and that of ethane of the water–ethane system are shown as functions of temperature in Figures 5.33–5.35. These functions increase with increasing temperature between 298 and 333 K.

Hydration and hydrophobic interaction are different phenomena not only due to the number of apolar molecules. When one studies the hydration process experimentally, the apolar molecule transfers to an aqueous environment and the number of water molecules around an apolar molecule are not the same all the time. Thus, the thermodynamic values may be similar but not equal.

The experimental residual chemical potential for the hydration process of xenon at 298 K temperature and 1 bar pressure is 5.623 kJ/mol [212] and the simulated residual chemical potential for the hydration of xenon (one xenon and 216 water molecules system) is 5.6602±0.03901 kJ/mol. The simulation results for the hydration of xenon are presented in Table 9.4 in Appendix C.

The calculated thermodynamic properties of water–xenon hydrophobic inter-

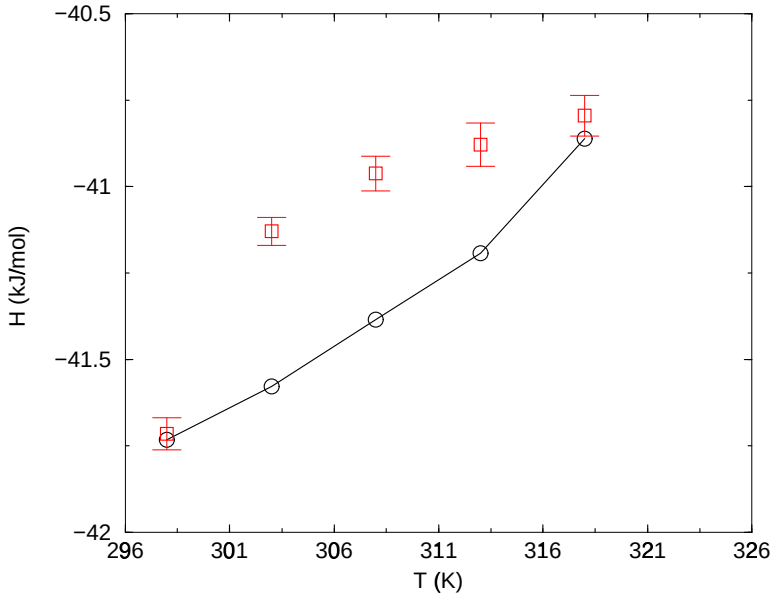

Figure 5.29: The simulated (red squares) and the experimental (solid line, black circles) enthalpy values of pure liquid water between 298 and 318 K at a pressure of 1 bar.

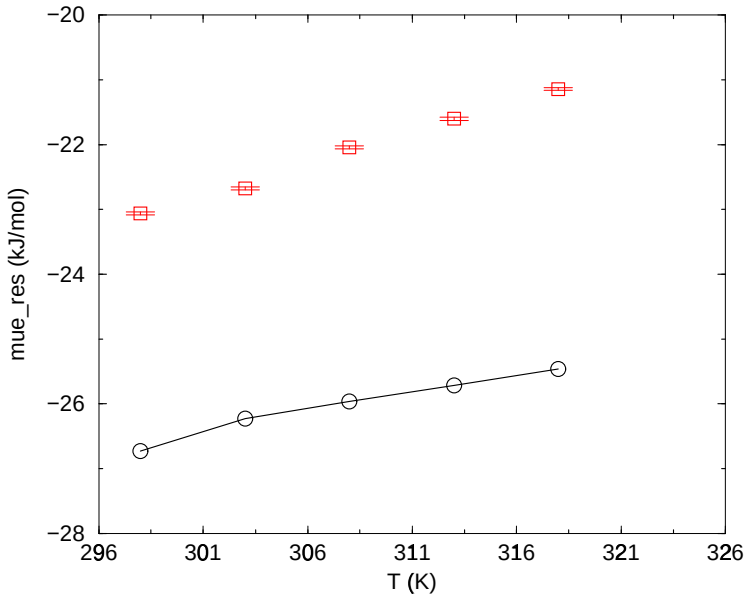

Figure 5.30: The simulated (red squares) residual chemical potential and the experimental chemical potential (solid line, black circles) of water with increasing temperature at 1 bar.

action process (2 xenon and 216 water molecules system) with increasing temperature are shown in Table 9.5 in Appendix C.

Figure 5.36 shows the enthalpy as a function of temperature. The enthalpy

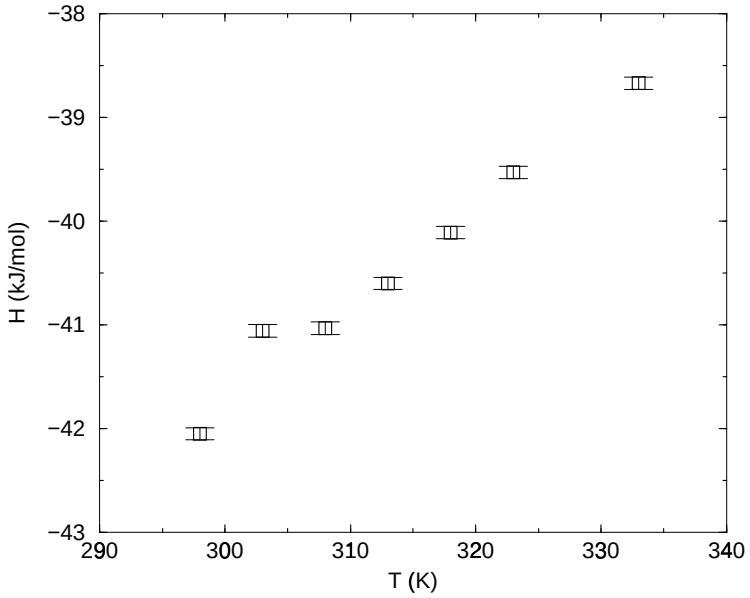

Figure 5.31: Temperature dependence of the enthalpy of the water–methane system at 1 bar pressure.

increases linearly with increasing temperature between 298 and 338 K.

The simulated residual chemical potential of xenon of the xenon hydration process with increasing temperature is in good agreement with the hydration experimental data [212]. In Figure 5.37 the simulated residual chemical potential of xenon, belonging to hydration process (1 xenon and 216 water molecules) and hydrophobic interaction (2 xenon and 216 water molecules) investigations, is presented.

The simulated residual chemical potential of water for hydration and hydrophobic interaction investigations, with increasing temperature and at 1 bar pressure, is presented in Figure 5.38.

5.3.2 Pressure dependence of the thermodynamic properties

The thermodynamic properties of pure water have been simulated and calculated with increasing pressure between 1 and 25 bar at 298 K temperature. The simulated and calculated properties are presented in Table 10.1 in Appendix D.

The volume, potential energy, and total chemical potential of pure liquid water show no clear dependence on increasing pressure between 1–25 bar at 298 K temperature.

The simulated and calculated pressure dependence of the thermodynamic properties of the water–methane system between 1–35 bar is presented in Table 10.2 in Appendix D. The volume, potential energy and residual chemical

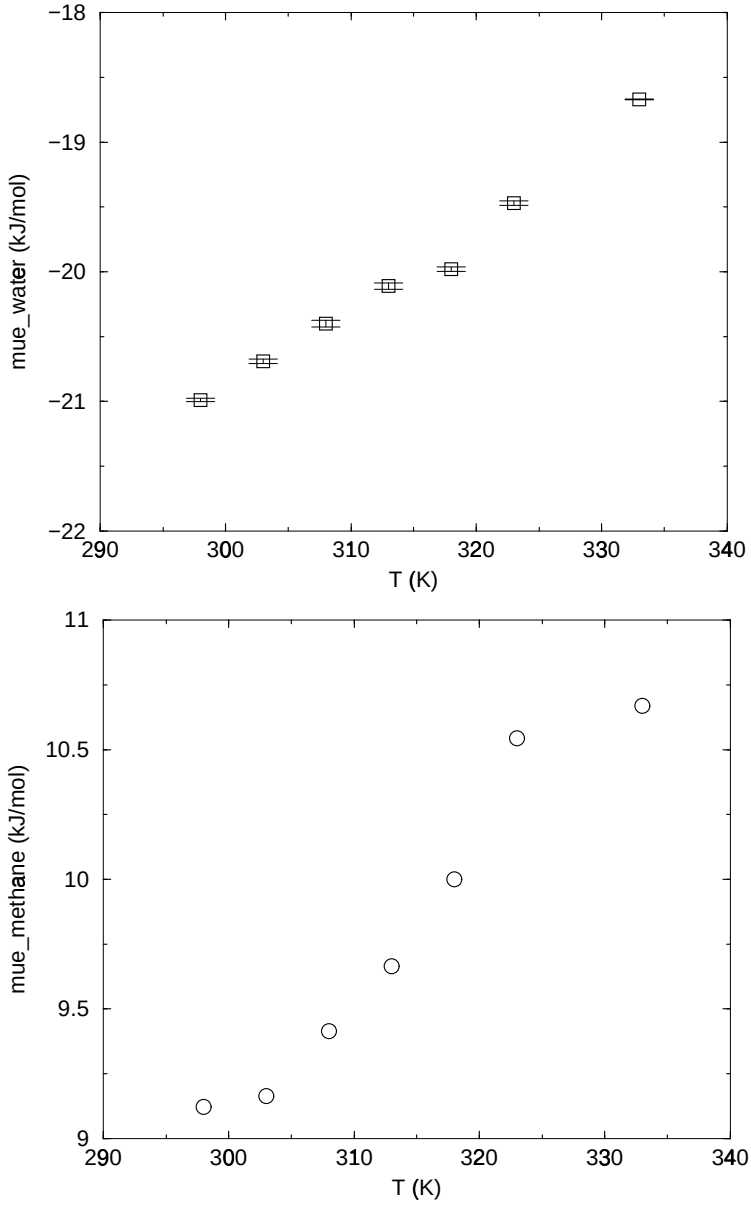

Figure 5.32: The residual chemical potential of water and the residual chemical potential of methane with increasing temperature at 1 bar pressure.

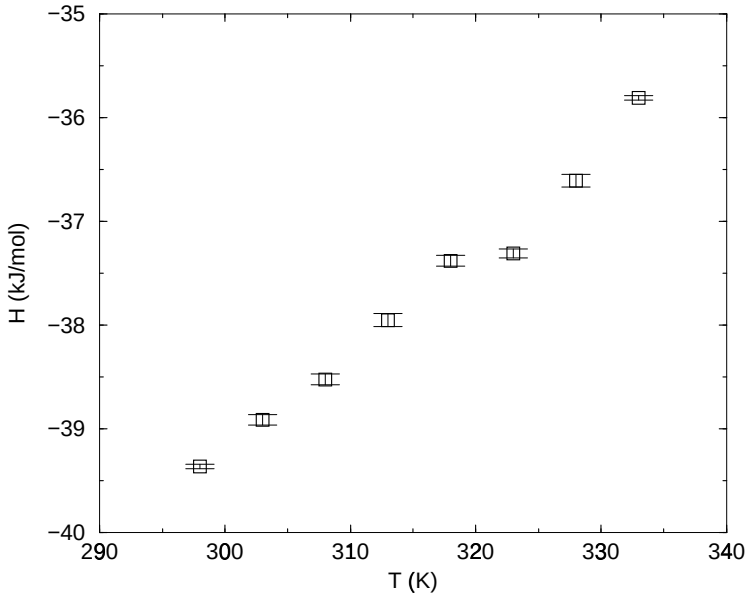

Figure 5.33: Temperature dependence of the enthalpy of the water–ethane system at 1 bar pressure.

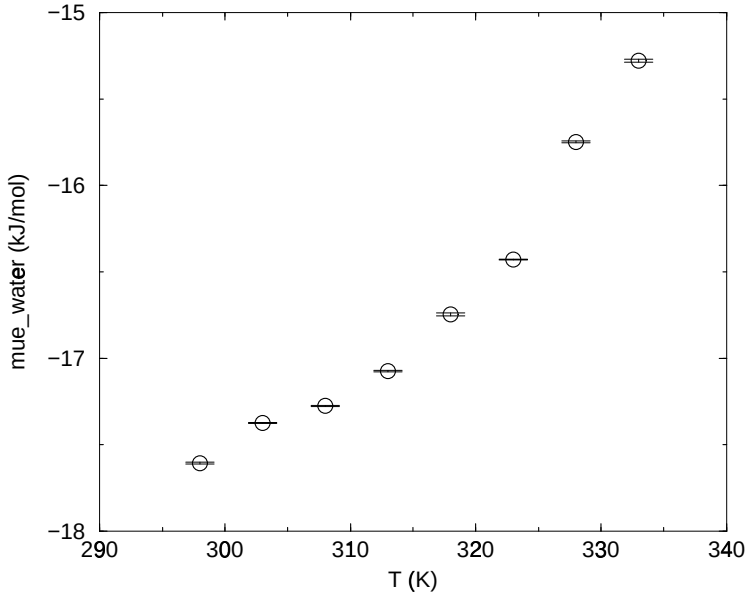

Figure 5.34: Temperature dependence of the residual chemical potential of water of the water–ethane system at 1 bar pressure.

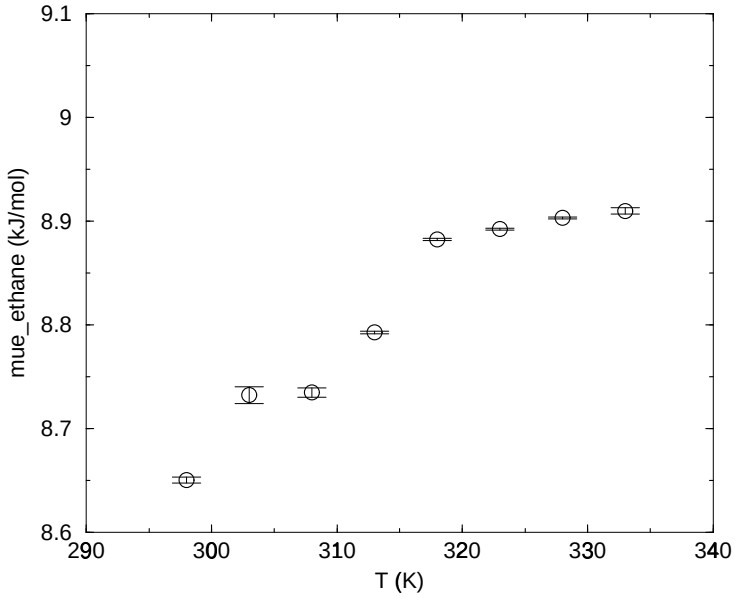

Figure 5.35: Temperature dependence of the residual chemical potential of ethane of the water–ethane system at constant 1 bar pressure.

potential of methane of the water–methane system stays almost constant with increasing pressure between 1 and 35 bar pressure.

The residual chemical potential of water of the water–methane system decreases with increasing pressure at 298 K temperature. This is illustrated in Figure 5.39.

Table 10.3 in Appendix D shows the simulated and calculated thermodynamic properties of the water–ethane system with increasing pressure between 1–30 bar at 298 K temperature. Table 10.4 in Appendix D presents the simulated thermodynamic properties of the water–xenon hydrophobic interaction investigations with increasing pressure between 1–35 bar. The volume, potential energy, residual chemical potential of water and the residual chemical potential of ethane and that of xenon show no clear dependence on increasing pressure.

5.4 A view of hydrophobic effetcs

A quantitative treatment of the thermophysical properties of hydrophobic interactions and the rearrangement and reorganization of water structure according to apolar molecules and increasing temperature is presented in this section.

This treatment is based on the behaviour of pure liquid water, water–methane, water–ethane and water–xenon systems as solution models. The thermophysical values used to develop this treatment are presented before.

A hydrophobic bond is considered to exist when two or more apolar molecules

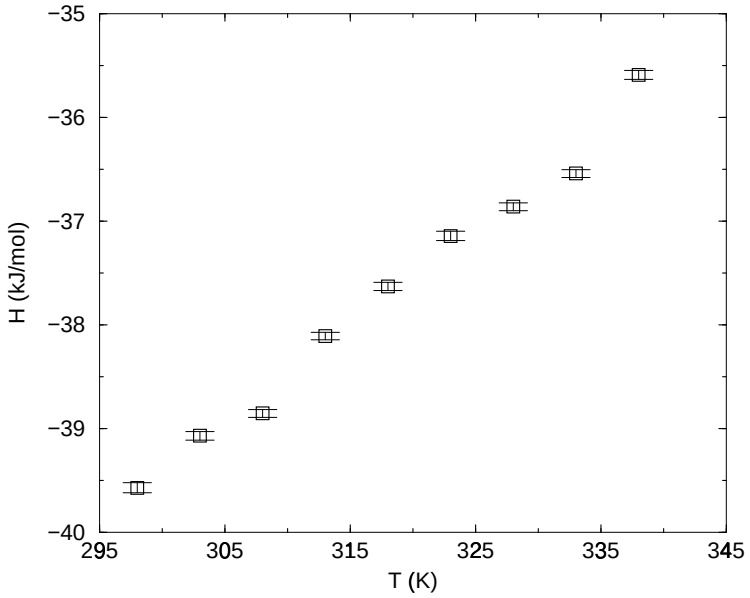

Figure 5.36: Temperature dependence of the enthalpy of the water–xenon system(hydrophobic interaction investigations) at 1 bar pressure.

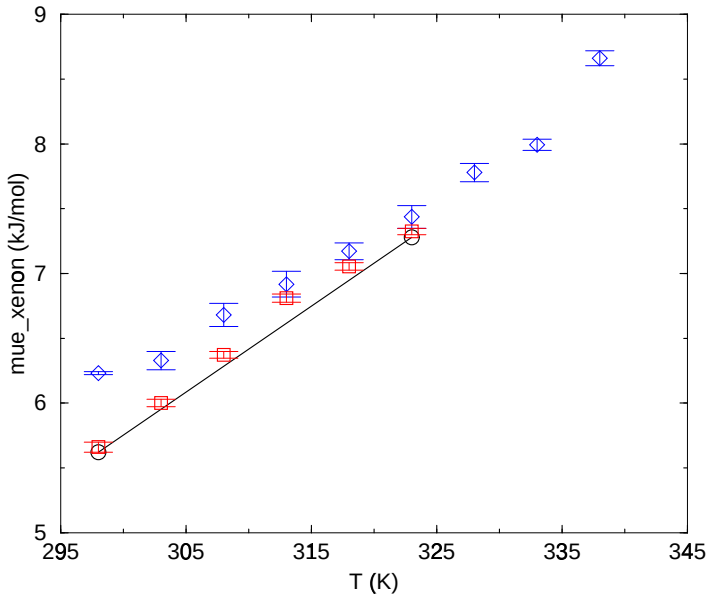

Figure 5.37: Temperature dependence of the simulated residual chemical potential: xenon hydration (red squares), xenon hydrophobic interaction simulations (blue diamonds) and experimental data (solid line, black circles) at 1 bar pressure.

come closer and contact each other. Thereby, the interaction with the surrounding water molecules should decrease in extent. It was recognized that the changes

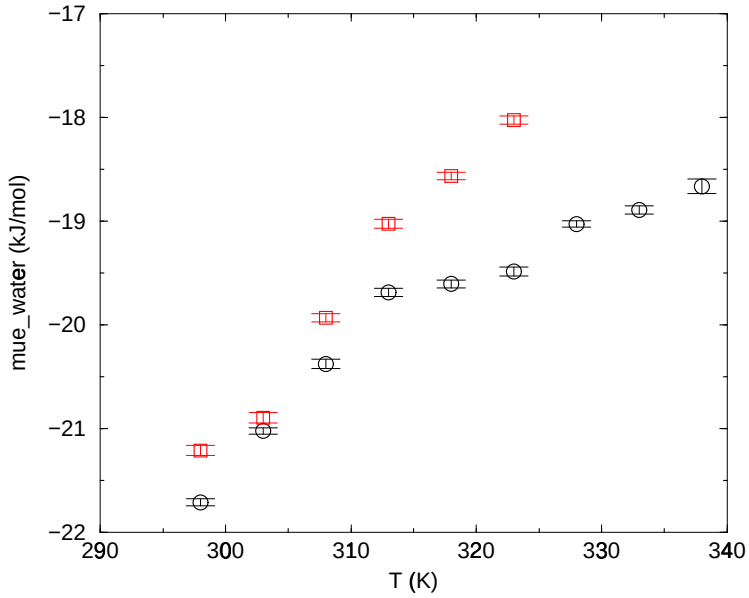

Figure 5.38: Teperature dependence of residual chemical potential of water: hydration process (black squares) and hydrophobic interaction investigations (red diamaonds) at constant 1 ar pressure.

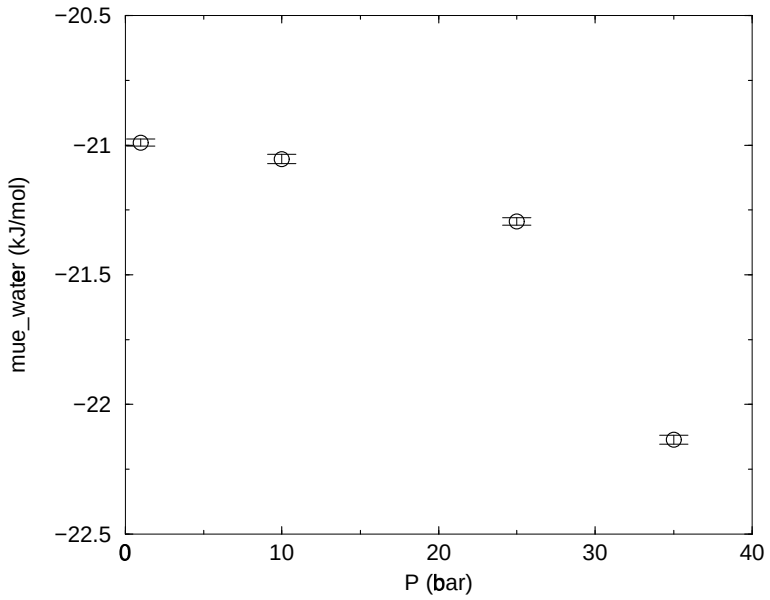

Figure 5.39: Pressure dependence of the residual chemical potential of water of the water–methane system between 1 and 35 bar and at 298 K temperature.

of water structure surrounding the apolar molecules has to play a crucial role in hydrophobic bonds formation [60, 216–218, 221, 222].

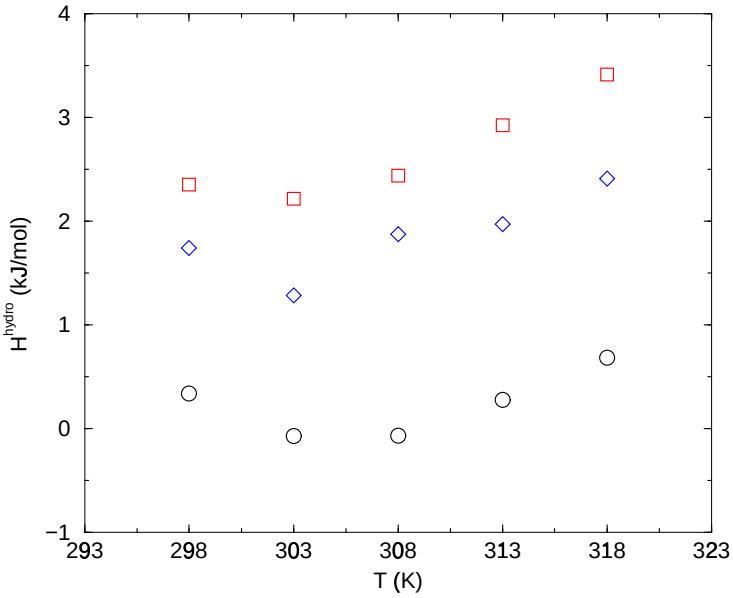

Figure 5.40: Temperature dependence of H_{hydro} of water/methane–water (black circles), water/ethane–water (red squares), water/xenon–water (blue diamonds) at 1 bar pressure.

When the hydrophobic bonds are formed, water–apolar molecules interactions decrease in extent and it should be accompanied by an energy loss according to Scheraga et al. [219, 221–223]. The H_{hydro} value is calculated for water–methane/water, water–ethane/water and water–xenon/water systems under same conditions and the results are presented in Figure 5.40. The change in the enthalpy is largest when one adds ethane molecules into water under same conditions and H_{hydro} decreases at low temperatures and increases slightly after 303 K.

The temperature dependence of μ_{hydro} is calculated for the water–methane/water, water–ethane/water and water–xenon/water systems under same conditions and the results are shown in Figure 5.41. The change in the residual chemical potential of water is largest when one adds two ethane molecules into water under same conditions. μ_{hydro} decreases slightly with increasing temperature for water–ethane/water and water–methane/water, μ_{hydro} for water–xenon/water, when one adds two xenon into water, does not present a clear temperature dependence.

5.5 Chemical potential methods and results

Figure 5.42 shows the simulated chemical potential of water with the Widom insertion method, Widom deletion method and particle deletion scheme method.

Generally, the Widom insertion method yielded the closest approximations to

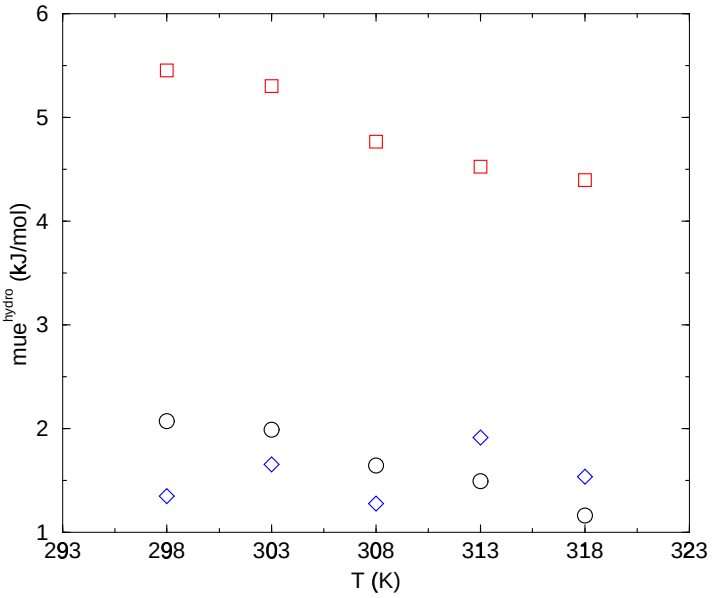

Figure 5.41: Temperature dependence of μ_{hydro} of water–methane/water (black circles), water–ethane/water (red squares) and water–xenon/water (blue diamonds) at 1 bar pressure.

the experimental data.

It is not possible to estimate correctly the chemical potential by the removal of a water molecule or the so-called Widom deletion method. Due to inefficient sampling of the highly positive energies felt by the removed water molecule. Parsonage believed that the inefficient sampling was due to importance sampling, where the system visits the most probable configurations, which does not provide an accurate estimation of the highly positive energy conformations that on the other hand contribute to the chemical potential value [29].

The particle deletion scheme method was tested for the Lennard–Jones fluid and the results were in agreement with the experimental data [161]. But this method failed for highly dense TIP5P water system due to the difference of a removed TIP5P water molecule and the inserted hard sphere into the remaining cavity. The positive energy felt by the removal of a TIP5P water molecule leads to a bias by sampling the configurations and this bias could not be removed by adding a hard sphere. This was the first time that the particle deletion scheme method has been used for TIP5P liquid water at different temperatures.

5.6 Solubility data

The solubility data (in mole fractions) of methane, ethane and xenon according to the Henrys coefficient calculations [225] are presented in Table 5.5.

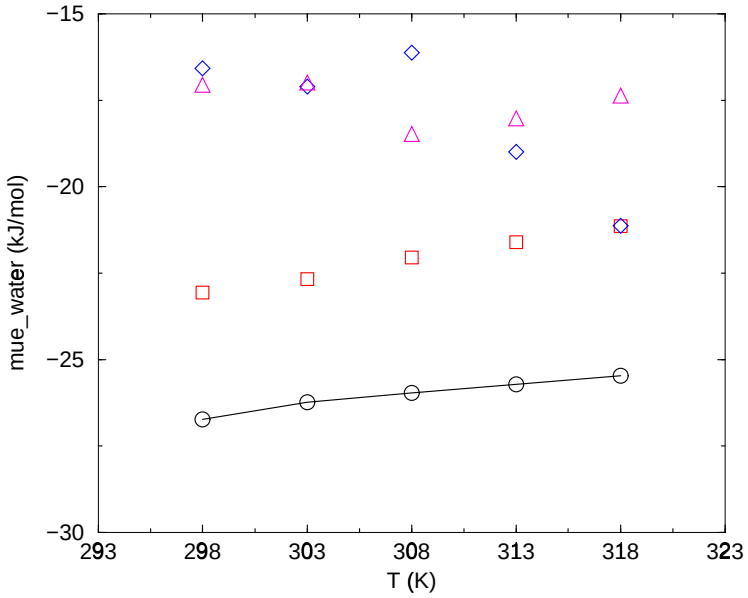

Figure 5.42: Simulated residual chemical potential of water with the Widom insertion method (red squares), Widom deletion method (blue diamonds), particle deletion scheme method (magenta triangles) with increasing temperature at 1 bar pressure. The solid line presents the experimental data [212] (black circles).

T (K)	X_{CH_4} 10^{-4}	$X_{C_2H_6}$ 10^{-4}	X_{Xe} 10^{-4}
298	1.44	2.50	6.82
303	1.25	2.35	6.66
308	1.17	2.15	6.29
313	0.63	2.11	5.78
318	0.54	2.08	5.22
323	0.36	2.06	4.94
328	0.27	1.91	4.50
333	0.18	1.87	4.41

Table 5.5: Temperature dependence of the solved mole fractions

The simulations have been performed in the metastable phase. The computers are still not enough developed to perform simulations in the stable phase with higher number of water molecules. The mole fraction of 2 methane, xenon and ethane molecules in 216 water molecules, used to investigate the hydrophobic interactions, is 0.00917. This indicates that a small part of the methane and ethane molecules is solved in water and the solubility of these apolar molecules decreases with increasing temperature. The experimental solubility data of xenon shows that more xenon is solved in water when compared with methane or ethane.

Chapter 6

Discussion

The temperature dependence of the structural and thermodynamic properties of pure water, water–methane, water–ethane, water–xenon systems and the hydration of one xenon atom in 216 water molecules has been investigated. This work was the first where the TIP5P model for water has been used to investigate hydrophobic interactions and hydration process by simulations.

The first and second peak of g_{OO}, g_{OH} and g_{HH} of pure water, water–methane, water–ethane and water–xenon systems decrease and broaden slightly with increasing temperature. The first peak of the methane–methane pair correlation function at about 4 increases remarkably between 313–318 K, and the second peak vanishes into the first peak with increasing temperature. The oxygen–oxygen, oxygen–hydrogen and hydrogen–hydrogen first hydration shell integrations show that the coordination numbers are higher for pure water and for the water–xenon system than for the water–methane and water-ethane systems under same conditions. The integration of the oxygen–hydrogen first hydration shell shows that the water–xenon system has the highest number of hydrogen bonds between the water molecules. The temperature dependence of the coordination number of oxygen–oxygen, oxygen–hydrogen and hydrogen–hydrogen is noticeable for the water–ethane system.

The methane–methane coordination number increases sharply between 313 and 318 K. The experimental solubility data decreases remarkably between 313 and 318 K. The integration of the coordination number of methane–methane in the first hydration shell yields small values. Thus, the water–separated methane pair probability is higher even the methane molecules attract each other with increasing temperature. The second peak of ethane–ethane correlation function, which represents the water–separated pair decreases and vanishes into the first peak with increasing temperature. The integration of the ethane–ethane first hydration shell shows that the ethane–ethane coordination number increases, while the coordination number of the second hydration shell decreases. The integration of the first hydration shell yields large ethane coordination number, the contact–pair probability is high.

The xenon–xenon correlation function and the coordination number decrease slightly with increasing temperature but a strong dependence of the structural properties on the temperature has not been observed. The water–separated xenon pair probability is high and xenon is more soluble in water according to the experimental data.

The residual chemical potential change of water as a function of temperature is positive and the enthalpy change is positive. The change in enthalpy of the water–methane system is almost equal between 308–323 K. The positive residual chemical potential change of water of the water–methane system is the smallest between 308–313 K and the residual chemical potential change of methane is the largest between 308 and 313 K. This may provide the structural investigations that the methane molecules attract each other especially between 308–313 K, according to the correlation functions and coordination numbers. The residual chemical potential change of water of the water–ethane system with increasing temperature is positive. The enthalpy change of the water–ethane system with increasing temperature is positive and the values are larger than the residual chemical potential change values under same conditions. These results combined with the structural properties presented before, provide information that the entropy change may be larger for the ethane molecules and the water rearrangement causes a large entropy change of the water molecules. The residual chemical potential change of water of the xenon hydration process is positive and increases between 303–308 K and decreases between 313–318 K. The residual chemical potential change of xenon increases also slightly between 303–308 K and decreases between 313–318 K. The residual chemical potential change of water of the water–xenon system is highest between 308–313 K and that of xenon stays almost constant. The water rearrangement seems like to be stronger between 313–318 K for the water–xenon system. On the other hand, it seems like the water rearrangement is weakest between 308–313 K for the water–methane system and between 308–323 K for the water–ethane system. These are those temperatures where the methane and ethane molecules show a tendency to come closer. The rotational degrees of freedom of water showed a decrease upon xenon binding. Tilton et al. presented that local rearrangements of water might occur upon xenon binding [46, 47, 55, 56, 58, 59]. The conclusions above, indicate that water rearrangement is especially the case between 313–318 K when xenon is present in the system. The xenon shows structural properties of clathrate hydrates in which the xenon is surrounded by a cage in the lattice of host water molecules. Such an orientation allows the number of water-water hydrogen bonds in the hydration shell to be close to that in bulk water and the oxygen–hydrogen coordination numbers and correlation functions of the water–xenon system resembles to those of pure water under same condition.

The volume, potential energy, enthalpy and residual chemical potential of water and as well as of the solute increase almost linearly with increasing temperature for pure water and all mixtures studied in this work. When the strong

water-water attractive forces are replaced by the weaker water-apolar molecules ones, this could lead to a net positive enthalpy change that would explain the positive residual chemical potential change with increasing temperature.

To generate a view of the temperature dependence of the apolar molecule effects on water molecules, the thermodynamic property changes of water when two apolar molecules are added into water were investigated. The enthalpy change is largest when two ethane molecules are added, and smallest when methane molecules are added into water. The H_{hydro} values of all three comparisons are negative between 298–303 K, but positive above 303 K. The residual chemical potential change of water when two apolar molecules are added was investigated, too. This property shows the strongest change when ethane molecules are added, due to the large size of ethane molecules. The residual chemical potential change of water when two xenon molecules are added is positive between 303–308 K and 313–318 K, which indicates the water rearrangement in these ranges. The residual chemical potential change is a combination of a small decrease in enthalpy. Therefore, there must be a large decrease in the entropy change. The creation of a cavity would require an input of enthalpy.

The structural and thermodynamic properties of pure water, water–methane, water–ethane and water–xenon systems have been investigated with increasing pressure and at constant 298 K. The results, which are presented in Section 3 and Appendix B, show no clear dependence on increasing pressure.

Because it is still a problem to simulate the residual chemical potential of highly dense systems, as explained in Section 2, the Widom insertion [135], Widom deletion [28] and the particle deletion method [161], which are explained in Section 2, were coded and the obtained results were compared to each other. The Widom insertion method yields the residual chemical potential of water, which is comparable with the available experimental data. The bias, introduced by the removal of a particle from the system by Widom deletion method, disturbed the sampling process for the evaluation of the residual chemical potential. This bias was replaced by an addition of a hard sphere by particle deletion scheme method, but the residual chemical potential values show that this method fails for TIP5P, whereas Theodorou et al. showed that this method yields good results for a system of Lennard–Jones particles. The differences in the hard sphere and TIP5P potential may cause a perturbation in the evaluation of the residual chemical potential.

Chapter 7

Appendix A

In this appendix, the temperature dependence of the structural properties of water for the water–methane, water–ethane and water–xenon systems are presented. The description of these correlation functions can be found in Section 4.

7.1 Temperature dependence of the structural properties

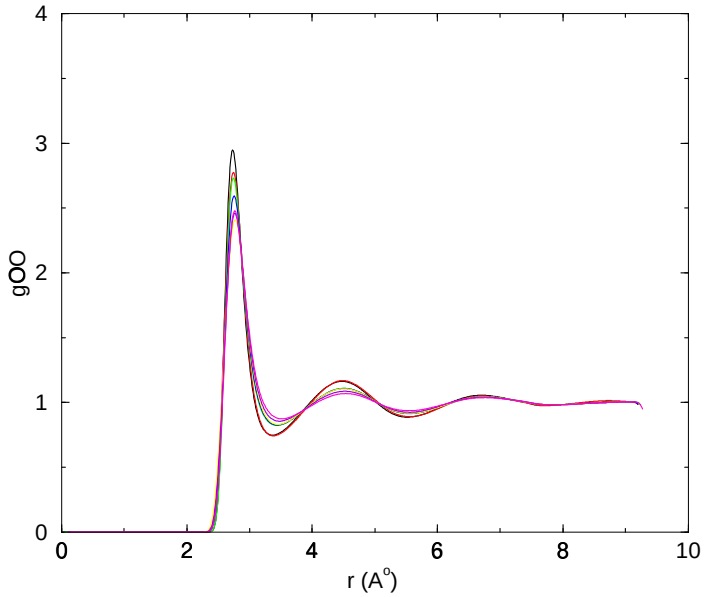

Figure 7.1: Temperature dependence of g_{OO} of the water–methane system, 298 K black, 303 K red, 308 K green, 313 K blue, 318 K yellow, 323 K violet, 328 K orange, 333 K magenta.

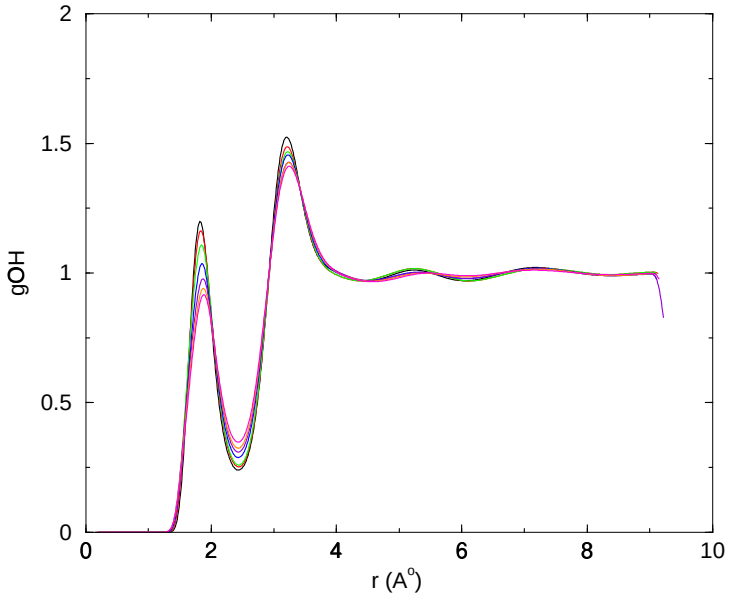

Figure 7.2: Temperature dependence of g_{OH} of the water–methane system, 298 K black, 303 K red, 308 K green, 313 K blue, 318 K yellow, 323 K violet, 328 K orange, 333 K magenta.

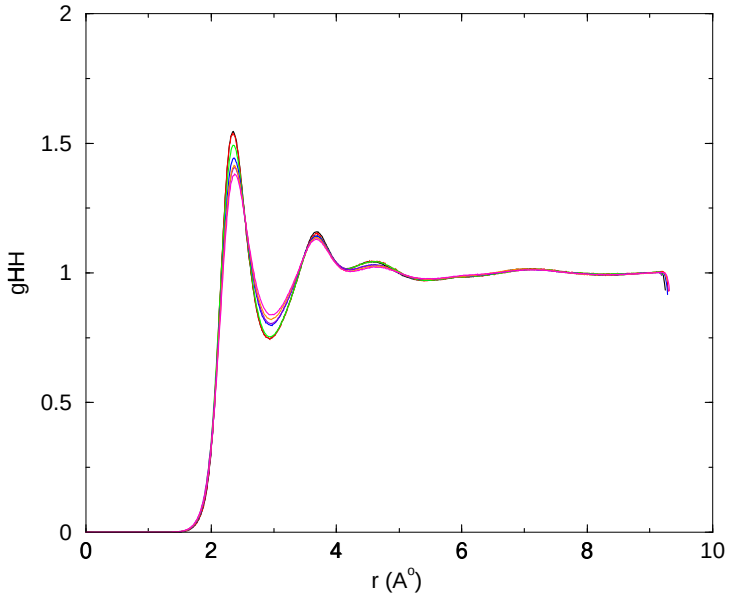

Figure 7.3: Temperature dependence of g_{HH} of the water–methane system, 298 K black, 303 K red, 308 K green, 313 K blue, 318 K yellow, 323 K violet, 328 K orange, 333 K magenta.

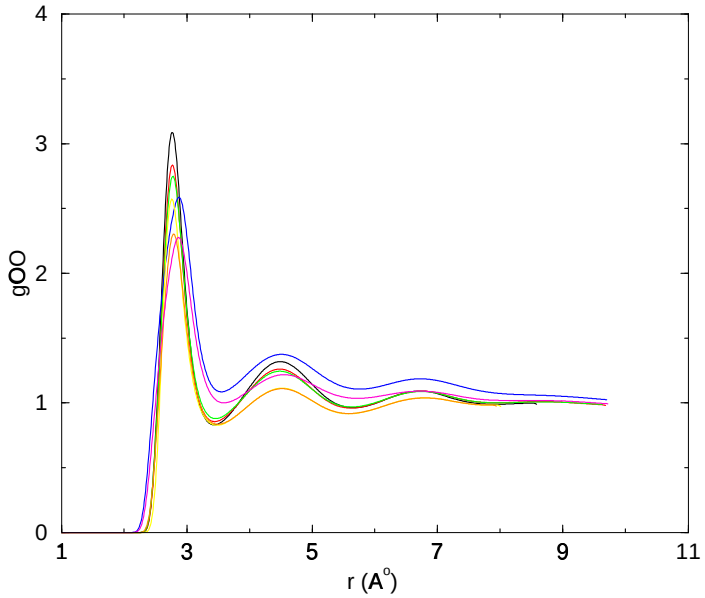

Figure 7.4: Temperature dependence of g_{OO} of the water–ethane system at 1 bar pressure. 298 K black, 303 K red, 308 K green, 313 K blue, 318 K yellow, 323 K violet, 328 K orange, 333 K magenta.

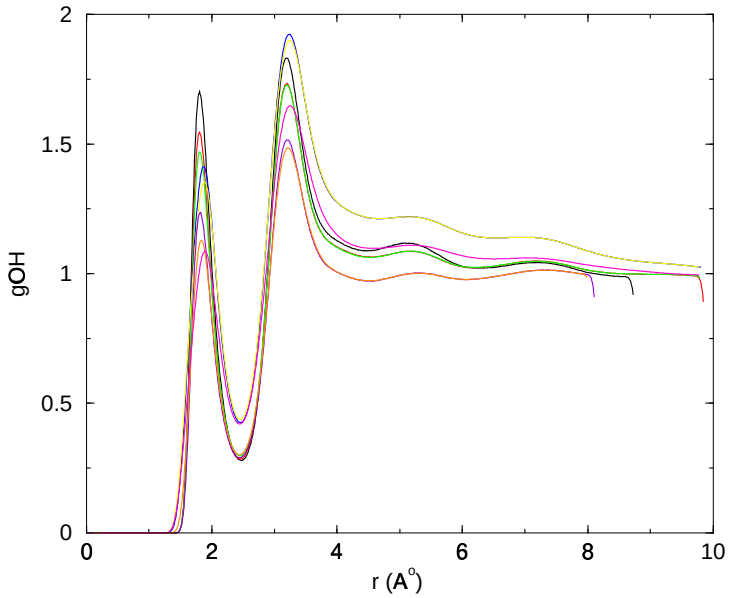

Figure 7.5: Temperature dependence of g_{OH} of the water–ethane system at 1 bar pressure. 298 K black, 303 K red, 308 K green, 313 K blue, 318 K yellow, 323 K violet, 328 K orange, 333 K magenta.

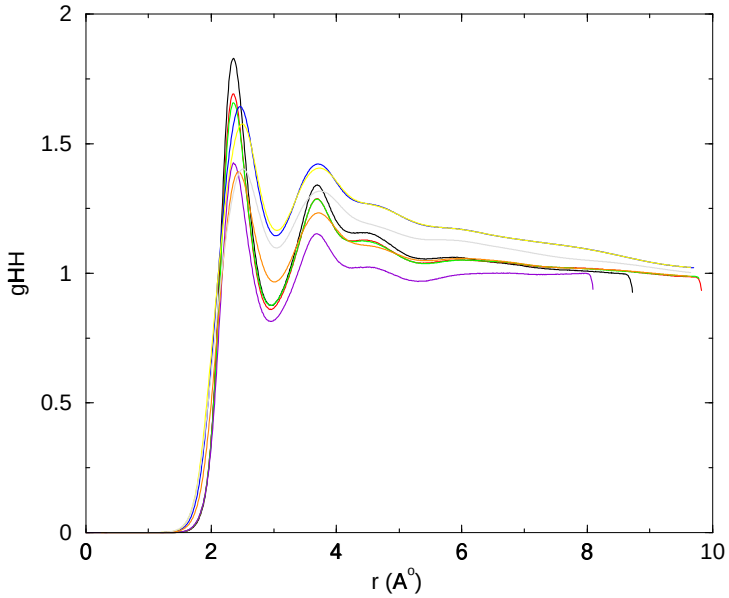

Figure 7.6: Temperature dependence of g_{HH} of the water–ethane system at 1 bar pressure. 298 K black, 303 K red, 308 K green, 313 K blue, 318 K yellow, 323 K violet, 328 K orange, 333 K magenta.

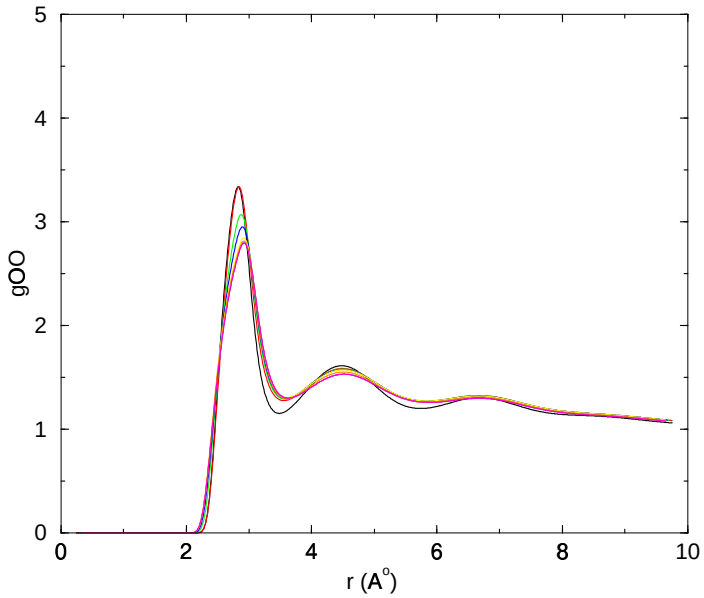

Figure 7.7: Temperature dependence of g_{OO} of the water–xenon system at 1 bar pressure, 298 K black, 303 K red, 308 K green, 313 K blue, 318 K yellow, 323 K violet, 328 K indigo, 333 K orange, 338 K magenta.

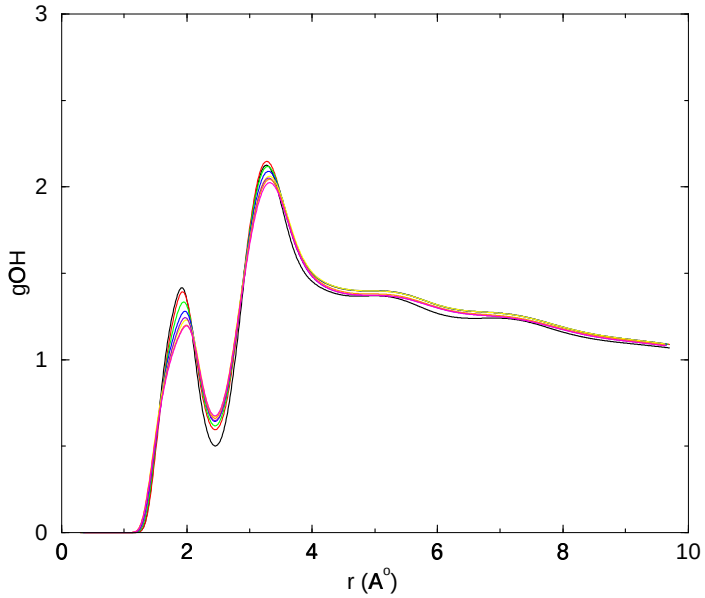

Figure 7.8: Temperature dependence of g_{OH} of the water–xenon system at 1 bar pressure, 298 K black, 303 K red, 308 K green, 313 K blue, 318 K yellow, 323 K violet, 328 K indigo, 333 K orange, 338 K magenta.

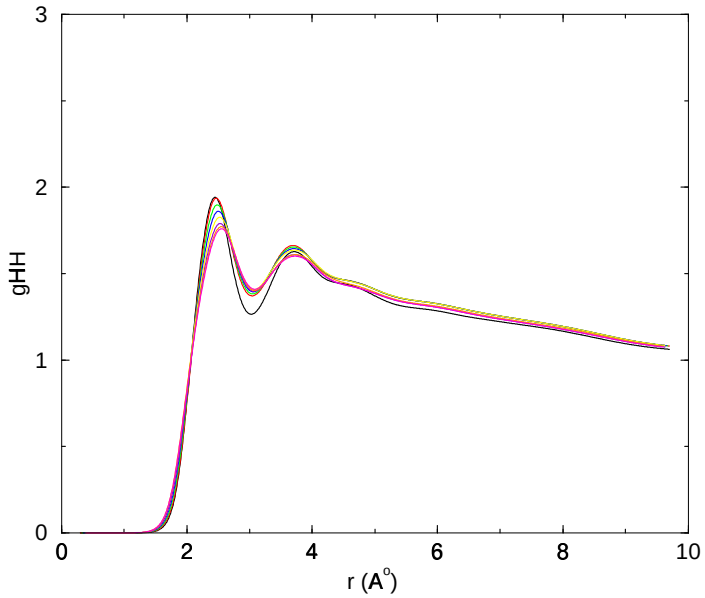

Figure 7.9: Temperature dependence of g_{HH} of the water-xenon system at 1 bar pressure, 298 K black, 303 K red, 308 K green, 313 K blue, 318 K yellow, 323 K violet, 328 K indigo, 333 K orange, 338 K magenta.

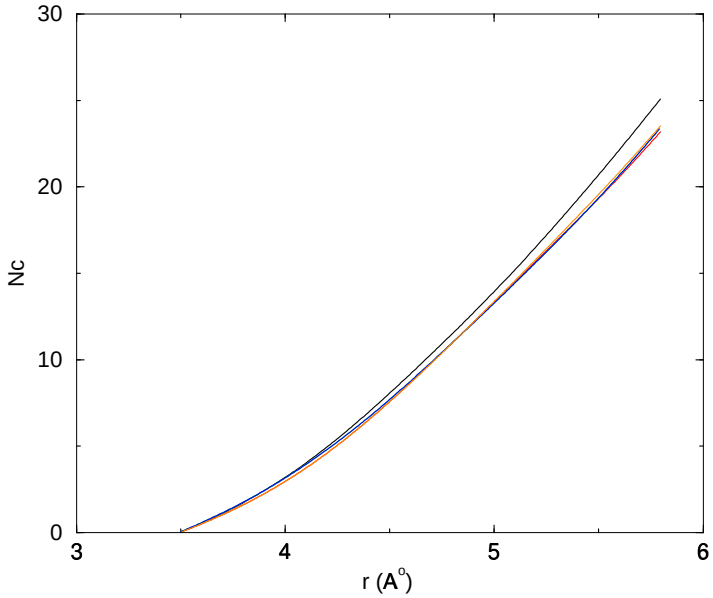

Figure 7.10: Temperature dependence of the oxygen–oxygen coordination number in the 2^{nd} hydration shell of pure water. 298 K black, 303 K red, 308 K green, 313 K blue, 318 K orange.

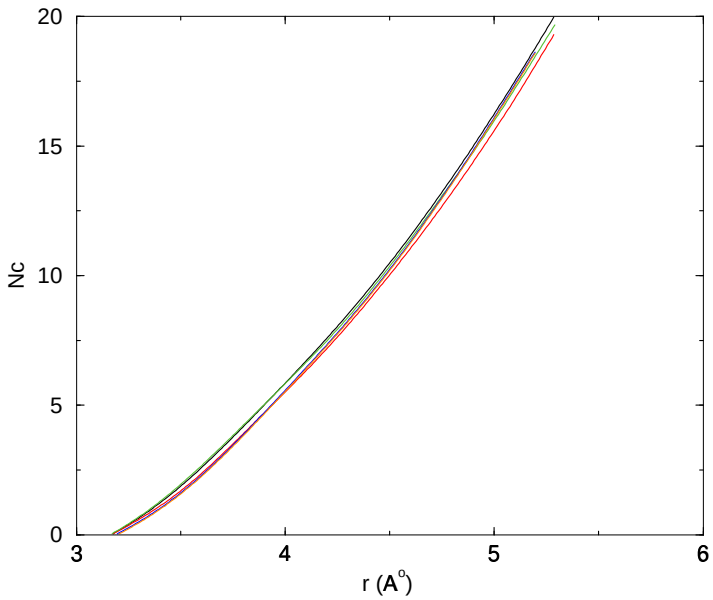

Figure 7.11: Temperature dependence of the hydrogen–hydrogen coordination number in the 2^{nd} hydration shell of pure water. 298 K black, 303 K red, 308 K green, 313 K blue, 318 K orange.

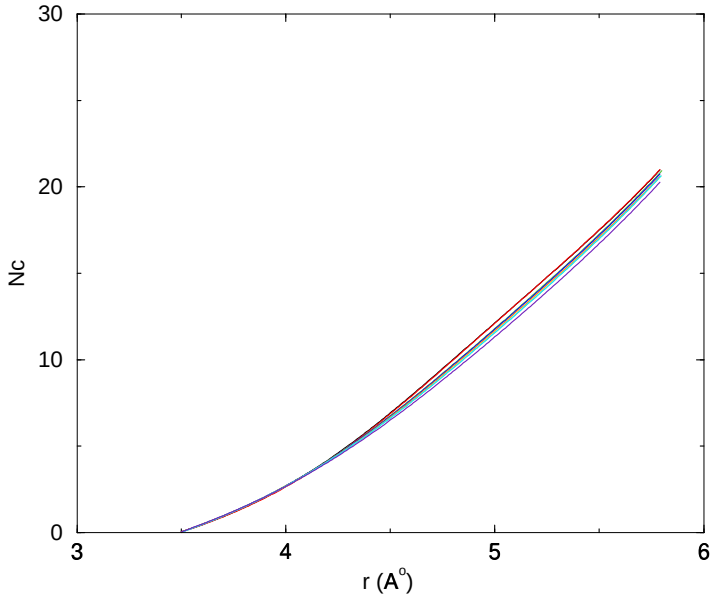

Figure 7.12: Temperature dependence of the oxygen–oxygen coordination number in the 2^{nd} hydration shell of the water–methane system. 298K black, 303 K red, 308 K green, 313 K blue, 318 K orange, 323 K brown, 328 K cyan, 333 K indigo.

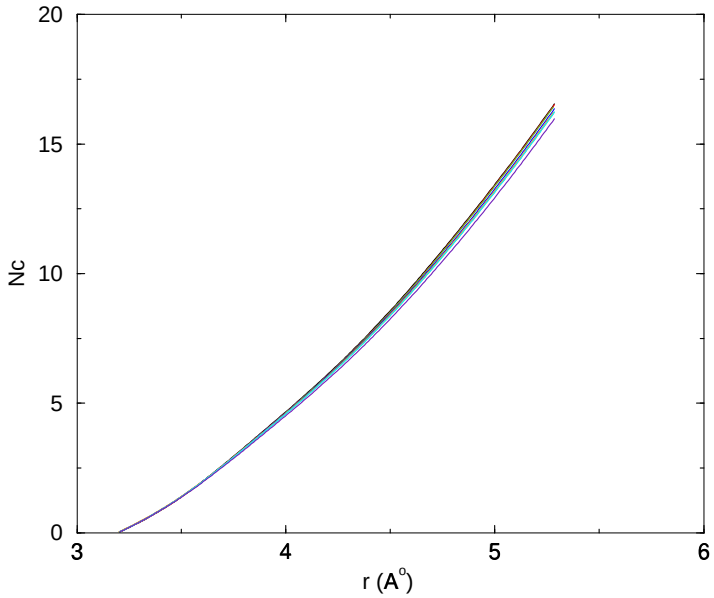

Figure 7.13: Temperature dependence of the hydrogen–hydrogen coordination number in the 2^{nd} hydration shell of the water–methane system. 298 K black, 303 K red, 308 K green, 313 K blue, 318 K orange, 323 K brown, 328 K cyan, 333 K indigo.

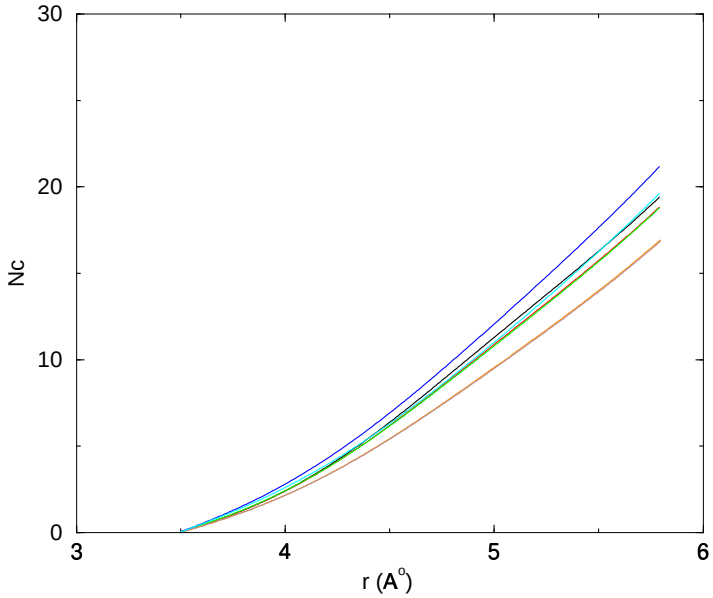

Figure 7.14: Temperature dependence of the oxygen–oxygen coordination number in the 2^{nd} hydration shell of the water–ethane system. 298 K black, 303 K red, 308 K green, 313 K blue, 318 K orange, 323 K brown, 328 K cyan, 333 K indigo.

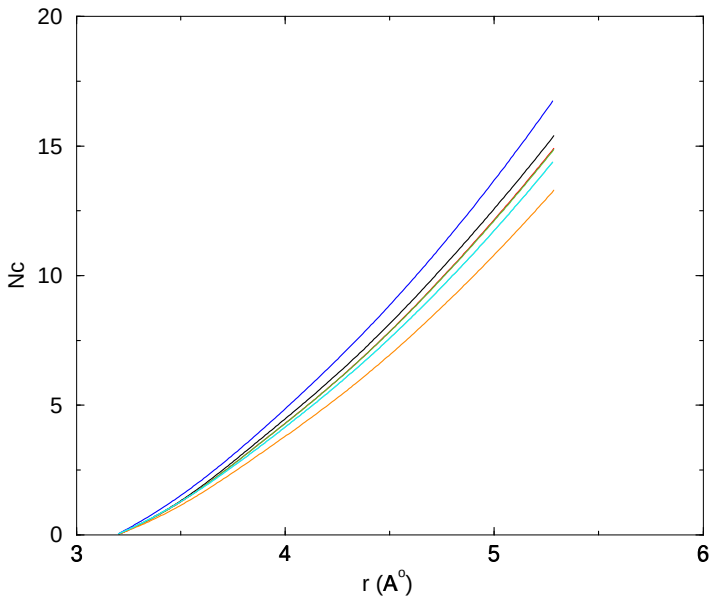

Figure 7.15: Temperature dependence of the hydrogen–hydrogen coordination number in the 2^{nd} hydration shell of the water–ethane system. 298 K black, 303 K red, 308 K green, 313 K blue, 318 K orange, 323 K brown, 328 K cyan, 333 K indigo.

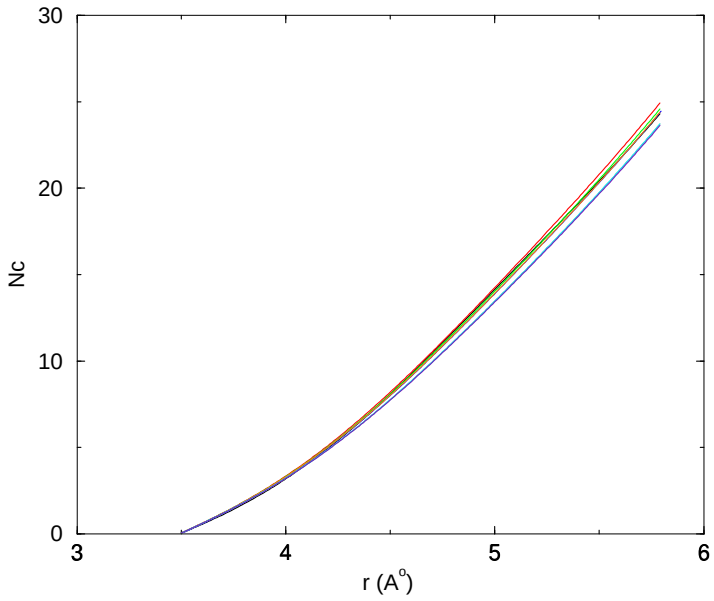

Figure 7.16: Temperature dependence of the oxygen–oxygen coordination number in the 2^{nd} hydration shell of the water–xenon system. 298 K black, 303 K red, 308 K green, 313 K blue, 318 K orange, 323 K brown, 328 K cyan, 333 K indigo, 338 K violet.

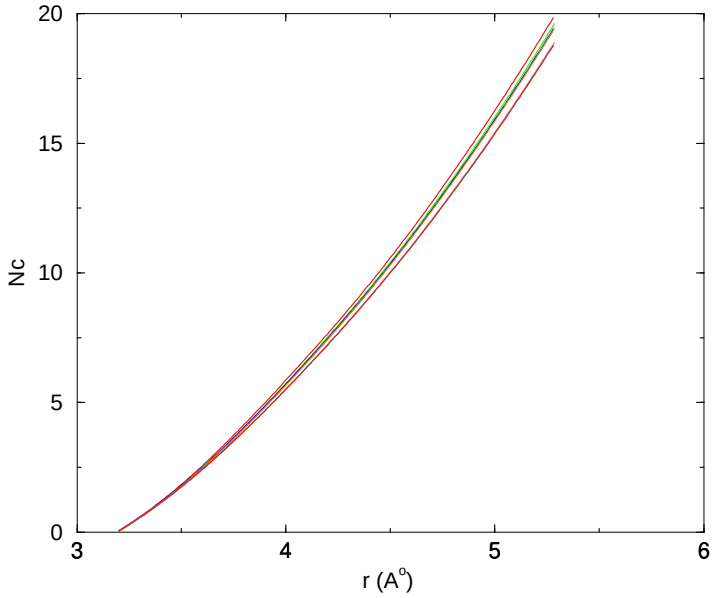

Figure 7.17: Temperature dependence of the hydrogen–hydrogen coordination number in the second hydration shell of the water–xenon system. 298 K black, 303 K red, 308 K green, 313 K blue, 318 K orange, 323 K brown, 328 K cyan, 333 K indigo, 338 K violet.

Chapter 8

Appendix B

8.1 Pressure dependence of the structural properties

In this appendix, the pressure dependence of the structural properties of water for the water–methane, water–ethane and water–xenon systems is presented. The description of these correlation functions can be found in Section 4.

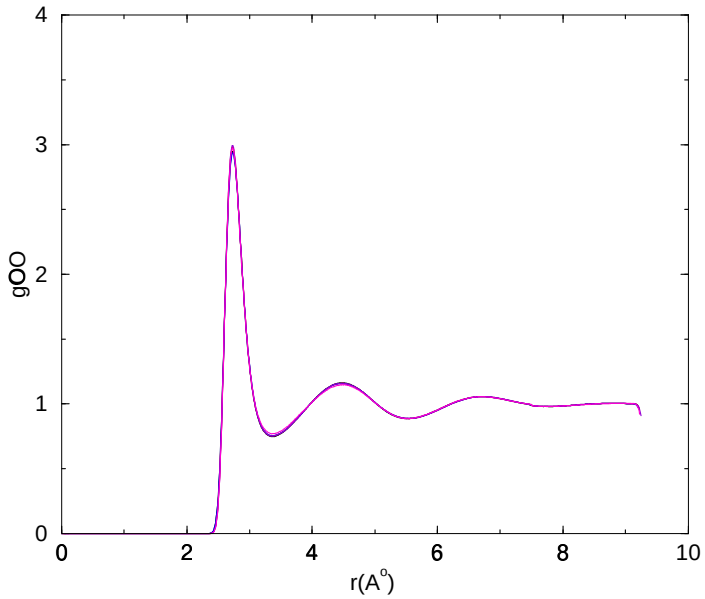

Figure 8.1: Pressure dependence of g_{OO} of the water–methane system with increasing pressure between 1 and 35 bar at 298 K temperature: 1 bar black, 5 bar red, 10 bar blue, 25 bar orange, 35 bar magenta.

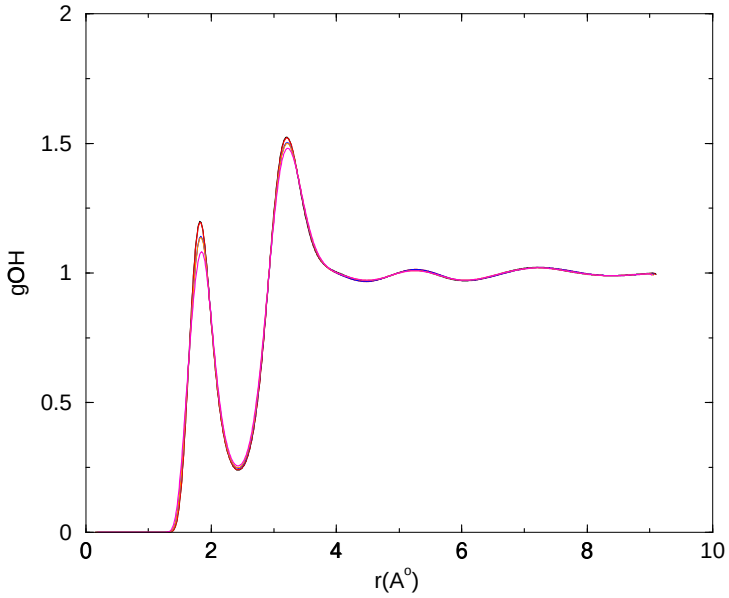

Figure 8.2: Pressure dependence of g_{OH} of the water–methane system with increasing pressure between 1 and 35 bar at 298 K temperature: 1 bar black, 5 bar red, 10 bar blue, 25 bar orange, 35 bar magenta.

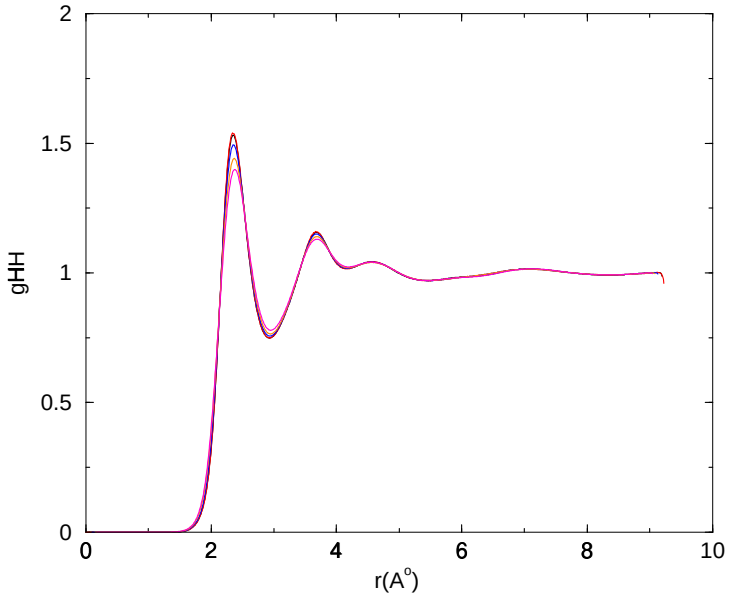

Figure 8.3: Pressure dependence of g_{HH} of the water–methane system with increasing pressure between 1 and 35 bar at 298 K temperature: 1 bar black, 5 bar red, 10 bar blue, 25 bar orange, 35 bar magenta.

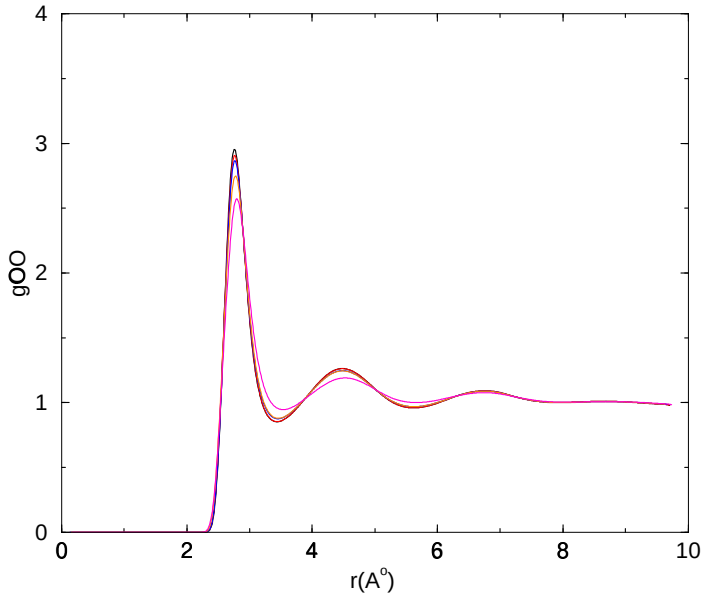

Figure 8.4: Pressure dependence of g_{OO} of the water–ethane system between 1–30 bar, at 298 K temperature: 1 bar black, 5 bar red, 10 bar blue, 15 bar violet, 20 bar orange and 30 bar magenta.

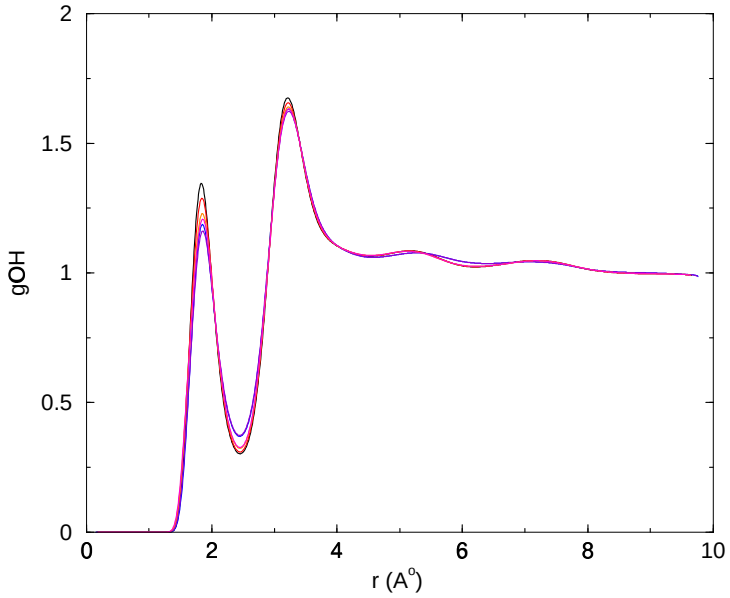

Figure 8.5: Pressure dependence of g_{OH} of the water–ethane system between 1–30 bar, at 298 K temperature: 1 bar black, 5 bar red, 10 bar blue, 15 bar violet, 20 bar orange and 30 bar magenta.

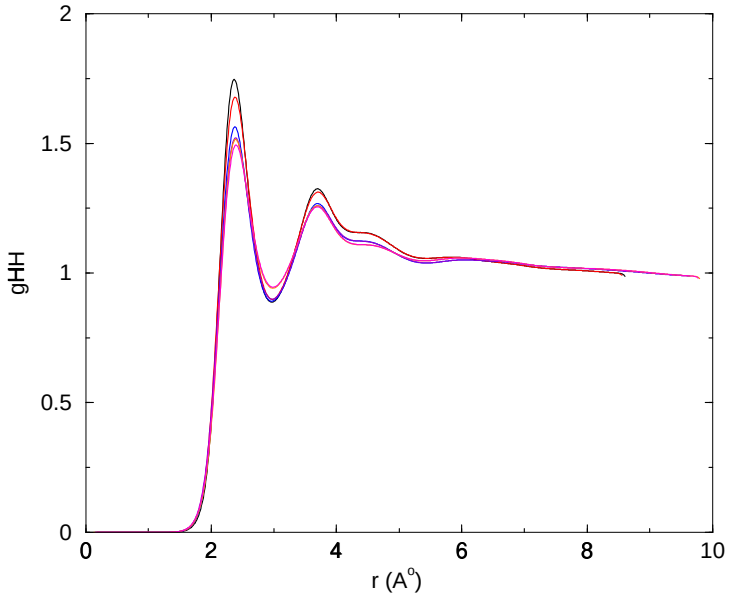

Figure 8.6: Pressure dependence of g_{HH} of the water–ethane system between 1–30 bar at 298 K temperature: 1 bar black, 5 bar red, 10 bar blue, 15 bar violet, 20 bar orange and 30 bar magenta.

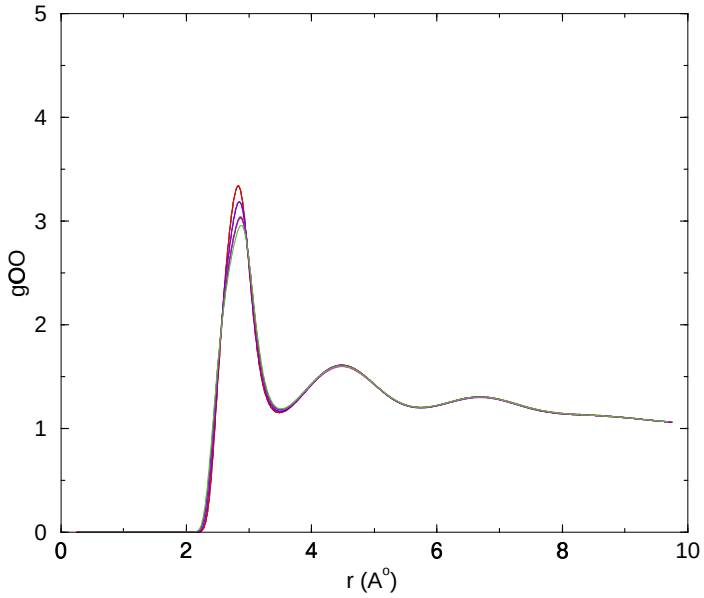

Figure 8.7: Pressure dependence of g_{OO} of the water–xenon system between 1–35 bar at, 298 K temperature: 1 bar black, 5 bar red, 10 bar blue, 15 bar violet, 20 bar orange, 25 bar magenta, 30 bar indigo and 35 bar green.

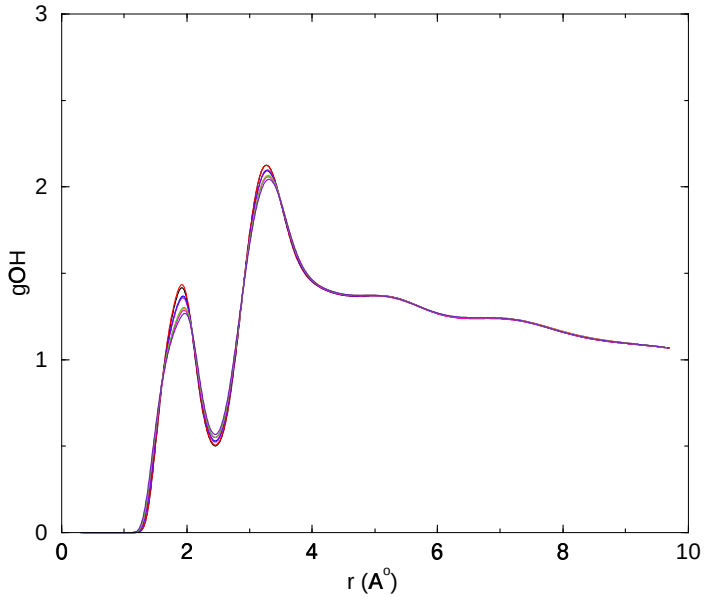

Figure 8.8: Pressure dependence of g_{OH} of the water–xenon system between 1–35 bar, at 298 K temperature: 1 bar black, 5 bar red, 10 bar blue, 15 bar violet, 20 bar orange, 25 bar magenta, 30 bar indigo and 35 bar green.

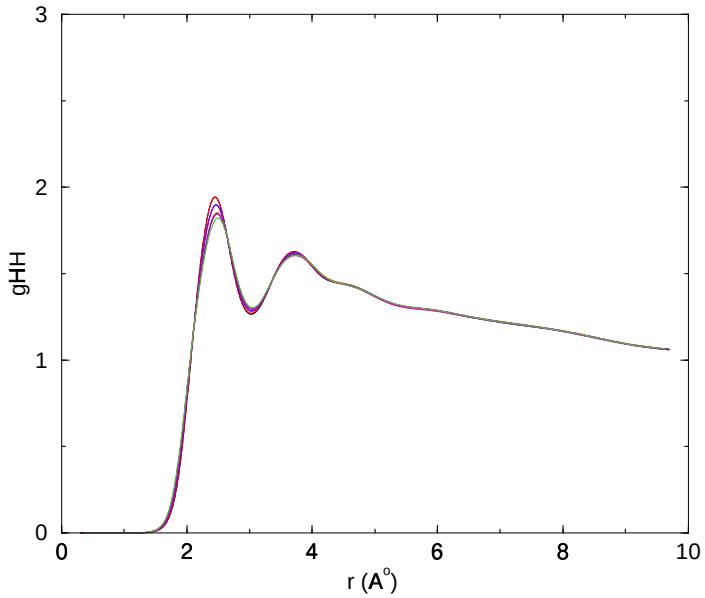

Figure 8.9: Pressure dependence of g_{HH} of the water–xenon system between 1–35 bar, at 298 K temperature: 1 bar black, 5 bar red, 10 bar blue, 15 bar violet, 20 bar orange, 25 bar magenta, 30 bar indigo and 35 bar green.

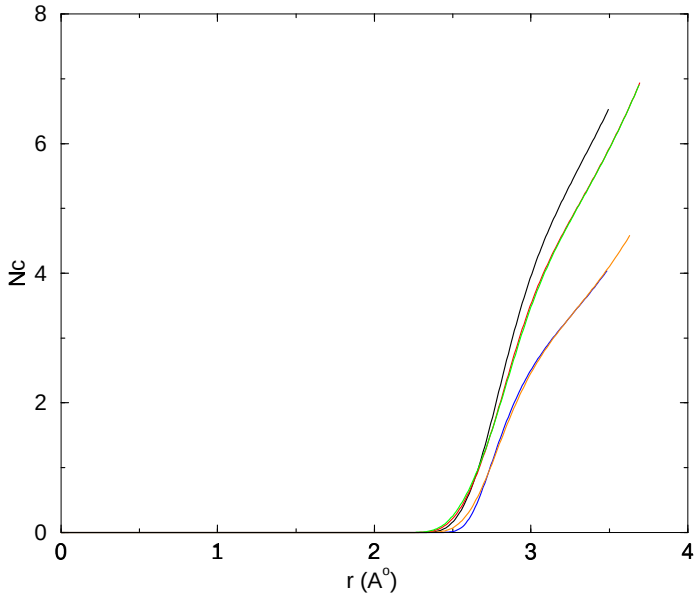

Figure 8.10: Pressure dependence of the oxygen–oxygen coordination number in the 1^{st} hydration shell of pure water: 1 bar black, 5 bar red, 15 bar green, 25 bar.

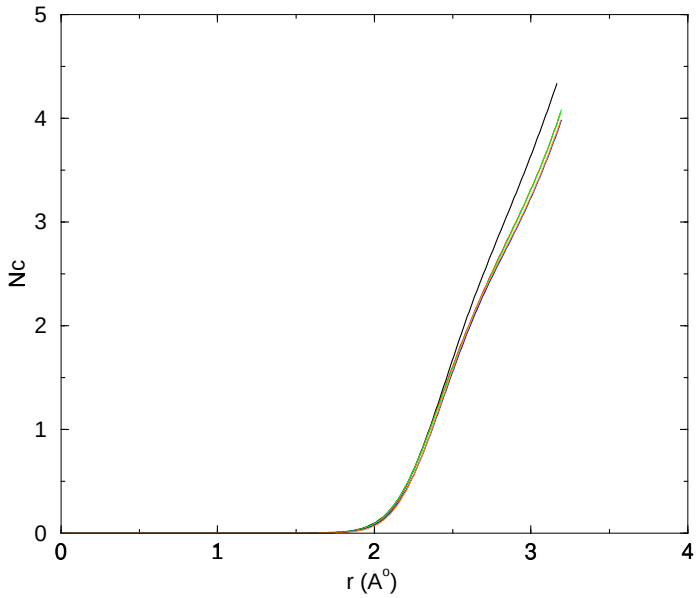

Figure 8.11: Pressure dependence of the hydrogen–hydrogen coordination number in the 1^{st} hydration shell of pure water: 1 bar black, 5 bar red, 15 bar green, 25 bar.

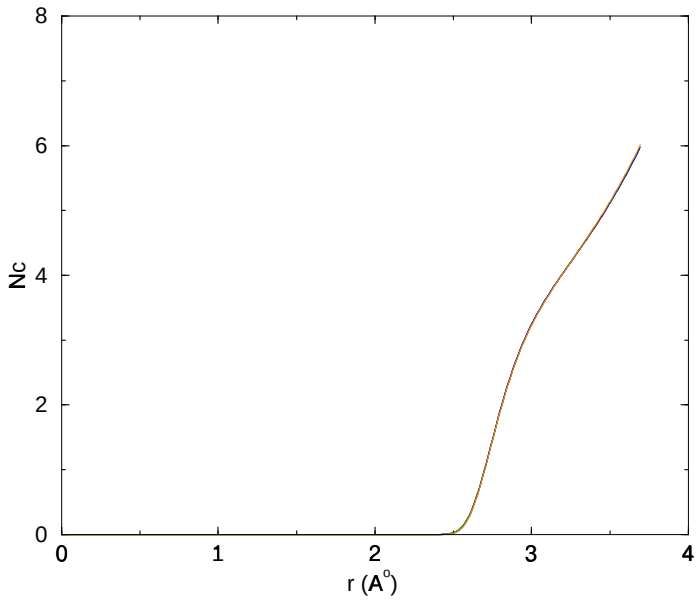

Figure 8.12: Pressure dependence of the oxygen–oxygen coordination number in the 1^{st} hydration shell of the water–methane system: 1 bar black, 5 bar red, 15 bar green, 25 bar blue, 30 bar orange, 35 bar brown.

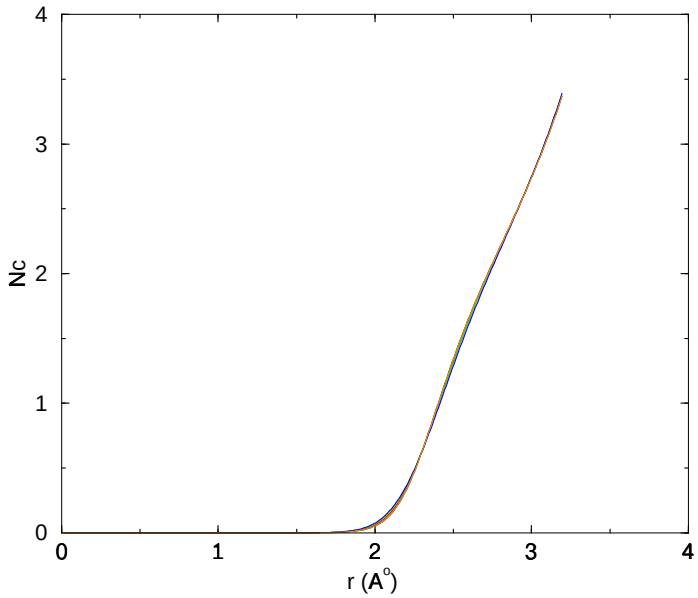

Figure 8.13: Pressure dependence of the hydrogen–hydrogen coordination number in the 1^{st} hydration shell of the water–methane system: 1 bar black, 5 bar red, 15 bar green, 25 bar blue, 30 bar orange, 35 bar brown.

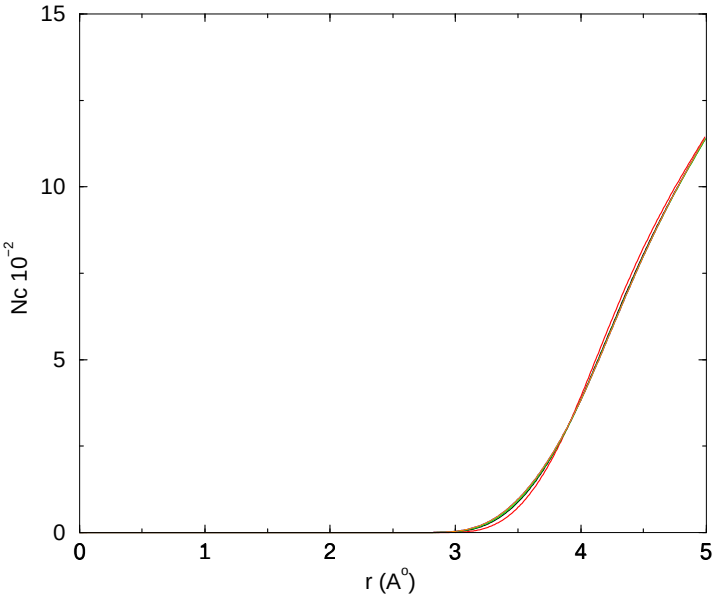

Figure 8.14: Pressure dependence of the methane–methane coordination number in the 1^{st} hydration shell of the water–methane system: 1 bar black, 5 bar red, 15 bar green, 25 bar blue, 30 bar orange, 35 bar brown.

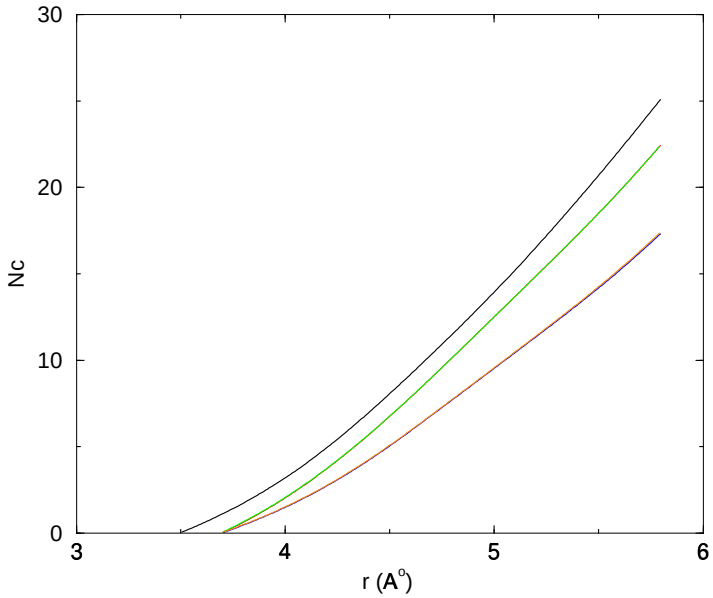

Figure 8.15: Pressure dependence of the oxygen–oxygen coordination number in the second hydration shell of water: 1 bar black, 5 bar red, 15 bar green, 25 bar blue.

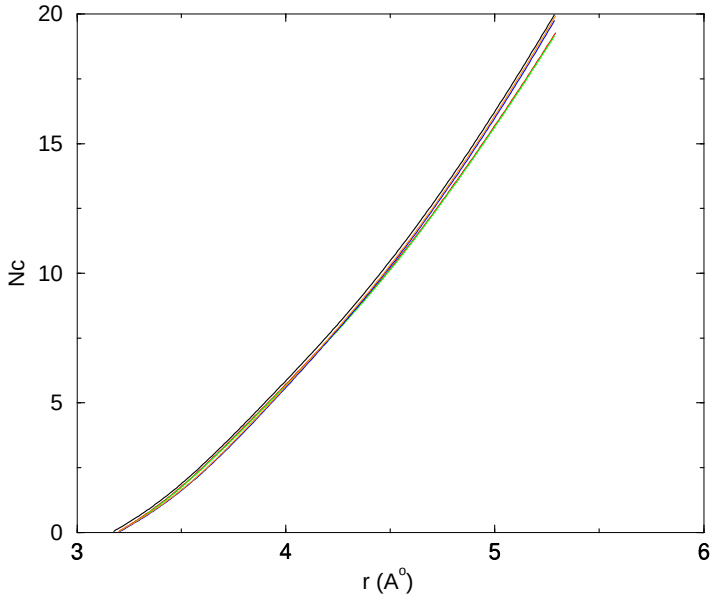

Figure 8.16: Pressure dependence of the hydrogen–hydrogen coordination number in the second hydration shell of water: 1 bar black, 5 bar red, 15 bar green, 25 bar blue.

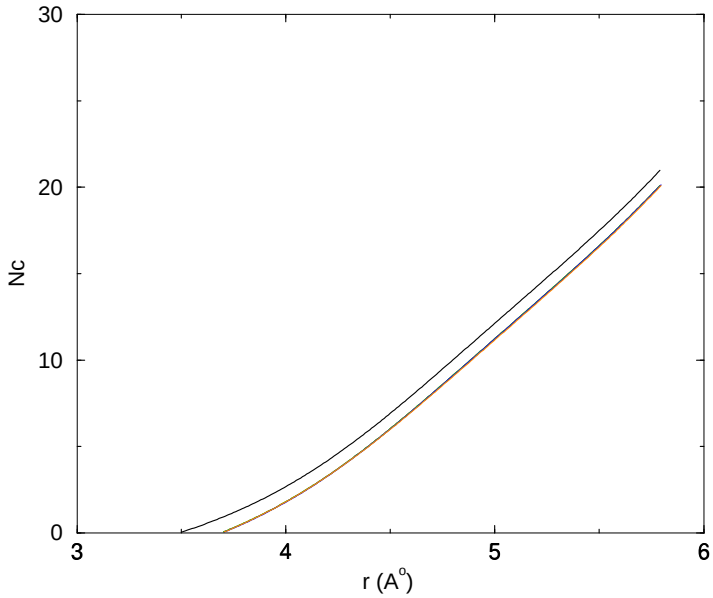

Figure 8.17: Pressure dependence of the oxygen–oxygen coordination number in the second hydration shell of the water–methane system: 1 bar black, 5 bar red, 15 bar green, 25 bar blue, 30 bar brown and 35 bar cyan.

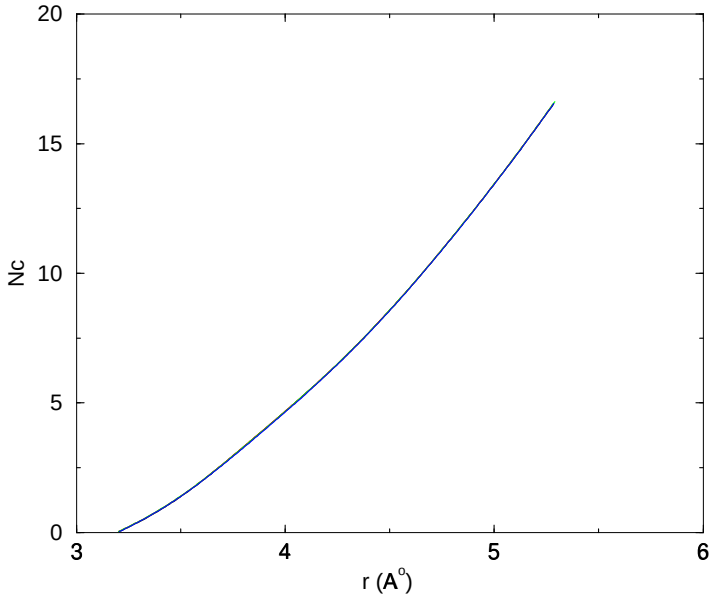

Figure 8.18: Pressure dependence of the hydrogen–hydrogen coordination number in the second hydration shell of the water–methane system: 1 bar black, 5 bar red, 15 bar green, 25 bar blue, 30 bar brown and 35 bar cyan.

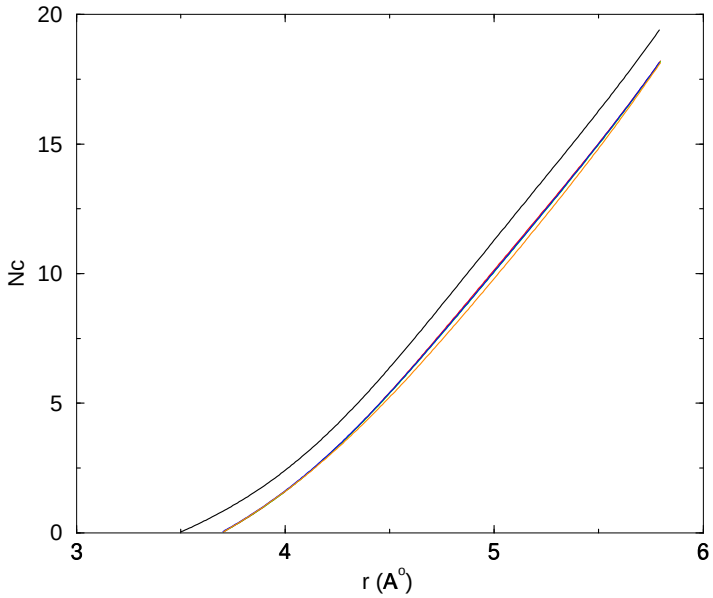

Figure 8.19: Pressure dependence of the oxygen–oxygen coordination number in the second hydration shell of the water–ethane system: 1 bar black, 5 bar red, 15 bar green, 25 bar blue, 30 bar brown and 35 bar cyan.

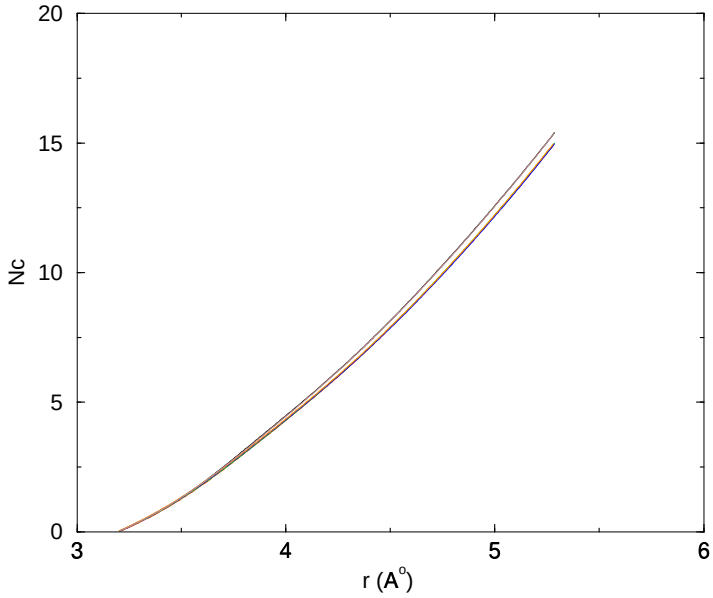

Figure 8.20: Pressure dependence of the hydrogen–hydrogen coordination number in the second hydration shell of the water–ethane system: 1 bar black, 5 bar red, 15 bar green, 25 bar blue, 30 bar brown and 35 bar cyan.

Chapter 9

AppendixC

9.1 Temperature dependence of the thermodynamic properties

T (K)	V 10^{-5} m^3/mol	E (kJ/mol)	ΔH_{vap} (kJ/mol)
298	1.8051±0.00022	-41.7404±0.0460	44.1839±0.02887
303	1.8217±0.00024	-41.1505±0.0418	43.6818±0.02929
308	1.8287±0.00029	-40.9747±0.0502	43.5563±0.02928
313	1.8344±0.00031	-40.8994±0.0460	43.4726±0.03054
318	1.8396±0.00030	-40.8241±0.0460	43.4308±0.03053

Table 9.1: Temperature dependence of the thermodynamic properties of pure water.

T (K)	V 10^{-5} (m^3/mol)	E (kJ/mol)	H (kJ/mol)	$\mu_{res}(H_2O)$ (kJ/mol)	$\mu_{res}(CH_4)$ (kJ/mol)
298	1.80±0.0003	-42.07±0.06	-42.05±0.06	-20.99±0.01	9.12±0.03
303	1.81±0.0004	-41.59±0.06	-41.06±0.06	-20.69±0.02	9.16±0.02
308	1.82±0.0003	-41.05±0.06	-41.03±0.06	-20.40±0.03	9.41±0.02
313	1.82±0.0003	-40.61±0.06	-40.60±0.06	-20.11±0.02	9.66±0.02
318	1.83±0.0003	-40.12±0.06	-40.11±0.06	-19.98±0.02	9.99±0.01
323	1.84±0.0003	-39.55±0.06	-39.53±0.06	-19.47±0.02	10.54±0.01
333	1.86±0.0004	-38.69±0.06	-38.67±0.06	-18.67±0.004	10.67±0.01

Table 9.2: Temperature dependence of the thermodynamic properties of the water–methane system.

T (K)	V 10^{-5} (m^3/mol)	E (kJ/mol)	H (kJ/mol)	$\mu_{res}(H_2O)$ (kJ/mol)	$\mu_{res}(C_2H_6)$ (kJ/mol)
298	2.17±0.0006	-39.38±0.08	-39.36±0.02	-17.61±0.005	8.65±0.003
303	2.19±0.0005	-38.93±0.07	-38.91±0.05	-17.37±0.002	8.73±0.008
308	2.19±0.0004	-38.54±0.06	-38.52±0.05	-17.27±0.003	8.73±0.004
313	2.21±0.0005	-37.97±0.061	-37.95±0.06	-17.07±0.004	8.79±0.001
318	2.22±0.0004	-37.40±0.06	-37.38±0.05	-16.75±0.008	8.88±0.001
323	2.24±0.0004	-37.33±0.06	-37.31±0.04	-16.43±0.002	8.89±0.001
328	2.24±0.0005	-36.62±0.06	-36.61±0.061	-15.7482±0.00556	8.9031±0.001

Table 9.3: Temperature dependence of the thermodynamic properties of the water–ethane system.

T (K)	V 10^{-5} m^3/mol	E (kJ/mol)	H (kJ/mol)	μ_{res} water (kJ/mol)	μ_{res} xenon (kJ/mol)
298	2.15±0.0006	-39.99±0.05	-39.97±0.05	-21.21±0.04	5.66±0.04
303	2.15±0.0006	-39.86±0.05	-39.84±0.05	-20.89±0.05	6.00±0.03
308	2.17±0.0005	-39.11±0.06	-39.08±0.06	-19.93±0.04	6.37±0.02
313	2.17±0.0006	-38.92±0.05	-38.90±0.05	-19.02±0.04	6.81±0.03
318	2.17±0.0005	-38.40±0.05	-38.38±0.05	-18.56±0.04	7.05±0.03
323	2.20±0.0006	-37.93±0.05	-37.91±0.05	-18.02±0.04	7.32±0.02

Table 9.4: Temperature dependence of the thermodynamic properties of the water–xenon hydration process (1 xenon and 216 water molecules).

T (K)	V 10^{-5} m^3/mol	E (kJ/mol)	H (kJ/mol)	μ_{res} water (kJ/mol)	μ_{res} xenon (kJ/mol)
298	2.17±0.0002	-39.59±0.07	-39.57±0.04	-21.71±0.03	6.23±0.01
303	2.18±0.0002	-39.09±0.06	-39.07±0.04	-21.02±0.03	6.33±0.07
308	2.20±0.0003	-38.88±0.06	-38.85±0.04	-20.76±0.04	6.68±0.09
313	2.22±0.0002	-38.13±0.06	-38.11±0.03	-19.69±0.04	6.92±0.1
318	2.22±0.0003	-37.65±0.06	-37.63±0.04	-19.60±0.04	7.17±0.06
323	2.24±0.0004	-37.16±0.07	-37.14±0.04	-19.49±0.04	7.44±0.09
328	2.25±0.0002	-36.88±0.06	-36.86±0.04	-19.03±0.03	7.78±0.07
333	2.25±0.0002	-36.56±0.06	-36.54±0.04	-18.89±0.04	7.99±0.04
338	2.26±0.0003	-35.61±0.07	-35.59±0.04	-18.66±0.07	8.66±0.006

Table 9.5: Temperature dependence of the thermodynamic properties of the water–xenon system.

Chapter 10

AppendixD

10.1 Pressure dependence of the thermodynamic properties

P (bar)	V 10^{-5} (m^3/mol)	E (kJ/mol)	μ_{total} (kJ/mol)
1	1.80±0.002	-41.74±0.04	-41.75±0.04
10	1.83±0.002	-41.84±0.04	-38.32±0.05
15	1.82±0.002	-41.88±0.05	-38.28±0.03
25	1.81±0.002	-43.93±0.04	-38.62±0.04

Table 10.1: Pressure dependence of the thermodynamic properties of pure water.

P (bar)	V 10^{-5} (m^3/mol)	E (kJ/mol)	$\mu_{res}(H_2O)$ (kJ/mol)	$\mu_{res}(CH_4)$ (kJ/mol)
1	1.81±0.0003	-42.07±0.06	-20.99±0.01	9.12±0.03
10	1.80±0.0003	-41.87±0.03	-21.05±0.02	9.17±0.01
25	1.81±0.0002	-42.13±0.03	-21.29±0.01	9.15±0.02
35	1.81±0.0002	-41.42±0.06	-22.14±0.02	9.18±0.02

Table 10.2: Pressure dependence of the thermodynamic properties of the water–methane system.

P (bar)	V 10^{-5} (m^3/mol)	E (kJ/mol)	H (kJ/mol)	$\mu_{res}(H_2O)$ (kJ/mol)	$\mu_{res}(C_2H_6)$ (kJ/mol)
1	2.17±0.06	-39.38±0.8	-39.36±0.02	-17.61±0.006	8.65±0.003
5	2.17±0.04	-40.12±0.6	-38.79±0.03	-17.87±0.003	8.75±0.002
10	2.17±0.04	-39.29±0.8	-39.07±0.03	-17.42±0.006	8.69±0.003
15	2.17±0.04	-38.99±0.6	-38.67±0.02	-17.31±0.004	8.79±0.004
20	2.17±0.03	-38.32±0.6	-37.89±0.05	-17.44±0.002	8.75±0.004
30	2.16±0.04	-40.14±0.6	-39.50±0.06	-17.11±0.007	8.73±0.003

Table 10.3: Pressure dependence of the thermodynamic properties of the water–ethane system.

P (bar)	V 10^{-5} m^3/mol	E (kJ/mol)	H (kJ/mol)	H_2O μ_{res} (kJ/mol)	Xe μ_{res} (kJ/mol)
1	2.17±0.0002	-39.59±0.06	-39.57±0.04	-21.71±0.03	6.23±0.01
5	2.11±0.0002	-37.99±0.08	-37.88±0.03	-19.88±0.04	6.12±0.08
10	2.09±0.0002	-37.52±0.07	-37.31±0.07	-19.89±0.04	6.09±0.09
15	2.08±0.0003	-37.99±0.07	-37.68±0.1	-19.90±0.04	6.15±0.1
20	2.12±0.0002	-37.60±0.06	-37.18±0.08	-19.95±0.04	6.17±0.08
25	2.10±0.0002	-36.65±0.07	-36.14±0.08	-19.96±0.04	6.13±0.07
30	2.11±0.0001	-36.07±0.07	-36.13±0.08	-19.96±0.04	6.13±0.07
35	2.13±0.0002	-36.23±0.06	-36.23±0.08	-20.12±0.03	6.15±0.09

Table 10.4: Pressure dependence of the thermodynamic properties of the water–xenon system.

Chapter 11

Danksagung

Herrn Prof. Dr. U. K. Deiters möchte ich für die Betreuung der Arbeit und für die Möglichkeit der Durchführung der Forschungsarbeit an der Universität zu Köln danken.

Herrn Dr. K. Leonhard, Herrn Dr. M. Hloucha, Herrn Priv. Doz. Dr. T. Kraska und Herrn Dr. L. Yelash möchte ich für die stete Hilfsbereitschaft danken.

Der Arbeitsgruppe von Prof. Dr. U. K. Deiters danke ich für die stete Unterstützung.

Bei den Mitarbeitern des Regionalen Rechenzentrums der Universität zu Köln bedanke ich mich für die Bereitstellung von Rechenzeit auf den leistungsfähigen Rechenanlagen.

Ich versichere, daß ich die von mir vorgelegte Dissertation selbständig angefertigt, die benutzten Quellen und Hilfsmittel vollständig angegeben und die Stellen der Arbeit – einschließlich Tabellen, Karten und Abbildungen –, die anderen Werken im Wortlaut oder dem Sinn nach entnommen sind, in jedem Einzelfall als Entlehnung kenntlich gemacht habe; daß diese Dissertation noch keiner anderen Fakultät oder Universität zur Prüfung vorgelegen hat; daß sie noch nicht veröffentlicht worden ist sowie, daß ich eine solche Veröffentlichung vor Abschluß des Promotionsverfahrens nicht vornehmen werde. Die Bestimmungen dieser Promotionsordnung sind mir bekannt. Die von mir vorgelegte Dissertation ist von Prof. Dr. U. K. Deiters betreut worden.

Köln, 8th September 2003

O. Coskuner

Lebenslauf

Persönliche Daten

Name	Orkide Coskuner
Addresse	Heidmann str. 22
	D-42855 Remscheid
Geburtsdatum	25. 09. 1973
Geburtsort	Remscheid
Familienstand	ledig

Schulausbildung

1980–1984	Kremenholler Grundschule in Remscheid
1984–1990	Besuch des Dedeman und Kayseri College

Hochschulausbildung

1990–1996	Studium der Chemie METU
1996–2000	Studium der Chemie an der
	Universität zu Köln
seit 2000	Promotion in Physikalischer Chemie

Anstellungen

09/99-04/00	Studentische Hilfskraft an der
	Universität zu Köln
seit 09/00	Wissenschaftliche Hilfskraft an der
	Universität zu Köln

Bibliography

[1] W. L. Jorgensen, J. F. Blake, J. K. Buckner. *Chem. Phys.*, **129**: 193, 1989.

[2] B. Guillot, Y. Guissani, S. Bratos. *J. Chem. Phys.*, **95**: 3643, 1991.

[3] F. H. Stillinger. *J. Soln. Chem.*, **2**: 141, 1973.

[4] L. R. Pratt, A. Pohorille. *J. Am. Chem. Soc.*, **112**: 5066, 1990.

[5] L. R. Pratt, D. L. Chandler. *J. Chem. Phys.*, **73**: 3434, 1980.

[6] K. A. Dill. *Biochemistry*, **29**: 7133, 1990.

[7] R. D. Amos. *J. Am. Chem. Soc.*, **83**:1595, 1987.

[8] P. C. Harihan, J. A. Pople. *Mol. Phys.*, **27**: 209, 1974.

[9] A. Ben-Naim. *Solvation Thermodynamics. Plenum Press, NY, London*, 1987.

[10] J. A. V. Butler, W. S. Reid. *J. Chem. Soc.*, 1171, 1936.

[11] J. A. V. Butler. *Trans. Faraday Soc.*, 229, 1937.

[12] S. J. Gill, S. F. Dec, G. Olofsson, I. Wadso. *J. Phys. Chem.*, **89**: 3758, 1985.

[13] F. Franks. *In Water, a Comprehensive Treatise. Plenum Press, NY*, 1975.

[14] M. A. Klapper. *Prog. Bioorg. Chem.*, **2**: 55, 1973.

[15] P. M. Rodger. *J. Phys. Chem.*, **94**: 6080, 1990.

[16] T. Lazaridis, M. E. Paulaitis. *J. Phys. Chem.*, *96*: 3847, 192.

[17] S. Tiwari, B. V. B. Reddy. *Theor. Chem. Acc.*, **101**: 41, 1999.

[18] P.Y. Chou, G. D. Fasman. *Biochemistry*, **13**: 222, 1974.

[19] J. Garnier, D. J. Osguthorpe, B. Robson. *J. Mol. Biol.*, **62**: 613, 1978.

[20] B. Rost, C. Sander. *J. Mol. Biol.*, **232**: 584, 1993.

[21] B. Rost, C. Sander. *Proteins*, **19**: 55, 1994.

[22] N. T. Southall, K. A. Dill. *J. Phys. Chem. B*, **106**: 521, 2002.

[23] G. Hummer, A. Szabo. *J. Chem. Phys.*, **105**: 2004, 1996.

[24] D. Sitkoff, A. Sharp, B. Honig. *J. Phys. Chem.*, **98**: 1978, 1994.

[25] B. Guillot, Y. Guissani. *J. Chem. Phys.*, **99**: 8075, 1993.

[26] R. D. Broadbent, G. W. Neilson. *J. Chem. Phys.*, **100**: 7543, 1994.

[27] A. Ben-Naim. *J. Am. Chem. Soc.*, **82**: 792, 1978.

[28] N. G. Parsonage. *J. Chem. Soc. Faraday Trans.*, **91**: 2971, 1995.

[29] N. G. Parsonage. *J. Chem. Soc. Faraday Trans.*, **92**: 1129, 1996a.

[30] A. P. Lyubartsev, O. K. Forrisdahl, A. Laaksonen. *Second. Int. Conf. on Gas Hydrates, Toulose, France*, **June 2-6**: 311, 1996.

[31] H. Sun. *J. Phys. Chem.*, **102**: 7338, 1998.

[32] A. Ben-Naim, Y. Marcus. *J. Chem. Phys.*, **81**: 2016, 1984.

[33] D. M. Huang, D. Chandler. *Proc. Natl. Acad. Sci.*, **97**: 8324, 2000.

[34] R. A. Pierotti. *J. Phys. Chem.*, **69**: 281, 1965.

[35] S. W. Rick, B. J. Berne. *J. Phys. Chem. B*, **101**: 10488, 1997.

[36] V. Villani, J. M. Z. Comenges. *Theor. Chem. Acc.*, **104**: 290, 2000.

[37] R. A. Pierotti. *Chem. Rev.*, **76**: 717, 1976.

[38] G. Hummer, S. Garde, A. E. Garcia, M. E. Paulaitis, L. R. Pratt. *Chem. Phys.*, **2**: 1, 1998.

[39] V. N. Prorokov, V. V. Dolotov, G. A. Krestov. *Russ. J. Phys. Chem.*, **58**: 1153, 1984.

[40] R. Battino, H. L. Clever. *Chem. Rev.*, **66**: 395, 1966.

[41] A. N. Strakhov, G. A. Krestov, V. K. Abrosimov, V. G. Badelin. *Russ. J. Phys. Chem.*, **6**: 1583, 1975.

[42] O. Sifner, J. Klomfar. *J. Phys. and Chem. Ref. Data*, **23**: 63, 1994.

[43] T. Prange, M. Schiltz, L. Pernot, N. Colloc'h, S. Longhi, W. Bourget, R. Fourme. *Proteins*, **30**: 61, 1998.

[44] J. G. Ewing, S. Maestas. *J. Phys. Chem.*, **74**: 2341, 1970.

[45] B. P. Schoenborn. *Nature*, **208**: 760, 1996.

[46] B. P. Schoenborn. *Nature*, **214**: 1120, 1967.

[47] R. F. Tilton, I. D. Kuntz, G. A. Petsko. *Biochemistry*, **23**: 2849, 1984.

[48] R. F. Tilton, U. C. Singh, S. J. Weiner, M. L. Conolly, I. D. Kuntz, P. A. Kollmann. *J. Mol. Biol.*, **192**: 443, 1986.

[49] B. P. Schoenborn, R. M. Featherstone, P. O. Vogelhut, C. Suesskind. *Nature*, **202**: 695, 1964.

[50] S. C. Cullen, E. G. Gross. *Science*, **113**: 580, 1951.

[51] M. Schiltz, T. Prange, R. Fourme. *J. Appl. Cryst.*, **27**: 950, 1994.

[52] M. Schiltz, W. Shepard, R. Fourme, T. Prange. *Acta Crystallography*, **53**: 78, 1997.

[53] M. H. B. Stowell, S. M. Soltis, C. Kisker, J. W. Peters, H. Schindelin, D. C. rees, D. Cascio, L. Beamer, P. J. Hart, M. C. Wiener, F. G. Whitby. *J. Appl. Cryst.*, **29**: 608, 1996.

[54] J. Vitali, A.H. Robins, S. C. Almo, R. F. Tilton. *J. Appl. Cryst.*, **24**: 931, 1991.

[55] M. L. Conolly. *J. Appl. Cryst.*, **16**: 548, 1983.

[56] S. J. Hubbard, K. H. Gross, P. Argos. *Protein Eng.*, **7**: 613, 1994.

[57] M. H. Klapper. *Biochim. Biophys. Acta*, **229**: 557, 1971.

[58] J. P. Kocher, M. Prevost, S. J. Wodak, B. Lee. *Structure*, **4**: 1517, 1996

[59] R. F. Tilton, I. D. Kuntz. *Biochemistry*, **21**: 6850, 1982.

bibitemIra1 Ira. N. Levine. *Quantum Chemistry*, **4th Edition** *Prentice Hall, New Jersey*, 1991.

[60] W. Kauzmann. *Adv. Protein Chem.*, **14**: 1, 1959.

[61] J. R. Pratt, D. Chandler. *J. Chem. Phys.*, **67**: 3683, 1977.

[62] J. R. Pratt, D. Chandler. *J. Chem. Phys.*, **73**: 3434, 1980.

[63] I. Yu, B. Roux, M. Karplus. *J. Chem. Phys.*, **92**: 5020, 1990.

[64] F. Hirata, J. Rossky, B. M. Pettitt. *Chem. Phys. Lett.*, **83**: 329, 1981.

[65] F. Hirata, J. Rossky, B. M. Pettitt. *J. Chem. Phys.*, **78**: 4133, 1983.

[66] C. Pangali, M. Rao, B. J. Berne. *J. Chem. Phys.*, **71**: 2975, 1979.

[67] K. Watanabe, H. C. Andersen. *J. Phys. Chem.*, **90**: 795, 1986.

[68] D. C. Rapaport, H. A. Scheraga. *J. Phys. Chem.*, **86**: 873, 1982.

[69] A. Laaksonen, P. Stilbs. *Mol. Phys*, **74**: 747, 1991.

[70] S. Swaminathan, D. L. Beveridge. *J. Am. Chem. Soc.*, **101**: 5832, 1979.

[71] G. Ravishanker, M. Mezei, D. L. Beveridge *Faraday Chem. Soc.*, **17**: 79, 1982.

[72] A. Wallqvist, B. J. Berne. *Chem. Phys. Lett.*, **145**: 26, 1988.

[73] D. Smith, A. D. J. Haymet. *J. Chem. Phys.*, **98**: 6445, 1993.

[74] D. L. Mancera, A. D. Buckingham. *Chem. Phys. Lett.*, **234**: 296, 1995.

[75] L. X. Dang. *J. Chem. Phys.*, **100**: 903, 1994.

[76] S. Luedemann, H. Schreiber, R. Abseher, O. Steinhauser. *J. Chem. Phys.*, **104**: 286, 1996.

[77] J. H. Cobos, A. D. Mackie, L. F. Vega. *J. Chem. Phys.*, **114**: 7527, 2001.

[78] S. Shimizu,H. S. Chan. *J. Chem. Phys.*, **113**: 4683, 2000.

[79] N .T. Skipper. *Chem. Phys. Lett.*, **207**: 424, 1993.

[80] D. L. Mancera, A. D. Bridgeman, A. D. Buckingham, N. T. Skipper. *Faraday Discuss.*, **103**: 414, 1996.

[81] X. L. Dang. *J. Chem. Phys.*, **100**: 9032, 1994.

[82] I. R. McDonnald, K. Singer. *Discuss. Faraday Soc.*, **43**: 40, 1967.

[83] N. Metropolis. *Los Alamos Science*, **12**: 125, 1987.

[84] M. Costas, B. Kronenberg, R. Silveston. *J. Chem. Soc. Faraday Trans.*, **90**: 1513, 1994.

[85] G. Peinel, H. Frischleder, F. Birnstock. *Theoret. Chim. Acta*, **57**: 245, 1980.

[86] P. Kollman. *Chem. Rev.*, **93**: 2395, 1993.

[87] P. Kollman. *J. Am. Chem. Soc.*, **99**: 4875, 1977.

[88] J. Gao. *J. Phys. Chem.*, **96**: 537, 1992.

[89] M. H. Abraham. *J. Am. Chem. Soc.*, **104**: 2085, 1982.

[90] V. Tran, B. Schwartz. *J. Phys. Chem. B*, **103**: 5570, 1999.

[91] T. L. Hill. *Statistical mechanics*, McGraw-Hill, New York, 1956.

[92] D. A. McQuarrie. *Statistical mechanics*, Harper and Row, New York, 1976.

[93] D. Frenkel, B. Smit. *Understanding Molecular Simulation. Academic Press*, 2002.

[94] M. P. Allen, D. J. Tildesley. *Computer Simulation of Liquids. Oxford Science Publications*, 1987.

[95] N. Metropolis. *J. Chem. Phys.*, **21**: 1087, 1953.

[96] F. Vesely. *Computerexperimente an Fl"ussigkeiten.* Physik Verlag, 1978.

[97] W. W. Wood. *Computer simulation of water and aqueous solutions. Physics of Simple Fluids*, pp. 115-230, Amsterdam, Netherlands.

[98] M. Born, T. von Karman. *Physik. Z.*, **13**: 297, 1912.

[99] L. R. Pratt, S. W. Haan. *J. Chem. Phys.*, **74**: 1862, 1981.

[100] P. Ewald. *Ann. Phys.*, **64**: 253, 1921.

[101] E. Madelung. *Phys. Z.*, **19**: 524, 1918.

[102] S. W. De Leeuw, J. W. Perram, E. R. Smith. *Proc. R. Soc. Lond.*, **A373**: 27, 1980.

[103] D. M. Heyes, J. H. R. Clark. *J. Chem. Soc. Faraday II*, **77**: 1089, 1981.

[104] C. Tanford. *Ben Franklin stilled the waves.. Duke University Press., Durham, NC*, 1989.

[105] I. Traube. *I. Ann. Chem. Liebigs.*, **27**: 265, 1981.

[106] I. Langmuir. *J. Am. Chem. Soc.*, **39**: 1848, 1917.

[107] J. Simpson, E. Weiner. *The Oxford English Dictionary. Oxford University Press.*, **2nd Edition**, 1989.

[108] H. Meyer. *Arch. Exptl. Pathol. Pharmakol.*, **42**: 110, 1989.

[109] J. W. McBain, C. S. Salmon. *J. Am. Chem. Soc.*, **42**: 426, 1920.

[110] E. Gorter, F. Grendel. *J. Exp. Med.*, **41**: 439, 1925.

[111] H. A. Davson. *J. Cellular Comput. Phys.*, **5**: 435, 1935.

[112] H. Bull. *Adv. Enzymol.*, **1**: 1, 1941.

[113] W. D. Harkings, R. W. Matton, M. L. Corrin, R. S. Stearns. *J. Chem. Phys.*, **13**: 534, 1945.

[114] J. C. Kendrew, G. Bodo, H. M. Dintzis,R. G. Parrish, D. C. Philips. *Nature*, **181**: 662, 1958.

[115] K. J. Palmer. *J. Phys. Chem.*, **48**: 12, 1944.

[116] P. Debye. *Ann. N. Y. Acad. Sci.*, **51**: 575, 1949.

[117] L. J. Pauling. *J. Am. Chem. Soc.*, **62**: 2643, 1940.

[118] J. Hildebrand. *J. Phys. Chem.*, **72**: 1841, 1968.

[119] M. H. Abraham. *J. Am. Chem. Soc.*, **104**: 2085, 1982.

[120] A. Ben-Naim, Y. Marcus. *J. Chem. Phys.*, **81**: 2016, 1984.

[121] L. Privalov, S. J. Gill. *Adv. Protein Chem.*, **39**: 191, 1988.

[122] M. Hloucha. *MC Simulationen an polarisierbaren Fl"ussigkeitsmodellen von Fluormethan*, *Shaker Verlag*, 1998.

[123] G. L. Pollack. *Science*, **251**: 1323, 1991.

[124] G. Nemethy, W. J. Peer, H. A. Sheraga. *Annu. Rev. Biophys. Bioeng.*, **10**: 59, 1981.

[125] M. Yacobi, A. Ben-Naim. *J. Phys. Chem.*, **78**: 175, 1974.

[126] E. E. Tucker, S. D. Christian. *J. Phys. Chem.*, **83**: 426, 1979.

[127] R. P. Keenan, G. L. Pollack. *J. Chem. Phys.*, **93**: 2724, 1990.

[128] E. E. Tucker, E. H. Lane, S. D. Christian. *J. Solut. Chem.*, **10**: 1, 1981.

[129] J. L. Alvarez, R. F. Prini. *J. Chem. Phys.* **96**: 3357, 1992.

[130] R. P. Keenan, G. L. Pollack. *J. Chem. Phys.*, **96**: 3359, 1992.

[131] A. Geiger, A. Rahman, F. H. Stillinger. *J. Chem. Phys.*, **70**: 263, 1978.

[132] D. W. Davidson. *in Water, a Comprehensive Treatise edited by F. Franks, Plenum, NY*, 1973.

[133] W. L. Jorgensen, J. K. Buckner, S. Boudon, J. Tirado-Rives. *J. Chem. Phys.*, **89**: 3742, 1988.

[134] N. T. Skipper, C. H. Bridgeman, A. D. Buckingham, R. L. Mancera. *Faraday Discuss.*, **103**: 414, 1996.

[135] B. Widom. *J. Chem. Phys.*, **39**: 2802, 1963.

[136] T. P. Straatsma, H. J. C. Berendsen, J. P. M. Postma. *J. Chem. Phys.*, **85**: 6720, 1986.

[137] D. A. Pearlman. *J. Phys. Chem.*, **98**: 1487, 1994.

[138] D. A. Pearlman. *J. Comp. Chem.*, **15**: 105, 1994.

[139] M. Mezei. *Mol. Simulations*, **10**: 225, 1993

[140] D. J. Adams. *Mol. Phys.*, **28**: 1241, 1974.

[141] D. E. Pearlman, P. A. Kollman. *J. Chem. Phys.*, **91**: 7831, 1989.

[142] P. A. Kollman. *Chem. Rev.*, **93**: 2395, 1993.

[143] C. A. Reynolds, P. M. King, W. G. Richard. *Mol. Phys.*, **76**: 251, 1992.

[144] J. P. Valleau, D. N. Card. *J. Chem. Phys.*, **57**: 5457, 1972.

[145] G. M. Torrie, J. P. Valleau. *J. Comp. Chem.*, **23**: 187, 1977.

[146] J. P. Valleau. *J. Comp. Chem.*, **96**: 193, 1991.

[147] M. Mezei. *J. Comp. Chem.*, **68**: 237, 1987.

[148] C. H. Bennet *J. Comp. Chem.*, **22**: 245, 1976.

[149] E. Rittger. *J. Comp. Chem.*, **79**: 1073, 1993.

[150] A. P. Lyubartsev, A. A. Martsinovskii, S. V. Shevkunov, P. N. Vorontsov-Velyaminov. *J. Chem. Phys.*, **96**: 1776, 1992.

[151] J. G. Kirkwood. *J. Chem. Phys.*, **3**: 300, 1935.

[152] N. Metropolis, A. W. Rosenbluth, M. N. Rosenbluth, A. H. Teller, E. J. Teller. *J. Chem. Phys.*, **21**: 1987, 1953.

[153] M. Mezei, S. Swaminathan, D. L. Beveridge. *J. Chem. Phys.*, **71**: 3366, 1979.

[154] P. K. Mehrotra, M. Mezei, D. L. Beveridge. *J. Chem. Phys.*, **78**: 3156, 1983.

[155] M. Rao, C. S. Pangali, B. J. Berne. *J. Chem. Phys.*, **37**: 1773, 1979.

[156] M. Mezei, S. Swaminathan, D. L. Beveridge. *J. Am. Chem. Soc.*, **100**: 3255, 1978.

[157] G. N. Sarkisov, V. G. Dashesky, G. G. Malenkov. *Mol. Phys.*, **27**: 1249, 1974.

[158] J. Owicki, H. A. Sheraga. *J. Am. Chem. Soc.*, **82**: 1257, 1978

[159] G. M. Torrie, J. P. Valleau. *J. Comp. Chem.*, **23**: 187, 1977.

[160] M. Mezei, D. L. Beveridge. *Comp. Sim. of Chem. and Biomol. Systems, Ann. of NY Acad. Sci.*, **482**, 1986.

[161] G. C. Boulougouris, I. G. Economou, D. N. Theodorou. *Mol. Phys.*, **96**: 905, 1999.

[162] M. W. Mahoney, W. L. Jorgensen. *J. Chem. Phys.*, **112**: 8909, 2000.

[163] I. Nezbeda, J. Slovak. *Mol. Phys.*, **90**: 353, 1997.

[164] I. Nezbeda. *J. Mol. Liquids*, **73**: 317, 1997.

[165] W. L. Jorgensen. *J. Chem. Phys.*, **79**: 926, 1983.

[166] W. L. Jorgensen, M. Matsuoka. *J. Chem. Phys.*, **64**: 1351, 1976.

[167] K. Watanabe, M. L. Klein. *Chem. Phys.*, **131**: 157, 1989.

[168] H. J. C. Berendsen, J. R. Grigera, T. P. Straatsma. *J. Phys. Chem.*, **91**: 6269, 1987.

[169] H. Popkie, H. Kistenmacher, E. Clementi. *J. Chem. Phys.*, **59**: 1325, 1973.

[170] F. H. Stillinger, A. Rahman. *J. Chem. Phys.*, **60**: 1545, 1974.

[171] J. D. Bernal, R. H. Fowler. *J. Chem. Phys.*, *1*: 515, 1933.

[172] W. L. Jorgensen, J. Chandrasekhar, J. D. Madura, R. W. Impey, M. L. Klein. *J. Chem. Phys.*, **79**: 926, 1983.

[173] W. L. Jorgensen, J. D. Madura. *Mol. Phys.*, **56**: 1381, 1985.

[174] H. J. C. Berendsen, J. R. Grigera, T. P. Straatsma. *J. Phys. Chem.*, **91**: 6269, 1987.

[175] J. D. Madura, B. M. Pettitt, D. F. Calef. *Mol. Phys.*, **64**: 325, 1988.

[176] H. J. C. Berendsen, J. P. M. Postma, W. F. van Gunsteren, J. Hermans. *in Intermolecular Forces. Reidel, Dordrecht, Holland*: 331, 1981.

[177] G. S. Kell. *J. Chem. Eng. Data*, **20**: 97, 1975.

[178] C. A. Angell, H. Kanno. *Science*, **193**: 1121, 1976.

[179] C. A. Angel, M. Oguni, W. J. Sichina. *J. Phys. Chem.*, **86**: 998, 1982.

[180] R. B. Hermann. *J. Phys. Chem.*, **76**: 2754, 1972.

[181] M. S. Jhon, E. R. van Artsdalen, J. Grosh, H. Eyring. *J. Chem. Phys.*, **44**: 1465, 1966.

[182] J. A. Reyolds, D. B. Gilbert, C. Tabford. *Proc. Natl. Acad. Sci.*, bf 71: 2925, 1974.

[183] W. L. Jorgensen, J. D. Madura, and C. J. Swenson. *J. Am. Chem. Soc.*, **106**: 6638, 1984.

[184] S. R. Billetter, P. M. King, W. F. van Gunsteren. *J. Chem. Phys.*, **100**: 6692, 1994.

[185] J. S. Gill, I. Wadso. *Proc. Natl. Acad. Sci.*, **73**: 2955, 1976.

[186] C. H. Cho, S. Singh, G. W. Robinson. *Phys. Rev. Lett.*, **76**: 1651, 1996.

[187] W. L. Jorgensen, C. Jenson. *J. Comput. Chem.*, **19**: 1179, 1998.

[188] P. H. Poole, F. Sciortino, U. Essman, H. E. Stanley. *Nature*, **360**: 324, 1992.

[189] L. A. Baez, P. Clancy. *J. Chem. Phys.*, **101**: 9837, 1994.

[190] A. H. Narten, H. A. Levy. *J. Chem. Phys.*, **55**: 2263, 1971.

[191] F. Sciortino, S. Sastry. *J. Chem. Phys.*, **100**: 3881, 1994.

[192] I. M. Svishchev, P. G. Kusalik, J. Wang, R. J. Boyd. *J. Chem. Phys.*, **105**: 4742, 1996.

[193] A. K. Soper, M. G. Phillips. *Chem. Phys.*, **107**: 47, 1986.

[194] H. Sato, M. Uematsu, K. Watanabe, A. Saul, W. Wagner. *J. Phys. Chem. Ref. Data*, **17**: 1439, 1988.

[195] A. Wallqvist, P. O. Astrand. *J. Chem. Phys.*, **102**: 6559, 1995.

[196] G. C. Lie, E. Clementi. *Phys. Rev. A*, **33**: 2679, 1986.

[197] O. Teleman, B. Jonsson, S. Engstrom. *Mol. Phys.*, **60**: 193, 1987.

[198] S. B. Zhu, S. Yao, J. B. Zhu, S. Singh, G. W. Robinson. *J. Phys.Chem.*, **95**: 6211, 1991.

[199] D. J. Swanton, G. B. Bacskay, N. S. Hush. *Chem. Phys.*, **82**: 303, 1983.

[200] D. J. Swanton, G. B. Bacskay, N. S. Hush. *J. Chem. Phys.*, **84**: 5715, 1986.

[201] A. I. Kitaigorodski. *Molecular Crystals and Molecules, Academis Press, NY*, 1973

[202] A. Warshel, S. Lifson. *J. Chem. Phys.*, **53**: 582, 1970.

[203] B. R. Gelin, M. Karplus. *Biochemistry*, **18**: 1256, 1979.

[204] W. L. Jorgensen, R. C. Binning, B Bigot. *J. Am. Chem. Soc.*, **103**: 4393, 1981.

[205] W.L. Jorgensen. *J. Phys. Chem.*, **87**: 5304, 1983.

[206] J. R. Durig, D. A. Compton. *J. Phys. Chem.*, **83**: 265, 1979.

[207] L. Verlet, J. J. Weis. *Mol. Phys.*, **24**: 1013, 1972.

[208] A. Habenschuss, E. Johnson, A.H. Narten. *J. Chem. Phys.*, **74**: 5234, 1981.

[209] A.H. Narten. *J. Chem. Phys.*, **67**: 2102, 1977.

[210] J. P. Ryckaert, A. Bellemans. *Discuss. Faraday Soc.*, **66**, 1978.

[211] L. G. Dunfield, A. Burgess, H. A. Scheraga. *J. Phys. Chem.*, **82**: 2609, 1978.

[212] Y. Marcus, A. Ben-Naim. *J. Chem. Phys.*, **83**: 4744, 1985.

[213] J. Ji, T. Cagir, B. M. Pettitt. *J. Chem. Phys.*, **96**: 1333, 1992.

[214] M. W. Mahoney, W. L. Jorgensen *J. Chem. Phys.*, **114**: 363, 2001

[215] W. Kauzmann. *A Symposium on the mechanism of enzyme action. W. D. McElroy, B. Glass, eds., John Hopkins Univ. Press. Baltimore*, **70**, 1954.

[216] J. G. Kirkwood. *Ref.* **61**: 16.

[217] H. S. Frank, M. W. Evans. *J. Chem. Phys.*, **13**: 507, 1945.

[218] D. F. Waugh. *Advan. Protein Chem.*, **9**: 352, 1954.

[219] G. Nemethy, H. A. Scheraga. *J. Chem. Phys.*, **66**: 1773, 1962.

[220] G. Nemethy. *Angew. Chem.*, **6**: 195, 1967.

[221] I. M. Klotz, S. W. Luborsky. *J. Am. Chem. Soc.*, **81**: 5119, 1959.

[222] I. M. Klotz. *Science*, **128**: 815, 1958.

[223] K.U. Linderstrom-Lang. *Cold Spring Harbor Symp. Quant. Biol.*, **14**: 117, 1950.

[224] L. R. Pratt. *Annu. Rev. Phys. Chem.*, **53**: 409, 2002.

[225] Landolt-Boernstein *Zahlenwerte und Funktionen* **2.Teil**: b.

[226] A. Ben-Naim. *Hydrophobic Intercations*, *Plenum Press, NY*, 1980.

[227] A. Ben-Naim. *J Chem. Phys.*, **42**: 1512, 1965.

[228] A. Ben-Naim. *J. Chem. Phys.*, **54**: 1387, 1971.